CONFIDENTIAL

Copy 343
RM L55J12

NACA RM L55J12

NACA

RESEARCH MEMORANDUM

SOME EFFECTS OF SWEEP AND THICKNESS ON THE EXPERIMENTAL DOWNWASH CHARACTERISTICS AT TRANSONIC SPEEDS OF A SERIES OF HIGHLY TAPERED WINGS WITH AN ASPECT RATIO OF 3

TRANSONIC-BUMP METHOD

By Albert G. Few, Jr.

Langley Aeronautical Laboratory
Langley Field, Va.

CLASSIFIED DOCUMENT

This material contains information affecting the National Defense of the United States within the meaning of the espionage laws, Title 18, U.S.C., Secs. 793 and 794, the transmission or revelation of which in any manner to an unauthorized person is prohibited by law.

CLASSIFICATION CHANGED TO UNCLASSIFIED
AUTHORITY: NACA RESEARCH ABSTRACT NO. 121
EFFECTIVE DATE: OCTOBER 14, 1957 WHL

NATIONAL ADVISORY COMMITTEE
FOR AERONAUTICS

WASHINGTON

February 16, 1956

CONFIDENTIAL

NATIONAL ADVISORY COMMITTEE FOR AERONAUTICS

RESEARCH MEMORANDUM

SOME EFFECTS OF SWEEP AND THICKNESS ON THE EXPERIMENTAL DOWNWASH CHARACTERISTICS AT TRANSONIC SPEEDS OF A SERIES OF HIGHLY TAPERED WINGS WITH AN ASPECT RATIO OF 3

TRANSONIC-BUMP METHOD

By Albert G. Few, Jr.

SUMMARY

An investigation by the transonic-bump technique of some effects of sweep and thickness on the transonic downwash and wake characteristics of a series of highly tapered semispan wings with an aspect ratio of 3 has been made in the Langley high-speed 7- by 10-foot tunnel. The Mach number range extended from 0.60 to 1.18 with corresponding Reynolds numbers ranging from about 0.78×10^6 to 0.93×10^6. The angle-of-attack range was from -2° to about 24°. The measurements of downwash and dynamic pressure were made for a range of vertical distances from the wing chord plane extended, but at only one spanwise station and for a given wing plan form, at only one longitudinal station.

Increases in wing sweep provided a decrease in the rate of change of downwash with angle of attack, $\frac{\partial \epsilon}{\partial \alpha}$, in the low angle-of-attack range for all Mach numbers, and provided less variation with Mach number at all distances from the wing chord plane. The rate of change of downwash with angle of attack reached a maximum near the wing chord plane for all wing sweep angles. Above the wing chord plane, $\frac{\partial \epsilon}{\partial \alpha}$ increased to maximum values exceeding unity with an increase in angle of attack for all conditions of wing sweep and thickness. For a quarter-chord sweep angle of 14.03° a decrease in wing thickness ratio from $t/c = 0.045$ to $t/c = 0.02$ produces increases in $\frac{\partial \epsilon}{\partial \alpha}$ at any distance from the wing chord plane extended up to a Mach number of about 1.09. Regardless of wing sweep or thickness, increasing the speed from subsonic to supersonic caused the wake center to be displaced toward the wing chord plane and, although the losses in wake dynamic pressure were reduced, there was a general thickening of the wake in going to supersonic speeds.

INTRODUCTION

In an effort to increase performance, particularly at transonic and supersonic speeds, considerable attention has been given to thin, highly tapered, low-aspect-ratio wings which also offer certain structural advantages over wings of less taper. Recent comparisons of some effects of sweep and thickness on the transonic-speed static longitudinal stability characteristics of such a series of wing plan forms have been published in reference 1. However, experimental downwash and wake characteristics behind thin, highly tapered, low-aspect-ratio wings and their influence on the horizontal tail effectiveness at the various vertical distances from the wing chord plane which may be considered in conjunction with these wings is limited, especially in the higher angle-of-attack range. Reliable theoretical methods for predicting the downwash behavior behind these wings at high angles of attack and in the transonic and supersonic speed range also are, for the most part, not available as pointed out in references 2 to 5.

The present investigation was made primarily for the purpose of obtaining, at transonic speeds, quantitative downwash and wake characteristics (particularly at high angles of attack) of a series of thin, highly tapered, low-aspect-ratio wings having quarter-chord sweep angles varying from 0° to 45°. The models included a series of four wings all having an aspect ratio of 3, a taper ratio of 0.143, and NACA 65A003 airfoil sections parallel to the plane of symmetry. In addition to models having NACA 65A003 airfoil sections, models having NACA 65A002 and NACA 65A004.5 airfoil sections were provided for one sweep angle of 14.03°. Measurements of downwash and dynamic pressure were made for a wide range of vertical distances from the wing chord plane, but at only one spanwise station and for a given wing plan form at only one representative longitudinal station.

The reflection-plane system utilized in the investigation consisted of semispan wing models mounted on a transonic bump in the Langley high-speed 7- by 10-foot tunnel. The Mach number range extended from 0.60 to 1.18 with corresponding Reynolds numbers varying from about 0.78×10^6 to 0.93×10^6. The angle-of-attack range extended from about -2° to 24°. The results presented herein were derived from point pressure surveys behind the models.

SYMBOLS

ϵ downwash angle, deg

α angle of attack, deg

$\left(\frac{\partial \epsilon}{\partial \alpha}\right)_{\alpha=0^\circ}$	rate of change of downwash angle with angle of attack at zero angle of attack
q	effective free-stream dynamic pressure over span of wing, $\frac{\rho V^2}{2}$, lb/sq ft
q_a	average chordwise local dynamic pressure, lb/sq ft
$\frac{q \text{ wake}}{q}$	ratio of dynamic pressure at point of survey to effective free-stream dynamic pressure
V	free-stream velocity, ft/sec
ρ	air density, slugs/cu ft
M	effective Mach number over span of wing
M_l	local Mach number
M_a	average chordwise local Mach number
R	Reynolds number of wing based on $\bar{c}$
$\bar{c}$	mean aerodynamic chord of wing, $\frac{2}{S}\int_0^{b/2} c^2 dY$, ft
c	local wing chord, ft
t	maximum wing thickness, ft
S	twice wing area of semispan model, sq ft
b	twice span of semispan model, ft
A	aspect ratio
$\Lambda_{c/4}$	sweep of wing quarter-chord line, deg
λ	wing taper ratio
X	distance in free-stream direction from quarter chord of wing mean aerodynamic chord to point of flow survey, wing semispans

Y spanwise distance from plane of symmetry to point of flow survey, wing semispans

Z vertical distance normal to X-Y plane from wing chord plane extended to point of flow survey, percent b/2

MODELS AND APPARATUS

The semispan models used in the investigation were constructed of steel to the dimensions given in figure 1. The models included a series of four wings all having an aspect ratio of 3, a taper ratio of 0.143, and NACA 65A003 airfoil sections parallel to the plane of symmetry with quarter-chord sweep angles varying from 0° to 45°. In addition to models having NACA 65A003 airfoil sections, models having NACA 65A002 and 65A004.5 airfoil sections were provided for a quarter-chord sweep angle of 14.03°.

The downwash angles and total-pressure surveys were measured by means of six small probes, details of which are shown in figure 2. The heads of each of the wedge-shaped probes contained two orifices 45° adjacent to the free stream and a total pressure orifice. A photograph of one of the models (with probes installed) mounted on the bump in the Langley high-speed 7- by 10-foot tunnel is shown as figure 3.

TESTS AND CORRECTIONS

The tests were made in the Langley high-speed 7- by 10-foot tunnel employing a curved surface of a bump located on the tunnel floor to obtain transonic speeds. This bump is identical to that used in reference 1.

Typical contours of local Mach number in the vicinity of the model location on the bump (obtained from surveys with no model in position) are shown in figure 4. The effective test Mach numbers were obtained from contour charts similar to those presented in figure 4 using the relationship

$$M = \frac{2}{S}\int_0^{b/2} cM_a \, dY$$

Similarly, the effective dynamic pressure was obtained from contour charts using the relationship

$$q = \frac{2}{S}\int_0^{b/2} cq_a \, dY$$

The investigation covered a range of angle of attack from about -2° to 24° and a range of Mach number from 0.60 to 1.18. The corresponding average test Reynolds numbers, based on the mean aerodynamic chord of the wings, varied from about 0.78×10^6 to 0.93×10^6.

Downwash angles and wake profiles were measured at one spanwise distance from the plane of symmetry ($Y = 0.20b/2$) and for a range of vertical distance from the wing chord plane extended. The point at which the downwash was measured remained fixed, while the angle of attack was varied, and corresponds to the physical case of downwash behind a variable incidence wing. Because of problems associated with the attachment of the models to the balance, the surveys could not be made conveniently at the same longitudinal station for all wing sweep angles and varied from $1.69b/2$ to $2.05b/2$. Based on theoretical predictions of reference 6, this variation is considered to be of little significance.

For these tests, the pressure probes were rotated 10° with respect to the bump center line in a positive angle-of-attack direction in order to obtain pressure measurements at the higher angles of attack within the linear portion of the pressure-probe calibrations. These calibrations were made over a sufficiently large range of Mach number so that data could be obtained over the Mach number range at which each probe was operating. Stream angle surveys with no model in position were made with the probes rotated 10° and the results were applied to the data throughout the Mach number range. The static-pressure values used in computing dynamic pressure ratios were obtained by use of a static probe with no model in position. Jet-boundary corrections have not been evaluated since the boundary conditions to be satisfied are not rigorously defined. However, inasmuch as the effective flow field is large compared to the model size, the corrections are believed to be small.

RESULTS AND DISCUSSION

Presentation of Results

The results of the present investigation are presented in the form of basic data and survey plots in the following figures:

Figure

Basic data:

Effects of angle of attack on the variation of angle of downwash with vertical distance from the wing chord plane extended, Y = 0.20b/2:

$\Lambda_{c/4} = 0^\circ$; X = 2.05b/2; t/c = 0.03 5

$\Lambda_{c/4} = 14.03^\circ$; X = 1.92b/2; t/c = 0.03 6

$\Lambda_{c/4} = 36.87^\circ$; X = 1.69b/2; t/c = 0.03 7

$\Lambda_{c/4} = 45^\circ$; X = 1.69b/2; t/c = 0.03 8

$\Lambda_{c/4} = 14.03^\circ$; X = 1.92b/2; t/c = 0.02 9

$\Lambda_{c/4} = 14.03^\circ$; X = 1.92b/2; t/c = 0.045 10

Data related to analyses of basic data:

Effects of vertical distance from wing chord plane extended on the variation of angle of downwash with angle of attack for various wing plan forms investigated at two representative Mach numbers 11

Effect of wing sweep on $\left(\frac{\partial \epsilon}{\partial \alpha}\right)_{\alpha=0^\circ}$ through the Mach number range investigated and for several distances from the wing chord plane extended 12, 13

Effect of wing sweep on the variation of $\frac{\partial \epsilon}{\partial \alpha}$ with angle of attack for several distances from the wing chord plane extended at two representative Mach numbers 14

Effect of wing thickness on the variation of $\left(\frac{\partial \epsilon}{\partial \alpha}\right)_{\alpha=0^\circ}$ with Mach number for several distances from the wing chord plane extended 15

Effect of wing thickness on the variation of $\frac{\partial \epsilon}{\partial \alpha}$ with angle of attack for several distances from the wing chord plane extended at two representative Mach numbers 16

Effect of wing sweep and thickness on the wake characteristics throughout the range of angle of attack investigated at two representative Mach numbers 17, 18

Downwash Characteristics

The variation of downwash angle with angle of attack for each of the six wings at two representative Mach numbers and for several distances from the wing chord plane extended is presented in figure 11. These data show that, in general, an increase in angle of attack is accompanied by an increase in slope of the downwash curves especially for distances above the wing chord plane extended. As pointed out in reference 4 this is probably attributable to the fact that for survey points above the wing chord plane the distance between the survey points and the wing vortex sheet decreases with increasing angle of attack.

The variation of the rate of change of downwash angle with angle of attack at zero angle of attack $\left(\left(\frac{\partial \epsilon}{\partial \alpha}\right)_{\alpha=0^\circ}\right)$ with Mach number for various distances from the wing chord plane extended is presented in figure 12 for the range of wing sweep angles investigated. In general, an increase in wing sweep provided a decrease in $\left(\frac{\partial \epsilon}{\partial \alpha}\right)_{\alpha=0^\circ}$ for all Mach numbers and less variation with Mach number for all distances from the wing chord plane extended. An increase in distance from the wing chord plane results in somewhat less variation of $\left(\frac{\partial \epsilon}{\partial \alpha}\right)_{\alpha=0^\circ}$ with Mach number for all wing sweep angles than is present near the wing chord plane. Although there is some variation in longitudinal station as shown in figure 2, it is believed to be of little significance (ref. 6) and the effects shown are believed to be attributed to changes in span loading with changes in wing plan form. These data also are for one spanwise station only $\left(Y = 0.20^{b/2}\right)$ which was considered to be representative of a reasonable position for the center of pressure of a horizontal tail. It is indicated in figure 13 that $\left(\frac{\partial \epsilon}{\partial \alpha}\right)_{\alpha=0^\circ}$ reaches a maximum for all wing sweep angles near the wing chord plane extended or wake center line and generally decreases for all Mach numbers investigated with an increase in distance from the wing chord plane.

The effect of wing sweep on the variation with angle of attack of the rate of change of downwash angle with angle of attack $\left(\frac{\partial \epsilon}{\partial \alpha}\right)$ for several distances from the wing chord plane is shown in figure 14. For Mach numbers of either 0.90 and 1.05 in a region near or below the wing chord plane, an increase in angle of attack for all wing sweeps is accompanied by a decrease in $\frac{\partial \epsilon}{\partial \alpha}$; however, for the range of distances above the wing

chord plane (Z = 0.20b/2 to 0.60b/2), $\frac{\partial \epsilon}{\partial \alpha}$ increases to maximum values exceeding unity with an increase in angle of attack as was evidenced from figure 11. These high values of downwash, accompanied by the loss of dynamic pressure shown in figures 17 and 18, would likely result in destabilizing tendencies at high angles of attack for a horizontal tail located at any of these distances from the wing chord plane extended. It will be noted that, in general, an increase in wing sweep provides increases in $\frac{\partial \epsilon}{\partial \alpha}$ at the higher angles of attack, whereas decreases in $\frac{\partial \epsilon}{\partial \alpha}$ with increasing sweep are evident in the low-angle-of-attack range (fig. 14). Maximum values of $\frac{\partial \epsilon}{\partial \alpha}$ for all wing sweep angles generally occurred at higher angles of attack as the distance from the wing chord plane was increased for both Mach numbers (fig. 14). In general, the overall variation of $\frac{\partial \epsilon}{\partial \alpha}$ with angle of attack for all wing sweep angles was greater at a Mach number of 0.90 than for 1.05 as was also evidenced from figure 11.

Some effects of wing thickness on the rate of change of downwash angle with angle of attack are presented in figures 15 and 16. It is indicated in figure 15 that for the wing having a quarter-chord sweep of 14.03° a decrease in wing thickness from $t/c = 0.045$ to $t/c = 0.02$ produces increases in $\left(\frac{\partial \epsilon}{\partial \alpha}\right)_{\alpha=0^\circ}$, up to a Mach number of about 1.09, at any distance from the wing chord plane. This probably results from the higher lift-curve slopes of the thinner wings noted in reference 1. The greatest variation of $\left(\frac{\partial \epsilon}{\partial \alpha}\right)_{\alpha=0^\circ}$ with Mach number occurred for the thickest wing (t/c = 0.045), particularly in a region near the wing chord plane. Figure 16 indicated no significant effects of thickness on $\frac{\partial \epsilon}{\partial \alpha}$ particularly at the high angles of attack for a Mach number of 0.90. However, at a Mach number of 1.05 the thinnest wing (t/c = 0.02) provides curves of $\frac{\partial \epsilon}{\partial \alpha}$ with angle of attack which seem to be generally less variant than those of the 3- and 4.5-percent-chord-thick wings.

Wake Characteristics

Figures 17 and 18 present some effects of wing sweep and thickness for Mach numbers of 0.90 and 1.05 on the wing wake characteristics throughout the angle-of-attack range investigated. At the lower angles of attack (from zero to approximately 10°), the maximum total-pressure decay may not be sufficiently defined due to the pressure probe spacing on the bump; however, a brief quantitative type analysis of the profiles at higher angles of attack can be made. Figures 17 and 18 indicate a general displacement in wake center toward the wing chord plane extended, at moderate and high angles of attack, with an increase in Mach number from 0.90 to 1.05 for all conditions of sweep and thickness. However, for a given Mach number, an increase in angle of attack is generally accompanied by an upward displacement of the wake above the wing chord plane extended, and by an increase in thickness of the wake. The increment of wake displacement toward the wing chord plane due to increasing Mach number is of the same order of magnitude for all conditions of sweep and thickness. Although the losses in wake dynamic pressure were reduced, there was a general thickening of the wake in going to supersonic speeds which probably was a result of wing boundary-layer separation and shock waves emanating from the wing such as has been pointed out in reference 4. The losses in wake dynamic pressure at supersonic speeds were reduced considerably when the wing thickness was decreased (fig. 18).

CONCLUSIONS

Results of an investigation, by the transonic-bump technique, of the downwash and wake characterics (measured at one spanwise station and for a given wing at only one longitudinal station) of a series of highly tapered, aspect-ratio-3 wings with varying degrees of sweep and thickness indicate the following conclusions:

1. Increases in sweep provided a decrease in $\left(\frac{\partial \epsilon}{\partial \alpha}\right)_{\alpha=0^\circ}$ for all Mach numbers and less variation with Mach number at all distances from the wing chord plane extended. Maximum values of $\left(\frac{\partial \epsilon}{\partial \alpha}\right)_{\alpha=0^\circ}$ were reached near the wing chord plane for all wing sweeps.

2. Above the wing chord plane, $\frac{\partial \epsilon}{\partial \alpha}$ increased to maximum values exceeding unity with an increase in angle of attack for all wing sweep angles and thicknesses.

3. For a quarter-chord sweep angle of 14.03°, a decrease in wing thickness from $t/c = 0.045$ to $t/c = 0.02$ produced increases in $\left(\frac{\partial \epsilon}{\partial \alpha}\right)_{\alpha=0^\circ}$ up to a Mach number of about 1.09 at any distance from the wing chord plane extended.

4. Regardless of wing sweep or thickness, increasing speed from subsonic to supersonic caused the wake center to be displaced toward the wing chord plane, and although the losses in wake dynamic pressure were reduced, there was a general thickening of the wake in going to supersonic speeds.

Langley Aeronautical Laboratory,
National Advisory Committee for Aeronautics,
Langley Field, Va., October 21, 1955.

REFERENCES

1. Few, Albert G., Jr., and Fournier, Paul G.: Effects of Sweep and Thickness on the Static Longitudinal Aerodynamic Characteristics of a Series of Thin, Low-Aspect-Ratio, Highly Tapered Wings at Transonic Speeds - Transonic-Bump Method. NACA RM L54B25, 1954.

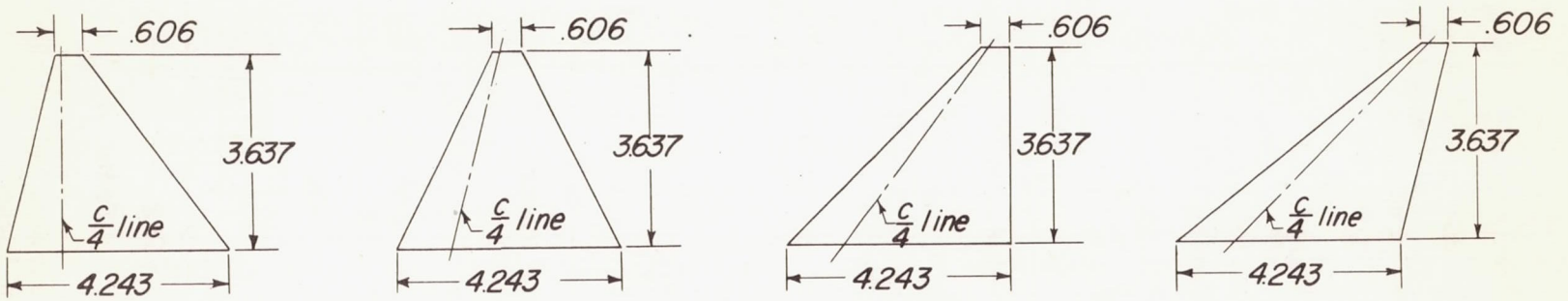
2. Weil, Joseph, Campbell, George S., and Diederich, Margaret S.: An Analysis of Estimated and Experimental Transonic Downwash Characteristics As Affected by Plan Form and Thickness for Wings and Wing-Fuselage Configurations. NACA RM L52I22, 1952.

3. Axelson, John A.: Downwash Behind a Triangular Wing of Aspect Ratio 3 - Transonic Bump Method. NACA RM A53I23, 1953.

4. Walker, Harold J., and Stivers, Louis S., Jr.: Investigation of the Downwash and Wake Behind a Triangular Wing of Aspect Ratio 4 at Subsonic and Supersonic Mach Numbers. NACA RM A50I14a, 1950.

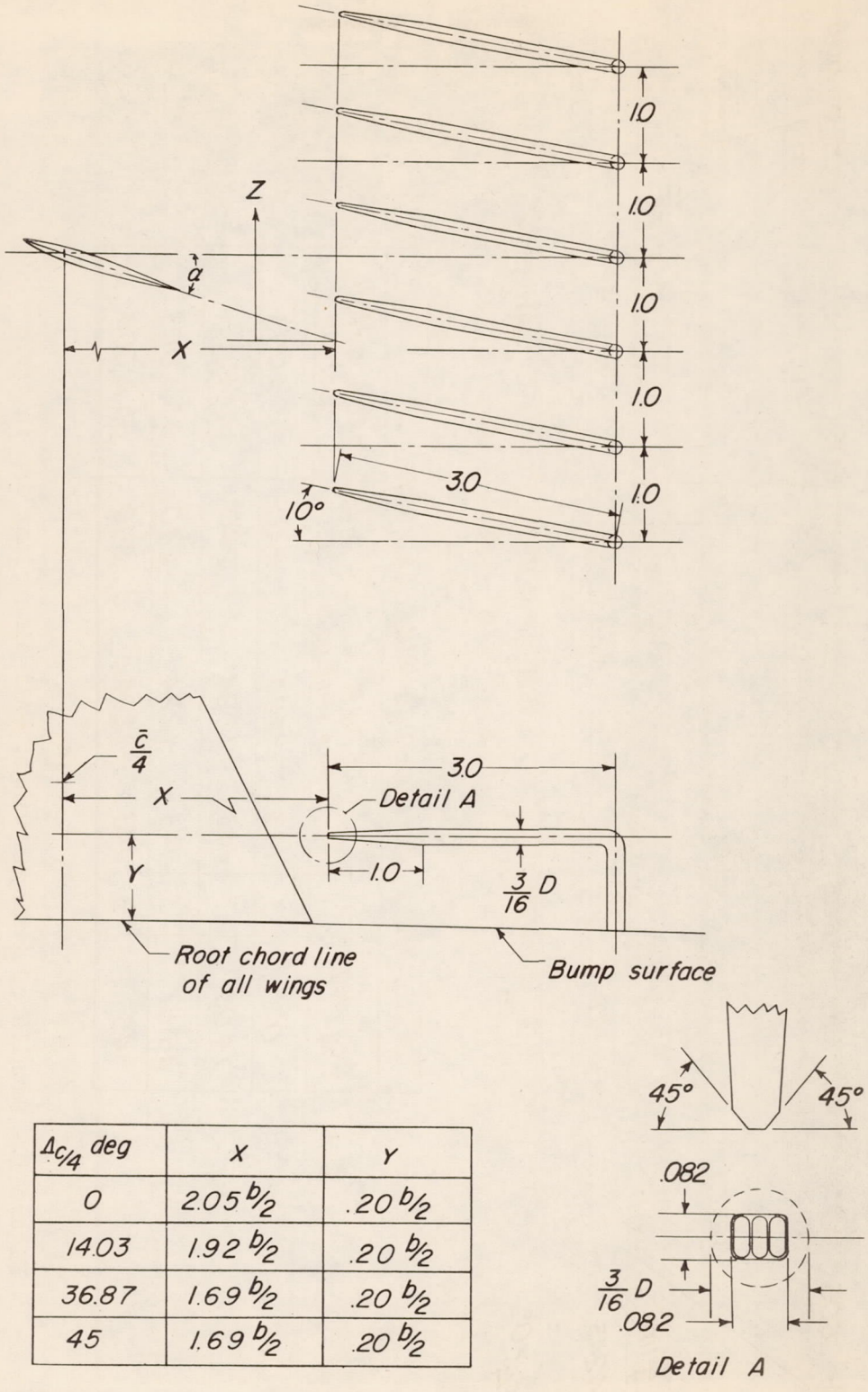
5. Boatright, William B.: An Analysis of Pressure Studies and Experimental and Theoretical Downwash and Sidewash Behind Five Pointed-Tip Wings at Supersonic Speeds. NACA RM L54B10, 1954.

6. DeYoung, John, and Barling, Walter H., Jr.: Prediction of Downwash Behind Swept-Wing Airplanes at Subsonic Speed. NACA TN 3346, 1955.



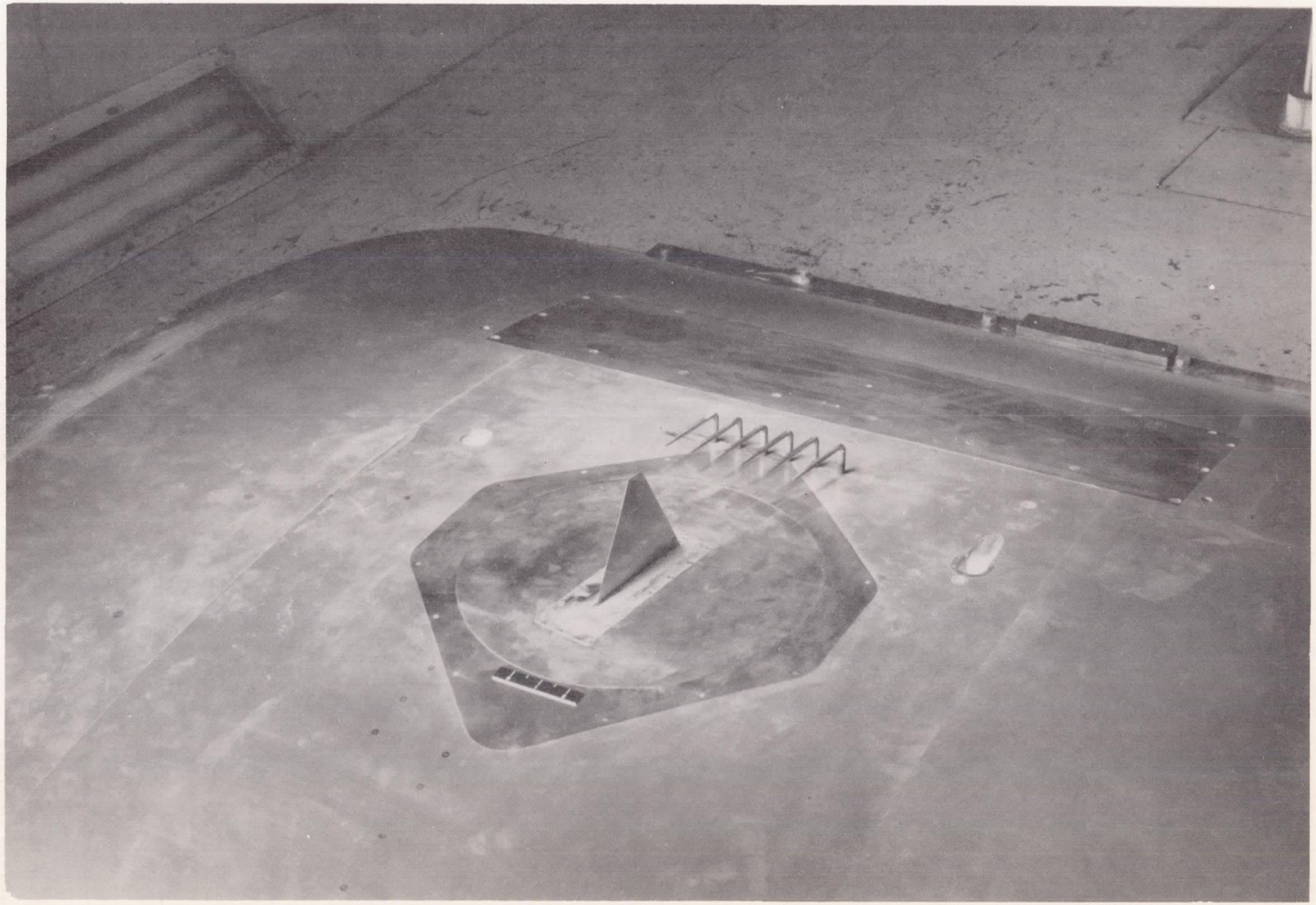
Physical characteristics of wings					
$\Lambda_{c/4}$, deg	A	λ	S, sq ft (twice semispan)	$\bar{c}$, ft	NACA airfoil section
0	3	.143	.1224	.240	65A003
14.03	3	.143	.1224	.240	65A002 65A003 65A004.5
36.87	3	.143	.1224	.240	65A003
45	3	.143	.1224	.240	65A003

Figure 1.- Details of semispan wings. All dimensions are in inches.



$\Delta_{c/4}$ deg	X	Y
0	$2.05\ b/2$	$.20\ b/2$
14.03	$1.92\ b/2$	$.20\ b/2$
36.87	$1.69\ b/2$	$.20\ b/2$
45	$1.69\ b/2$	$.20\ b/2$

Figure 2.- Details of pressure probes used for surveys behind the semispan models. All dimensions are in inches.



L-76833

Figure 3.- Photograph of wing mounted on transonic bump in the Langley high-speed 7- by 10-foot tunnel.

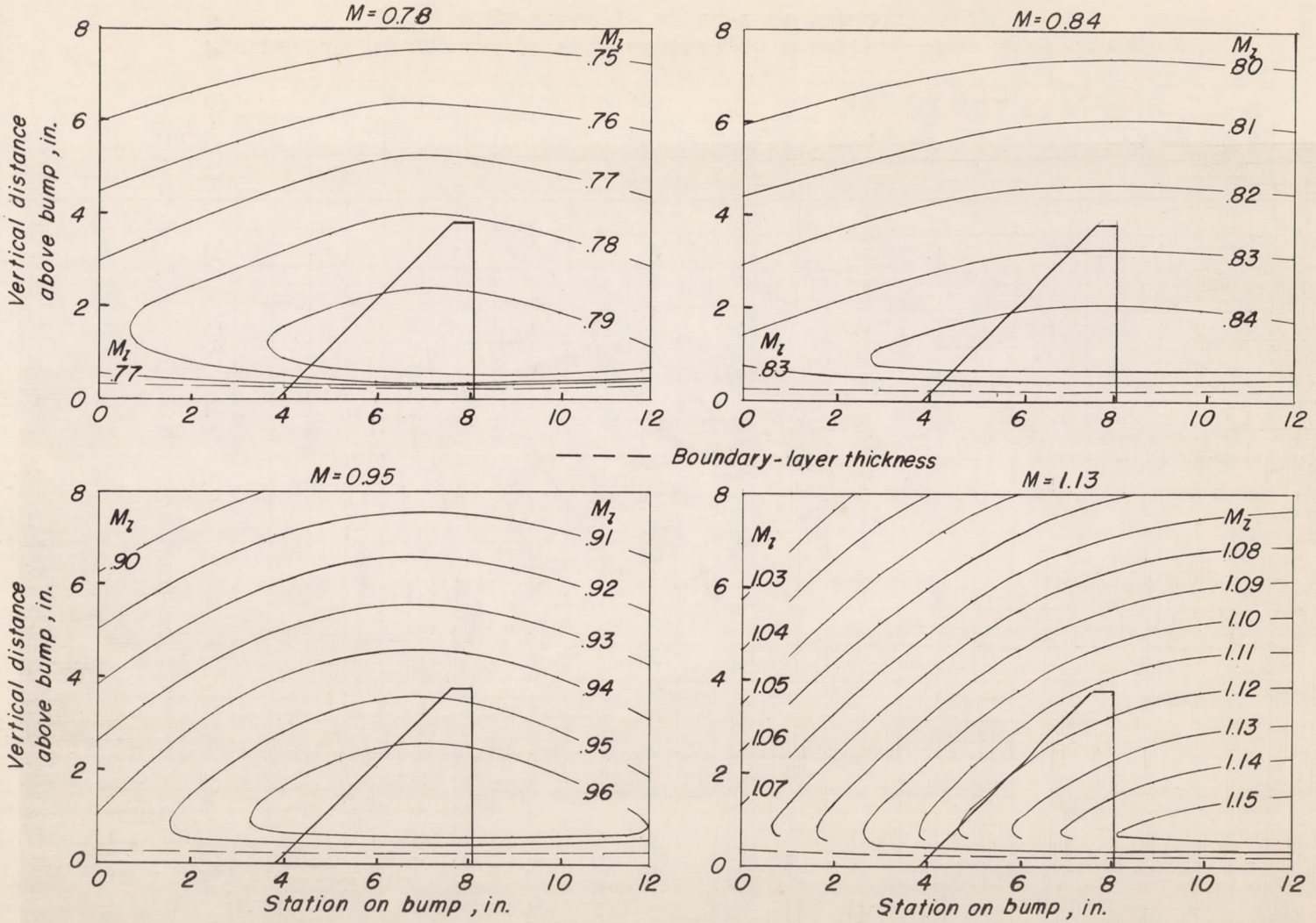
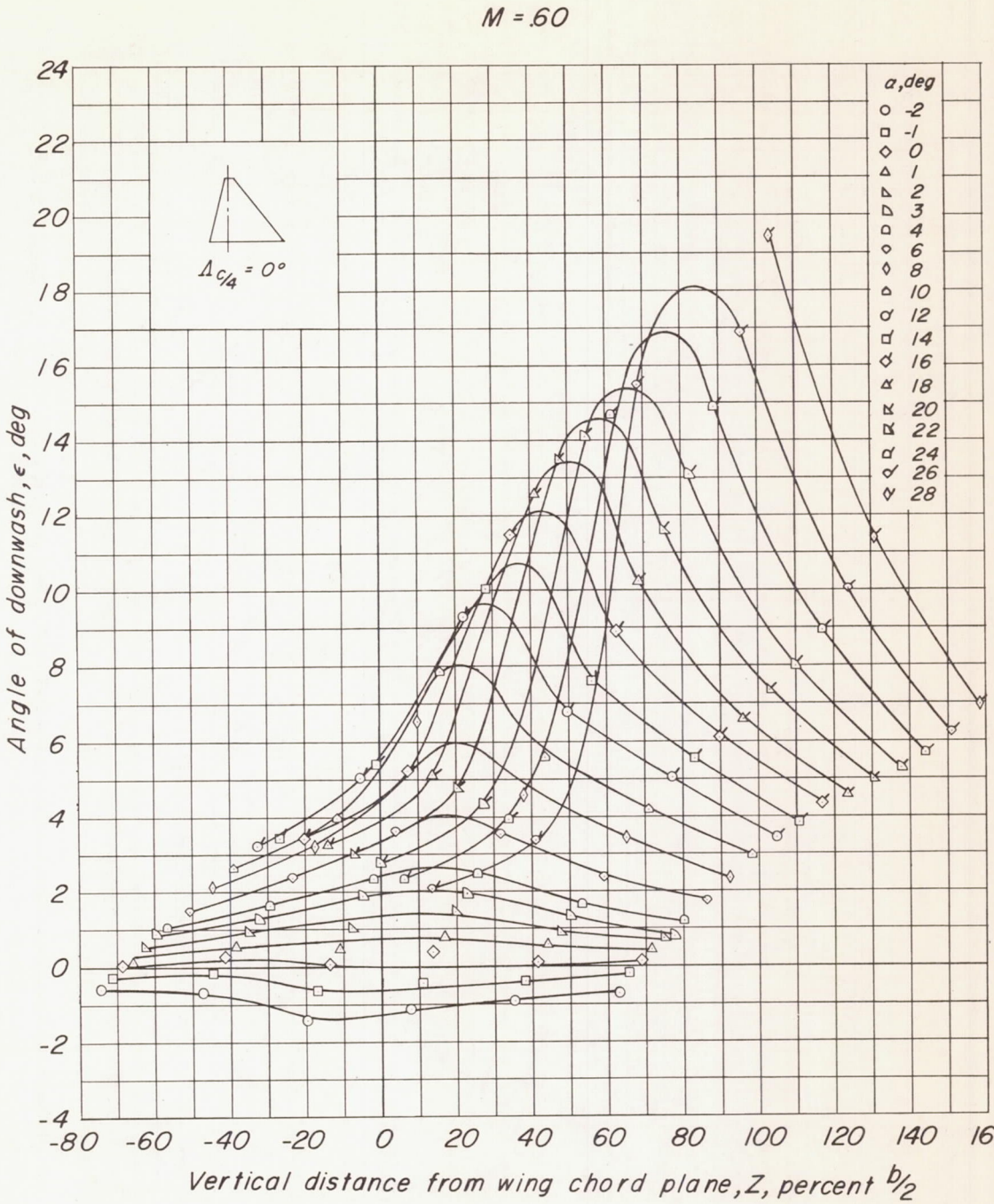
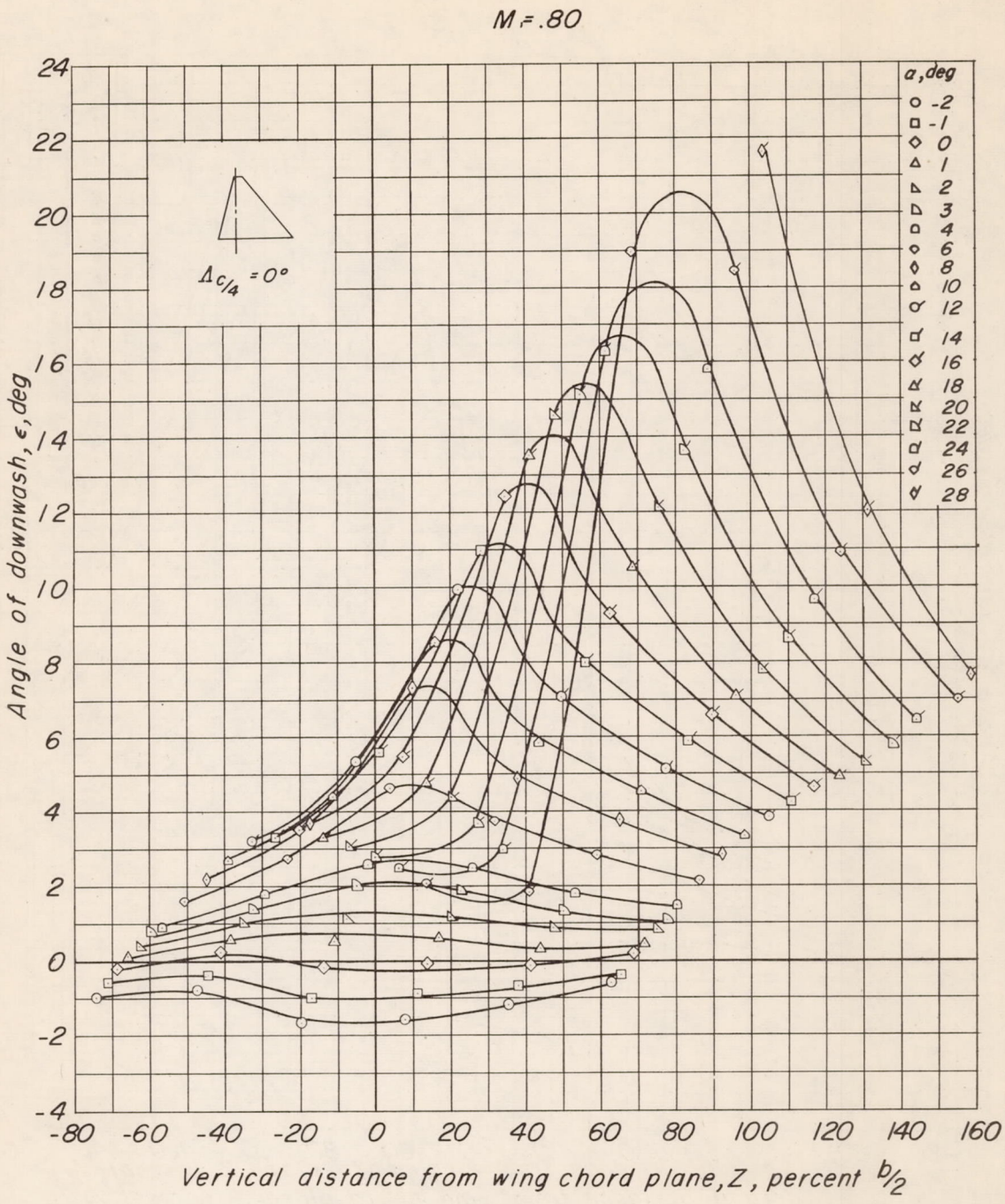


Figure 4.- Typical Mach number contours over transonic bump in region of model location.



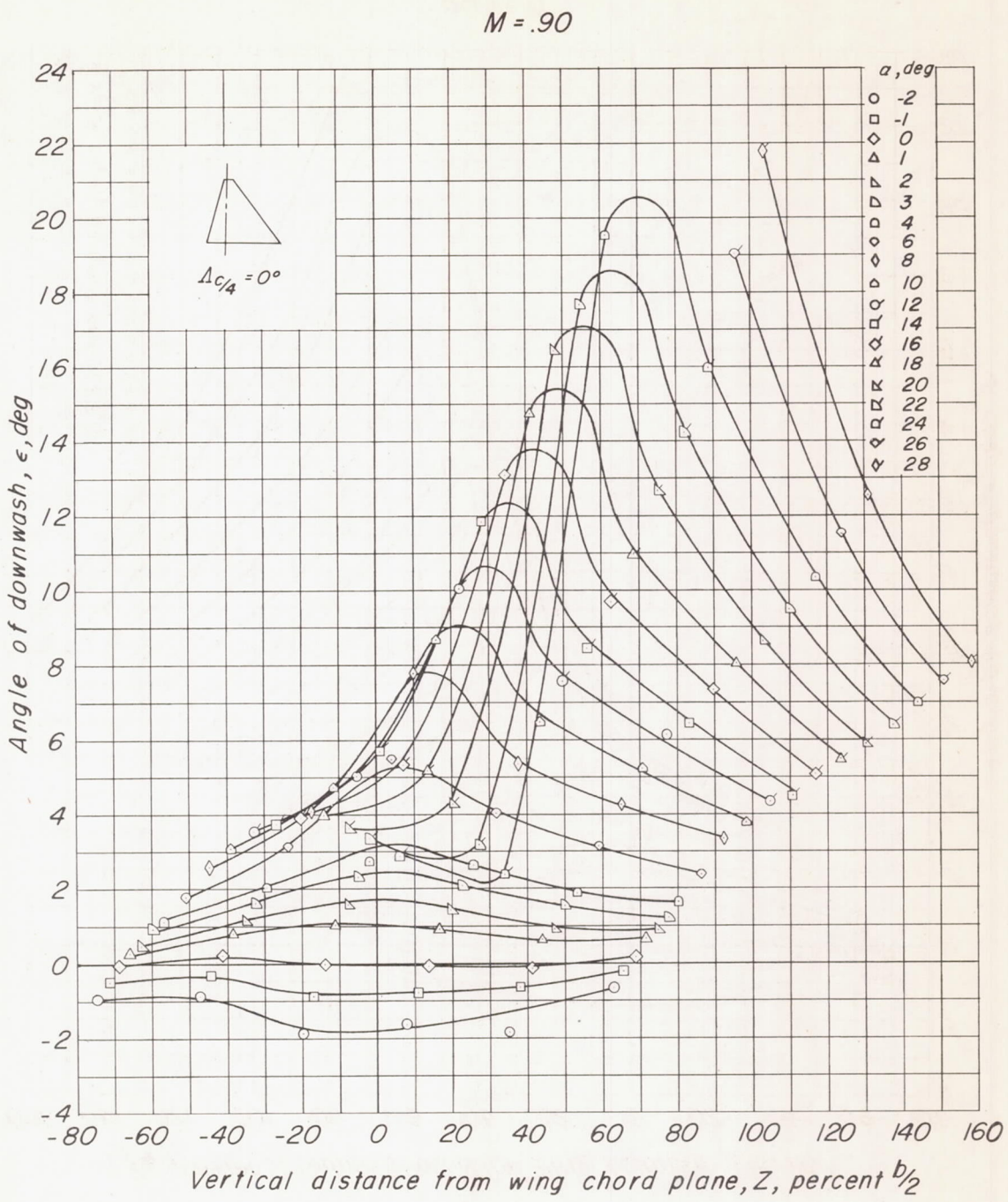
(a) M = 0.60.

Figure 5.- Effect of angle of attack on the variation of angle of downwash with vertical distance from the wing chord plane; Y = 0.20b/2; X = 2.05b/2; t/c = 0.03; $\Lambda_{c/4} = 0°$.



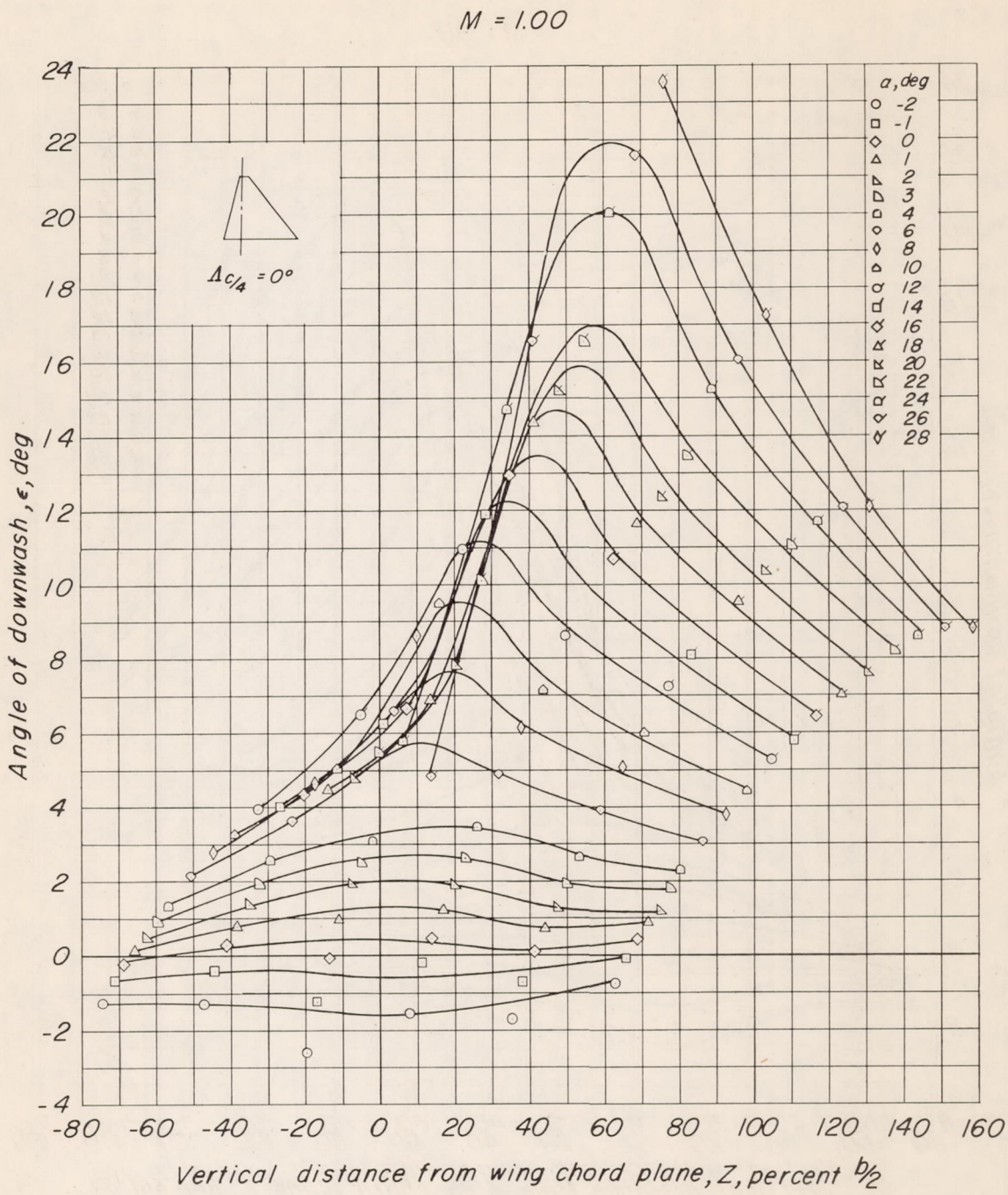
(b) M = 0.80.

Figure 5.- Continued.



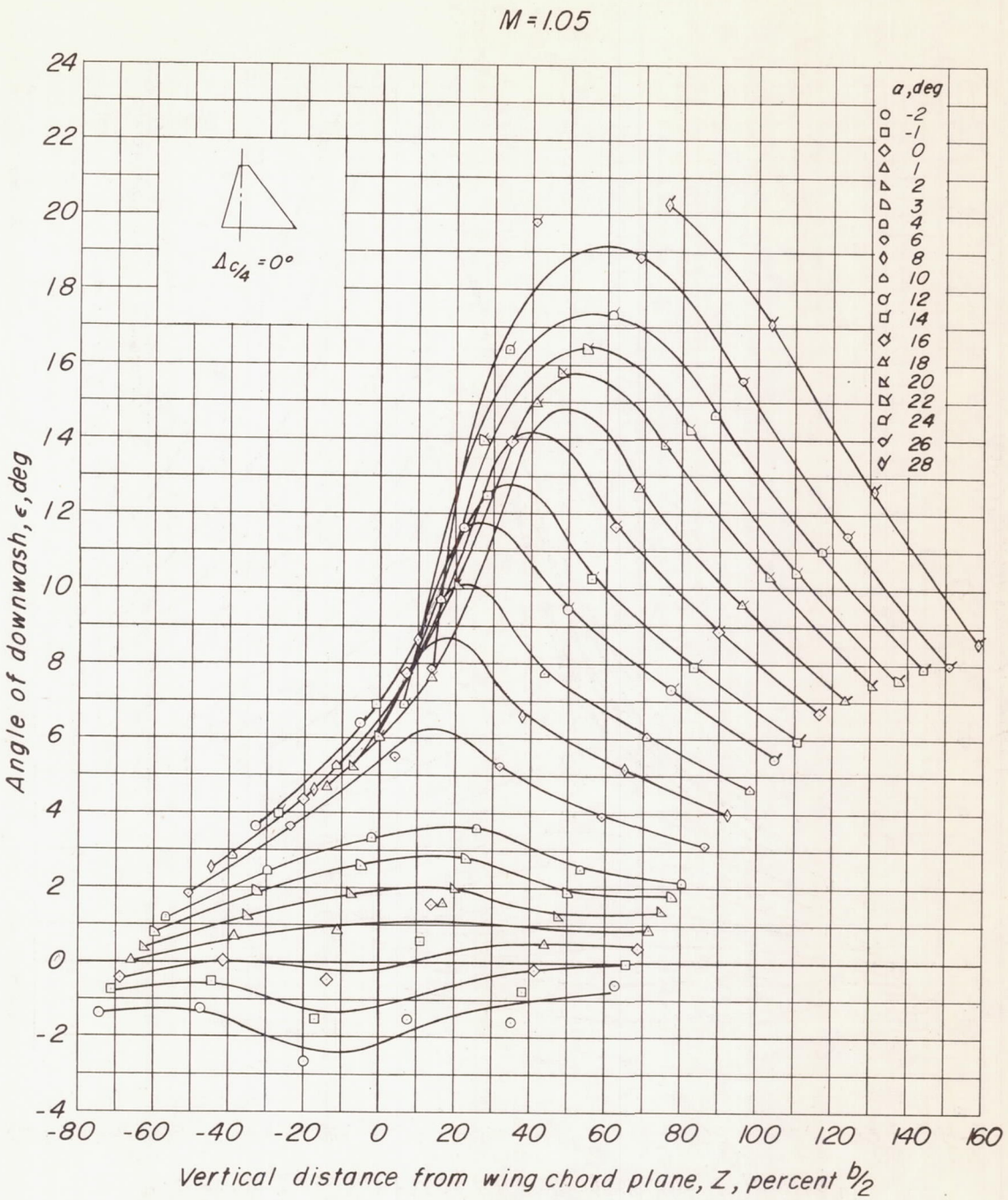
(c) M = 0.90.

Figure 5.- Continued.



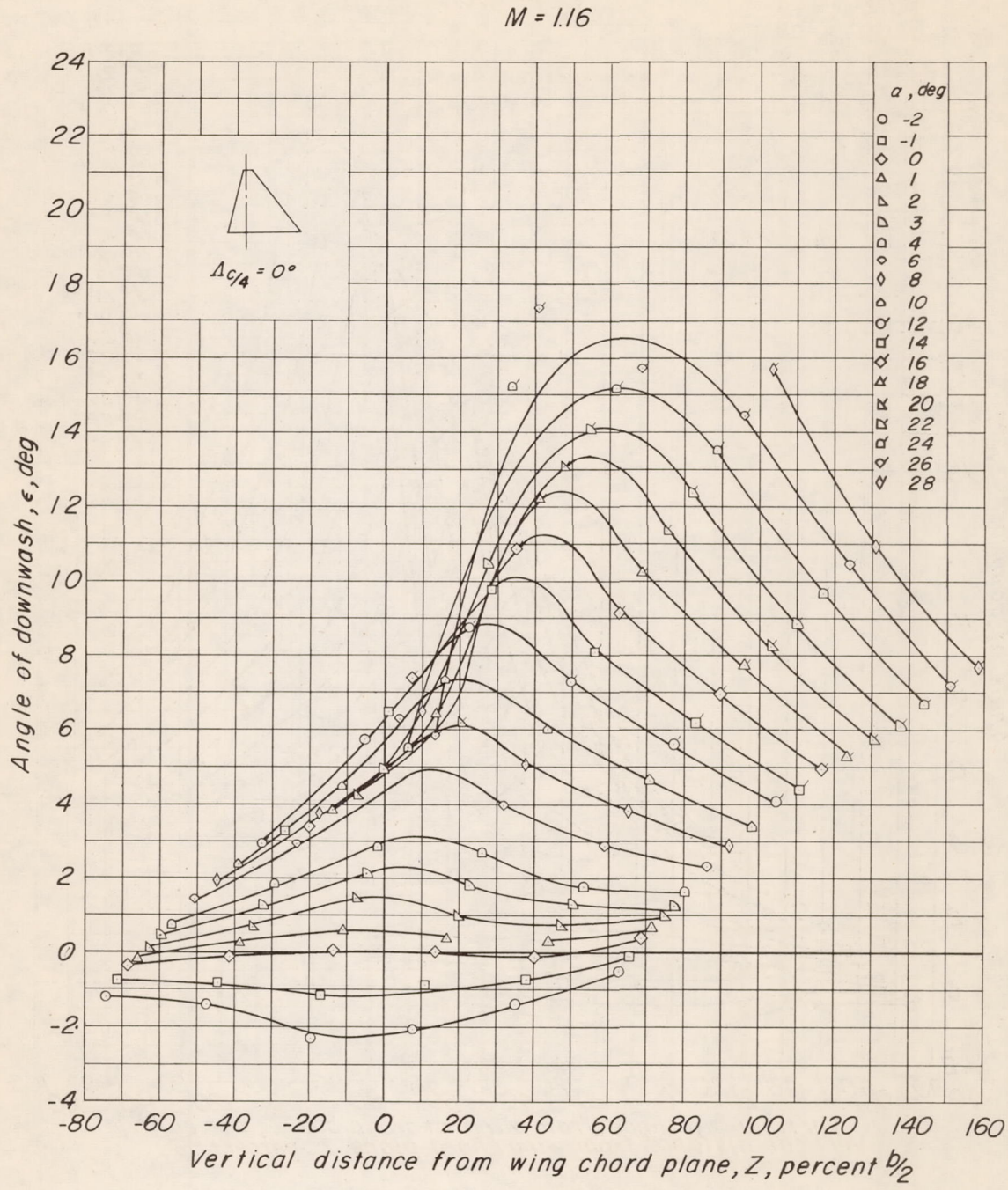
(d) M = 1.00.

Figure 5.- Continued.



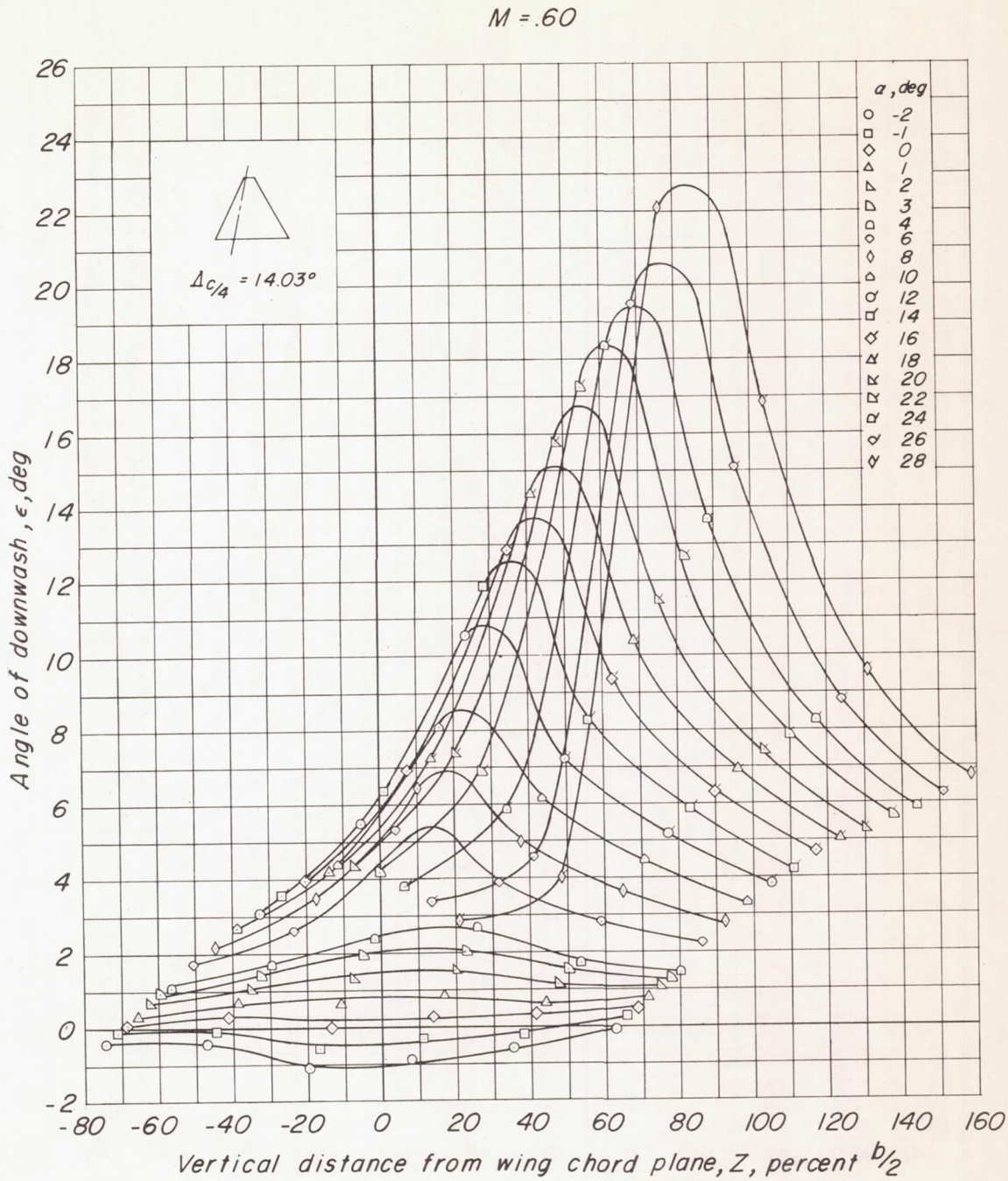
(e) M = 1.05.

Figure 5.- Continued.



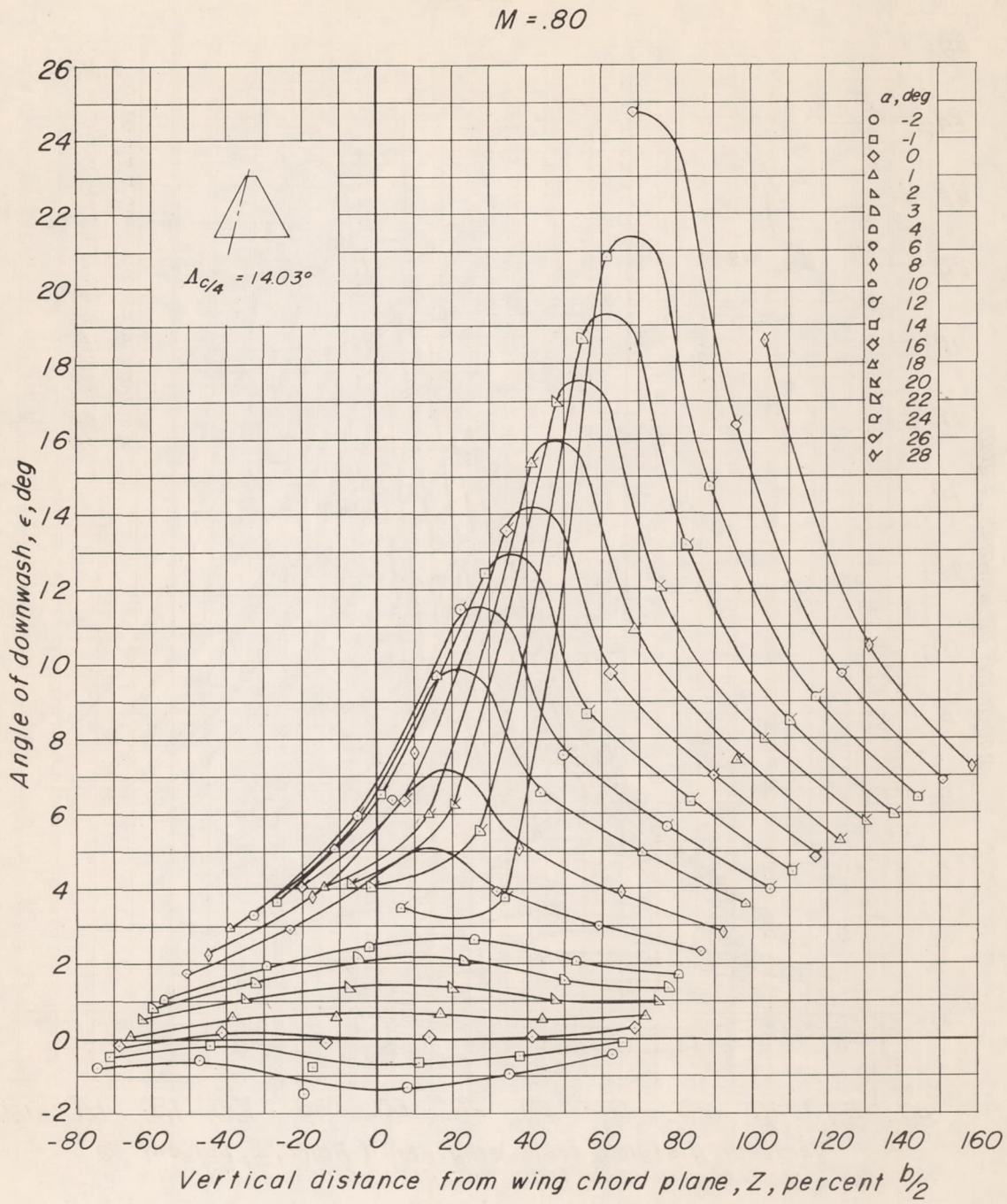
(f) M = 1.16.

Figure 5.- Concluded.



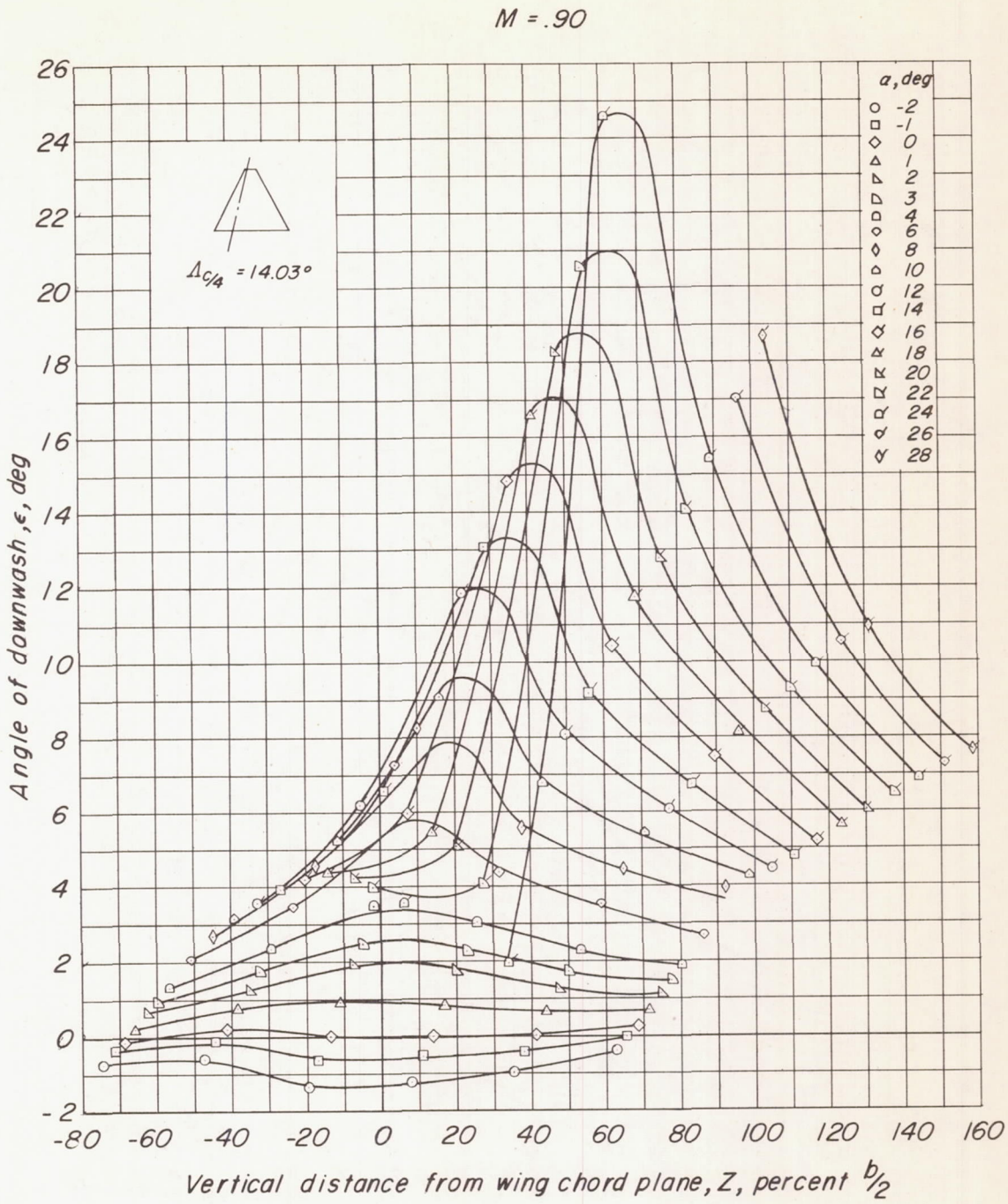
(a) M = 0.60.

Figure 6.- Effect of angle of attack on the variation of angle of downwash with vertical distance from the wing chord plane; Y = 0.20b/2; X = 1.92b/2; t/c = 0.03; $\Lambda_{c/4}$ = 14.03°.



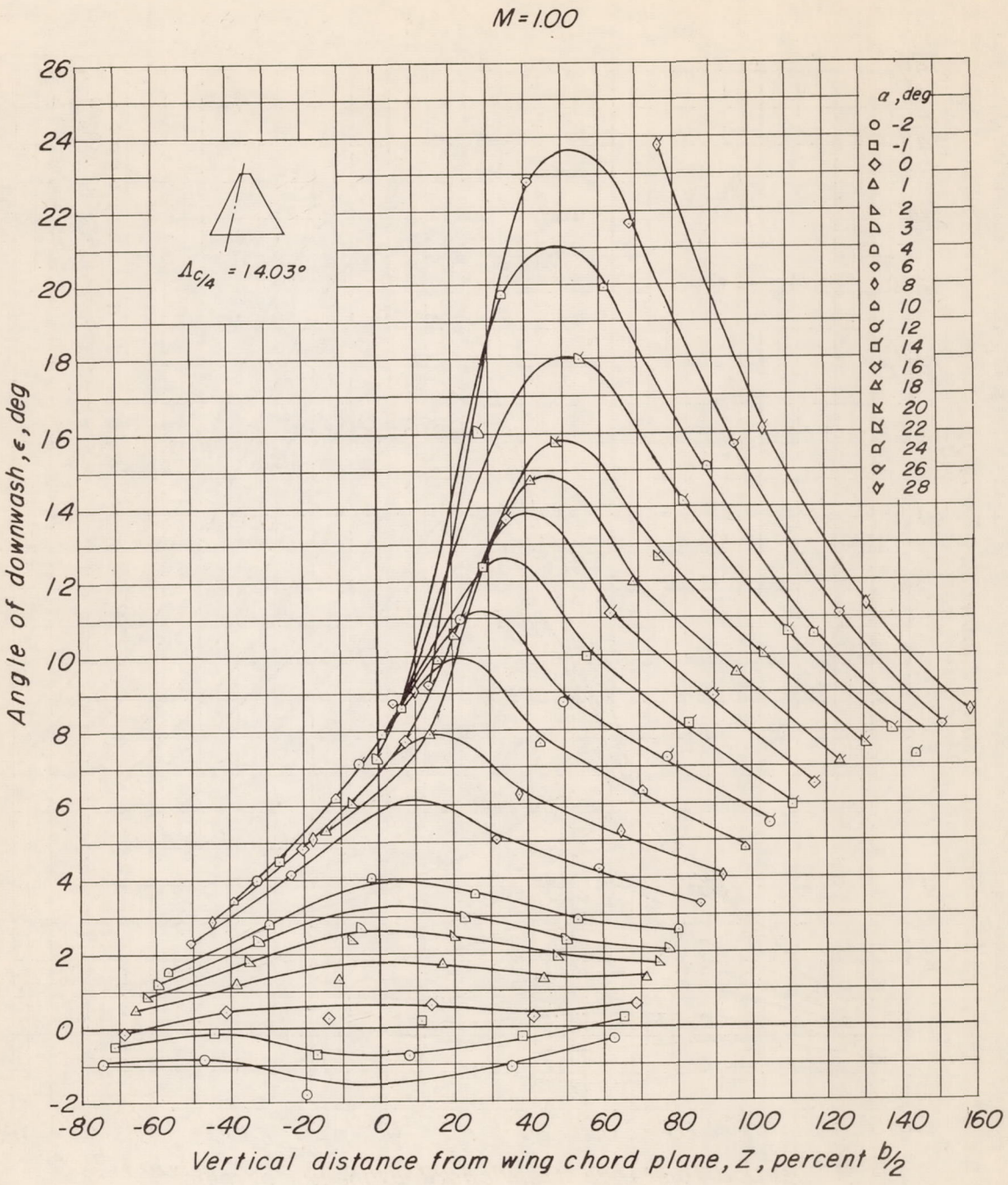
(b) M = 0.80.

Figure 6.- Continued.



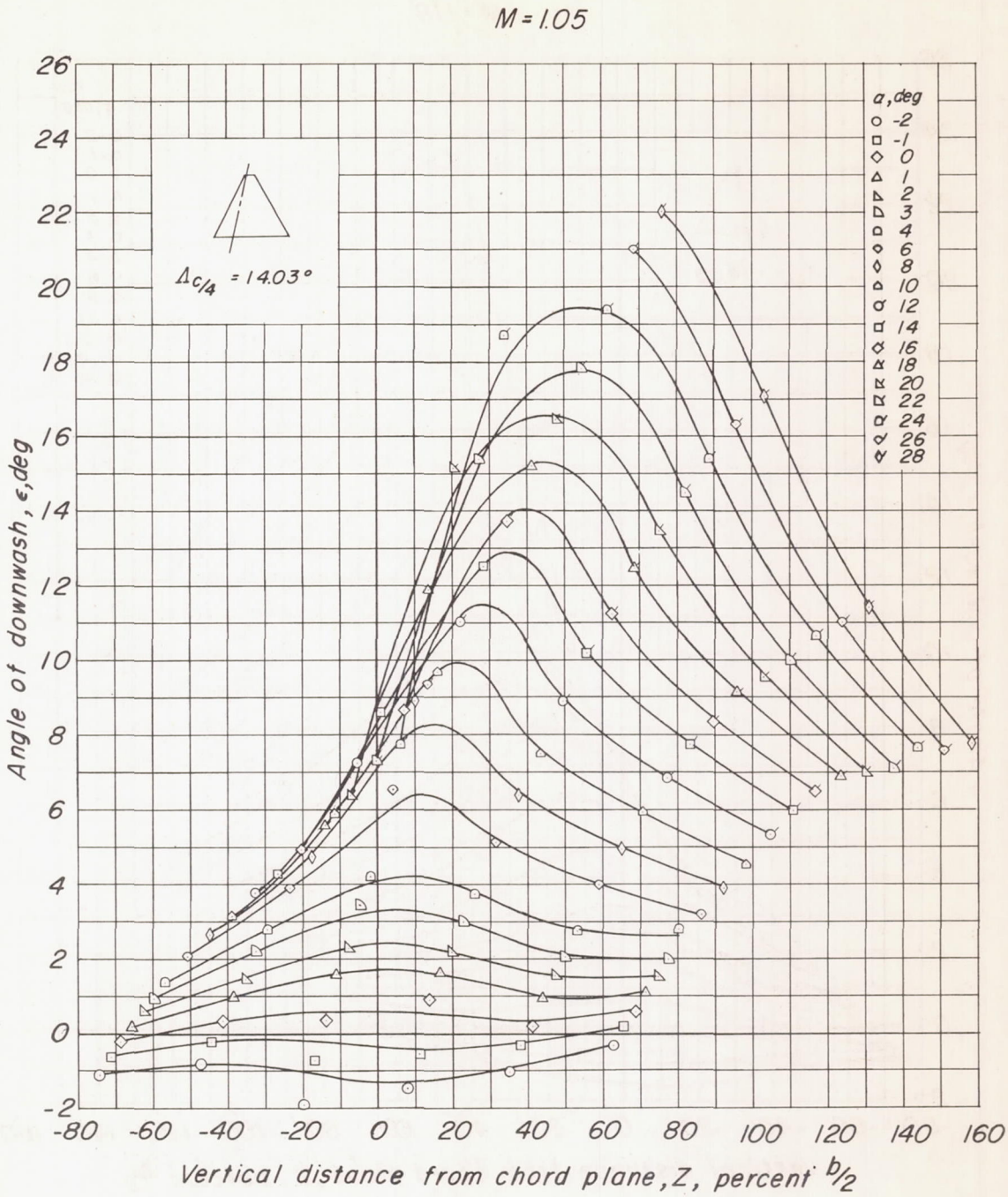
(c) M = 0.90.

Figure 6.- Continued.



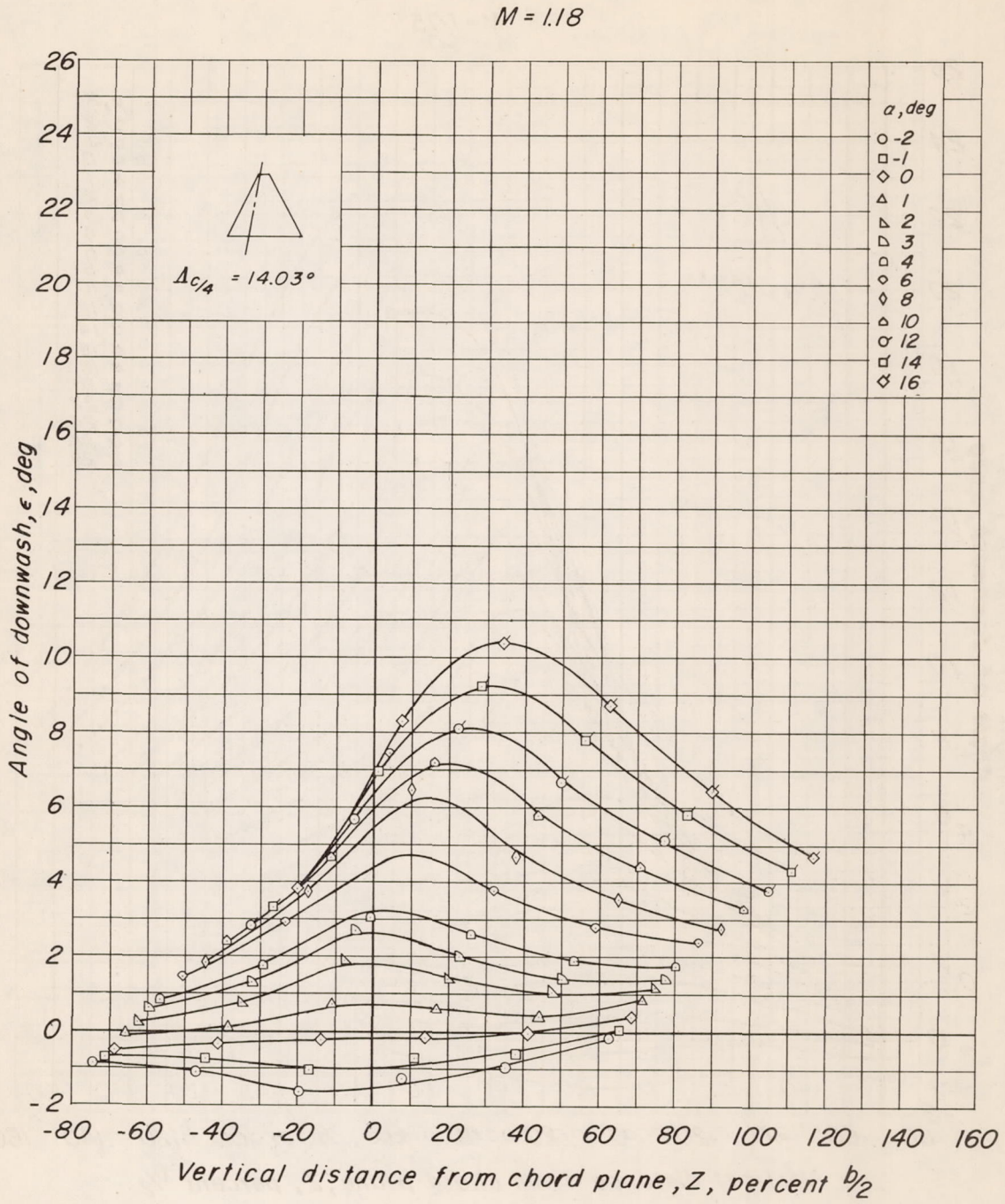
(d) M = 1.00.

Figure 6.- Continued.



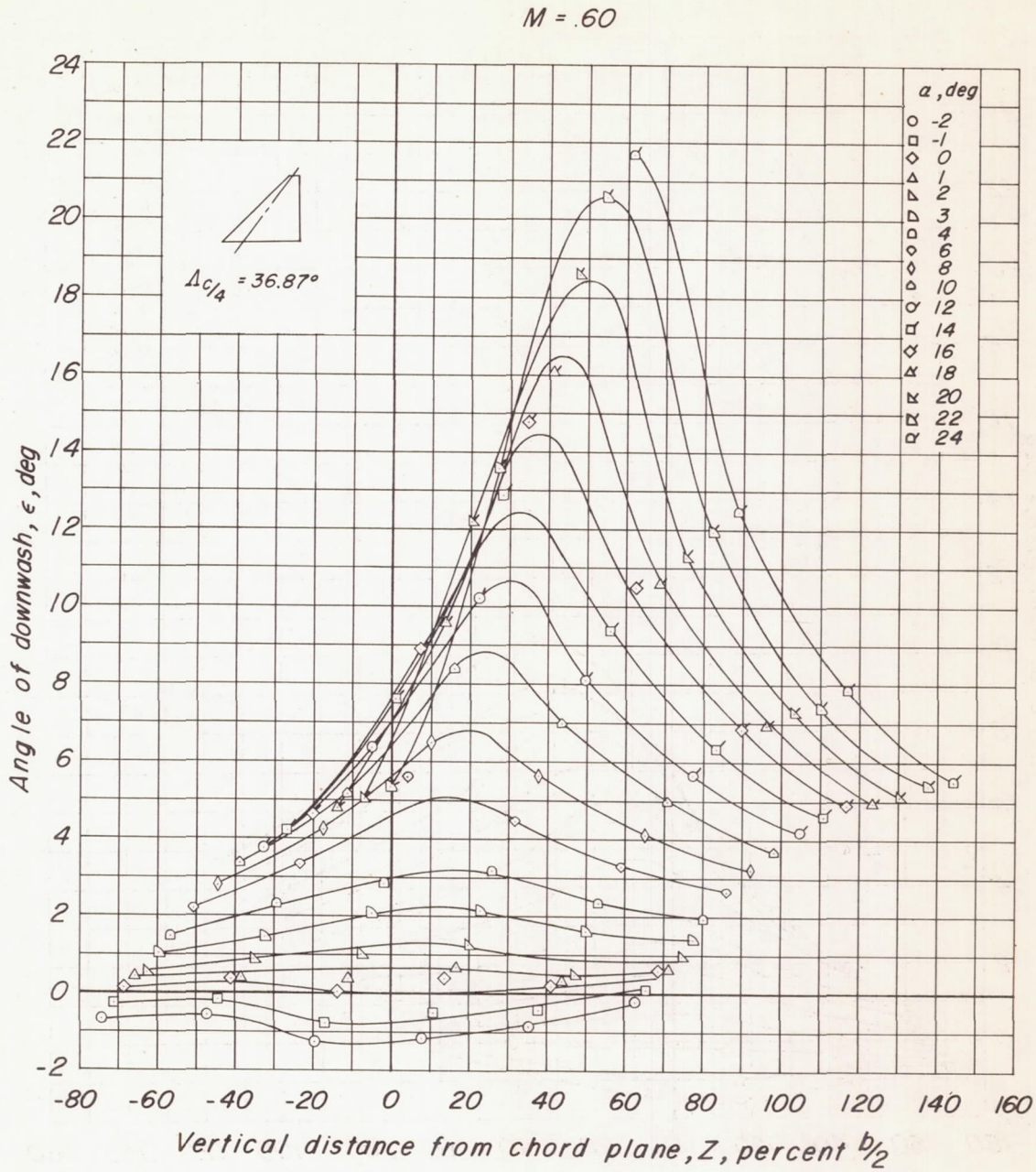
(e) M = 1.05.

Figure 6.- Continued.



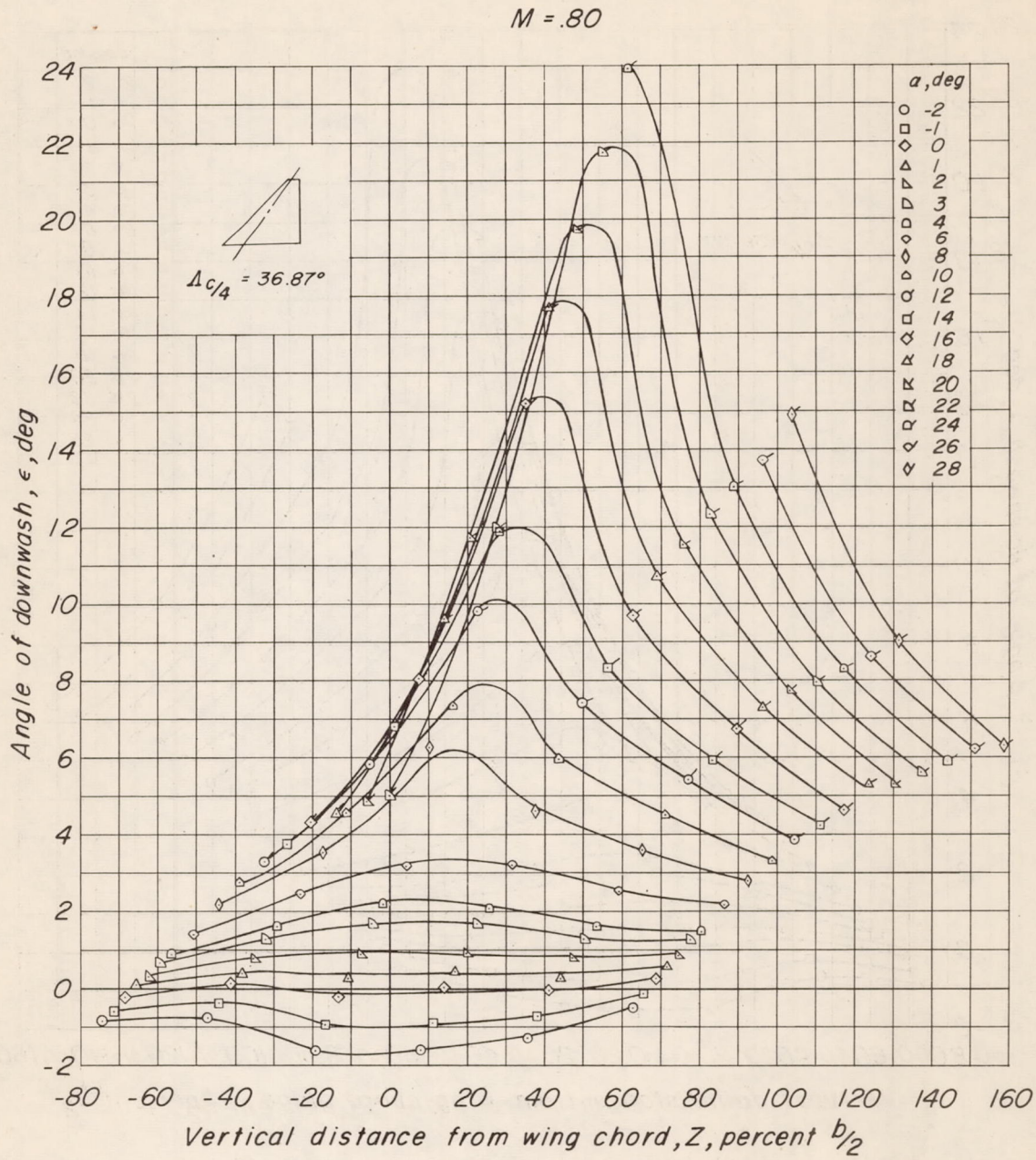
(f) M = 1.18.

Figure 6.- Concluded.



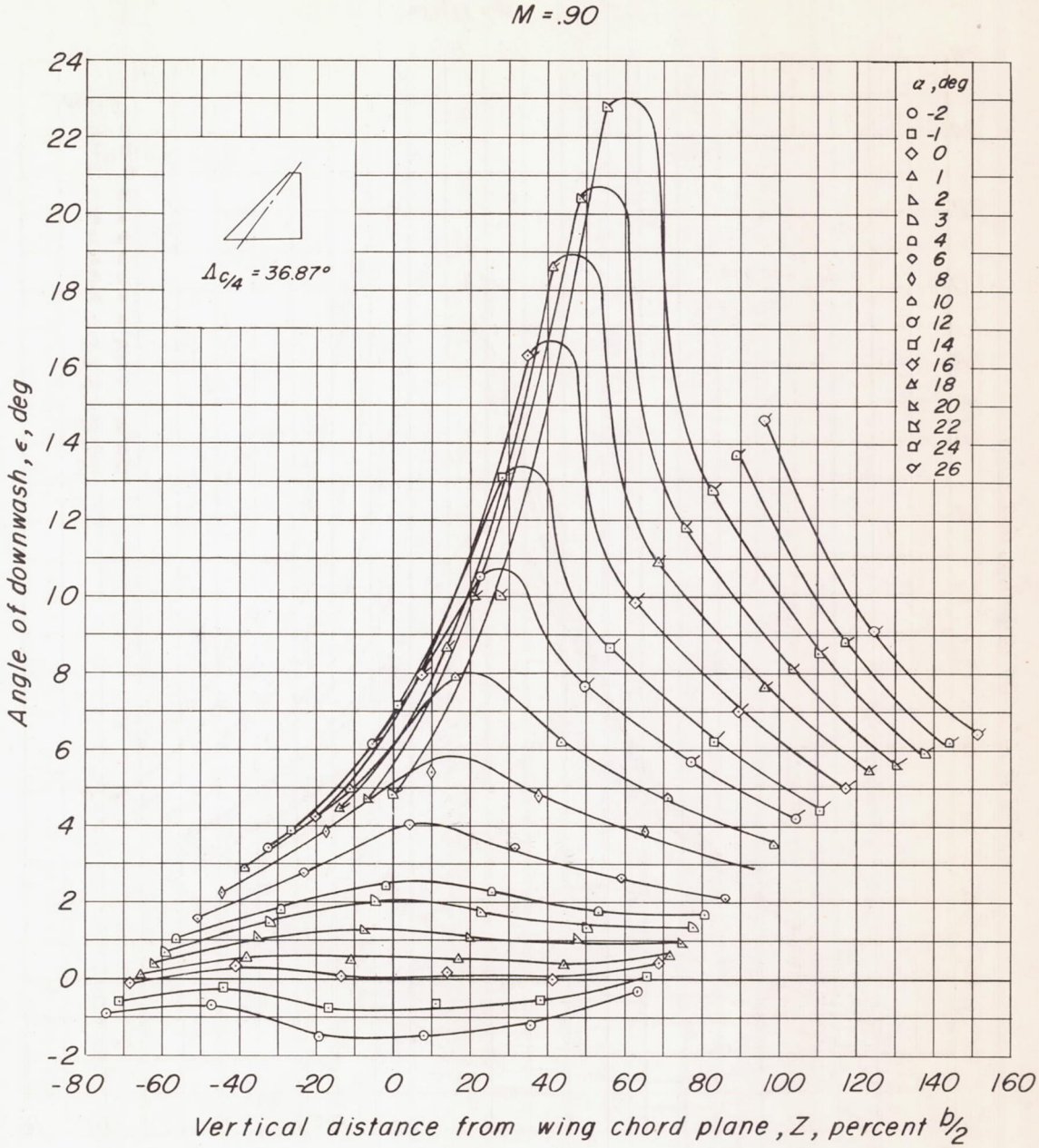
(a) M = 0.60.

Figure 7.- Effect of angle of attack on the variation of angle of downwash with vertical distance from the wing chord plane; Y = 0.20b/2; X = 1.69b/2; t/c = 0.03; $\Lambda_{c/4}$ = 36.87°.



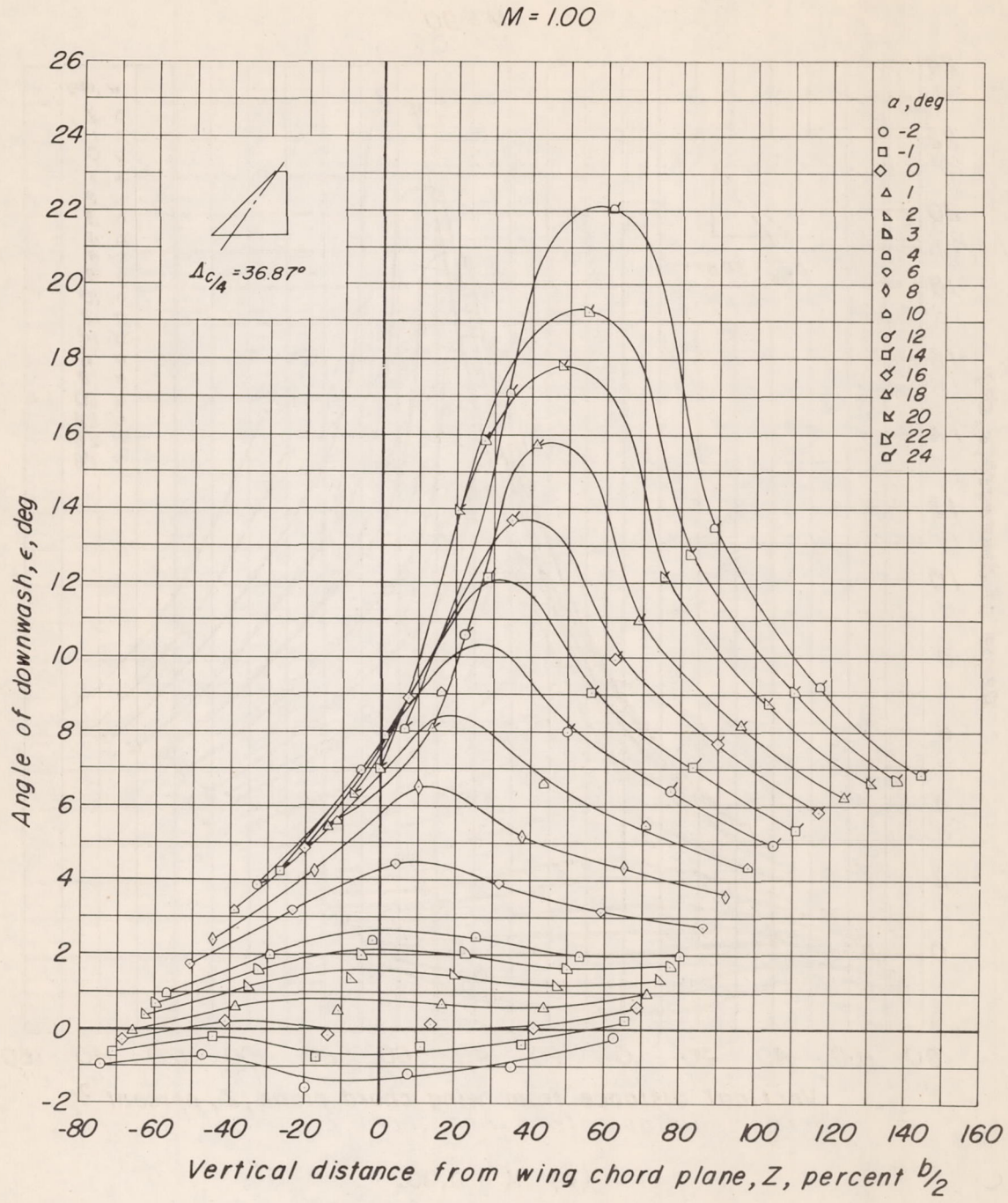
(b) M = 0.80.

Figure 7.- Continued.



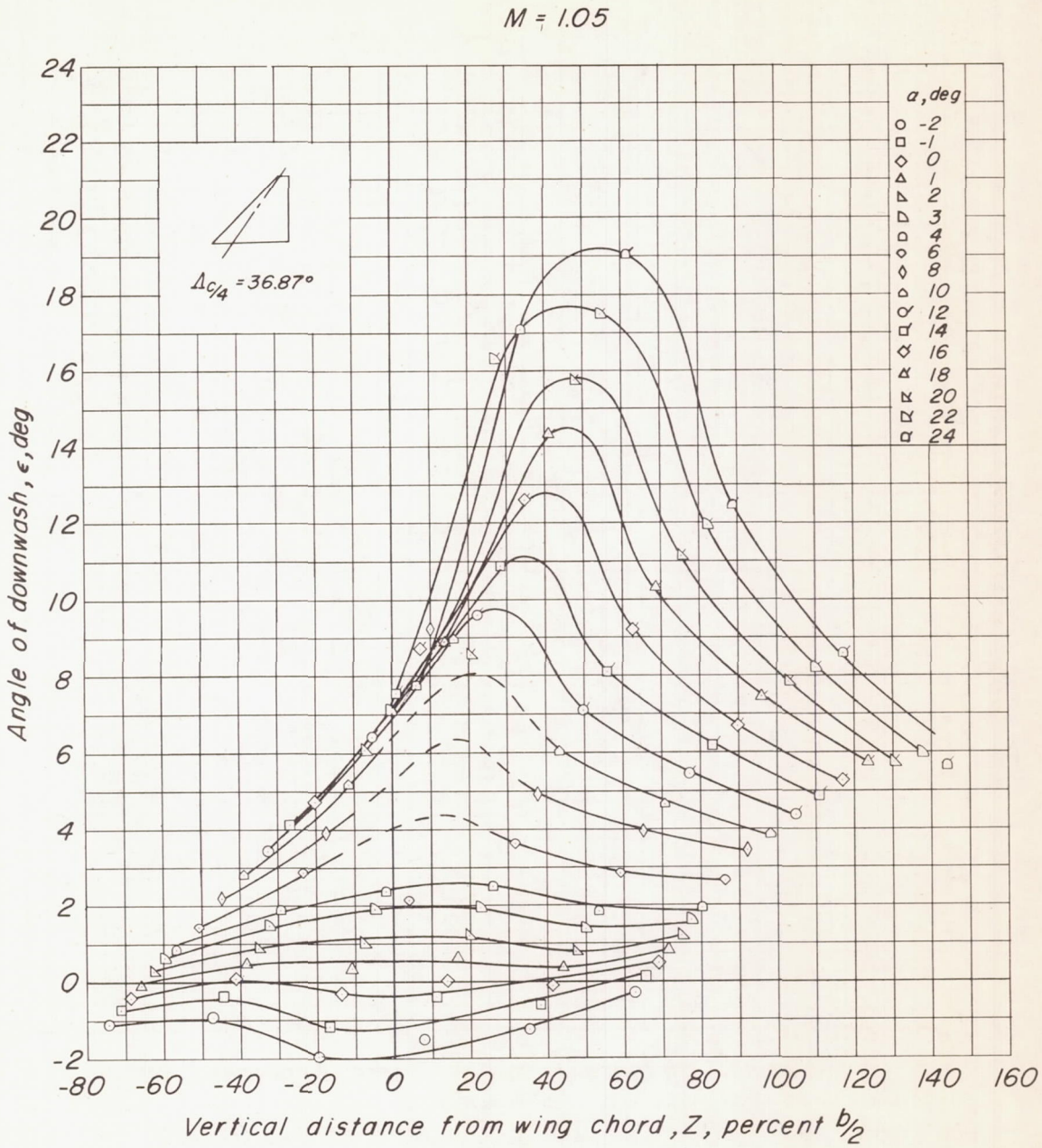
(c) M = 0.90.

Figure 7.- Continued.



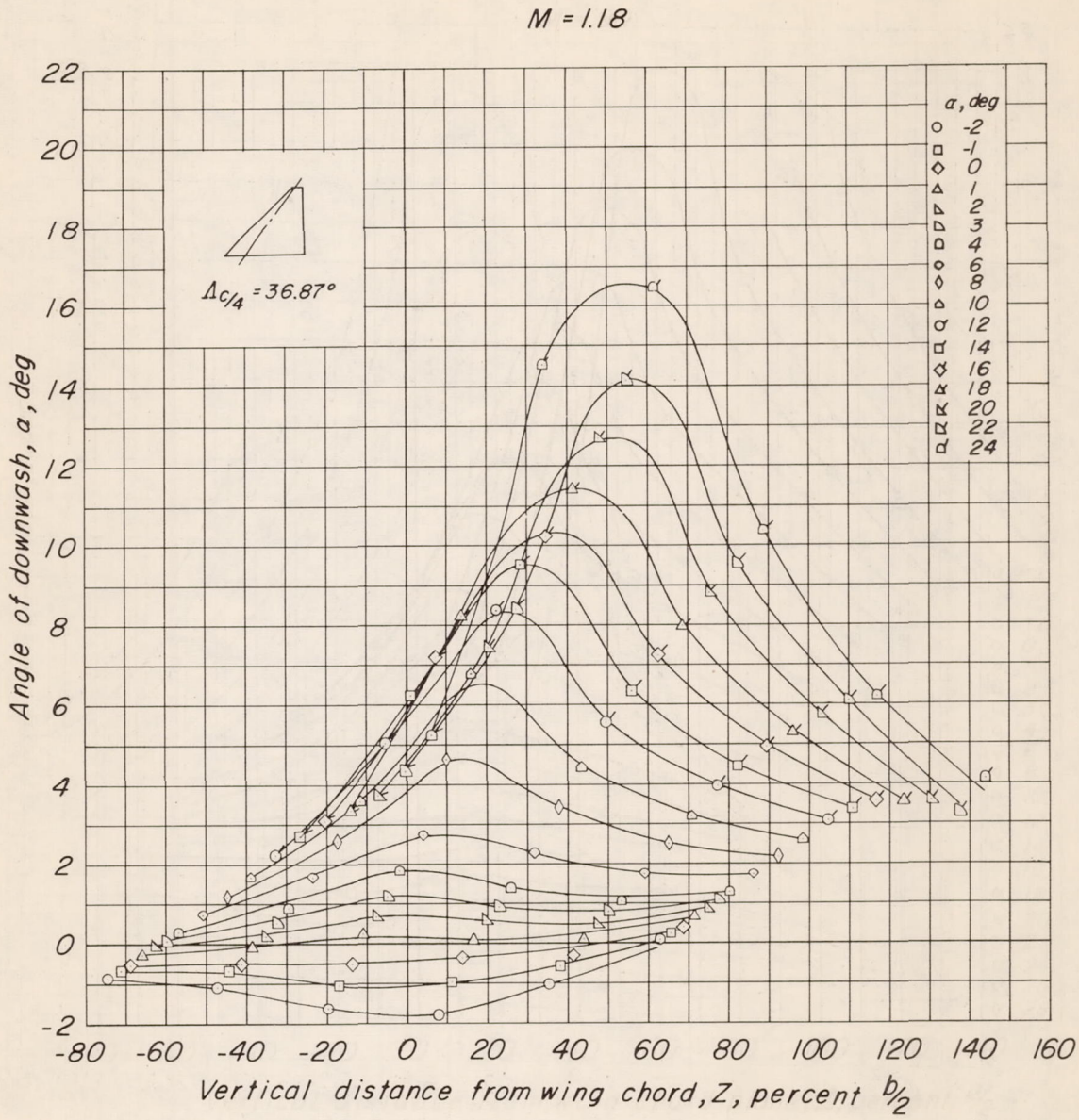
(d) M = 1.00.

Figure 7.- Continued.



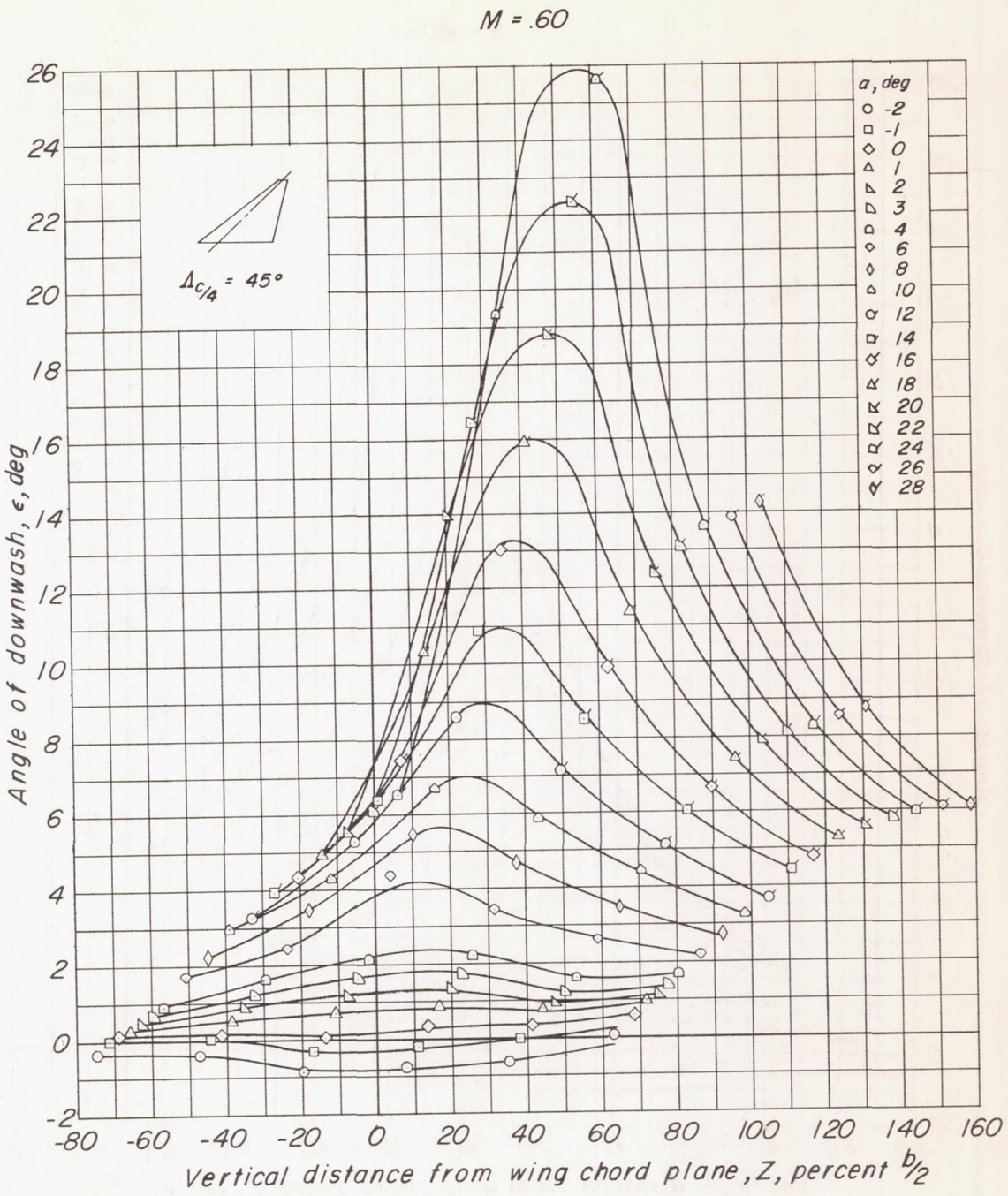
(e) M = 1.05.

Figure 7.- Continued.



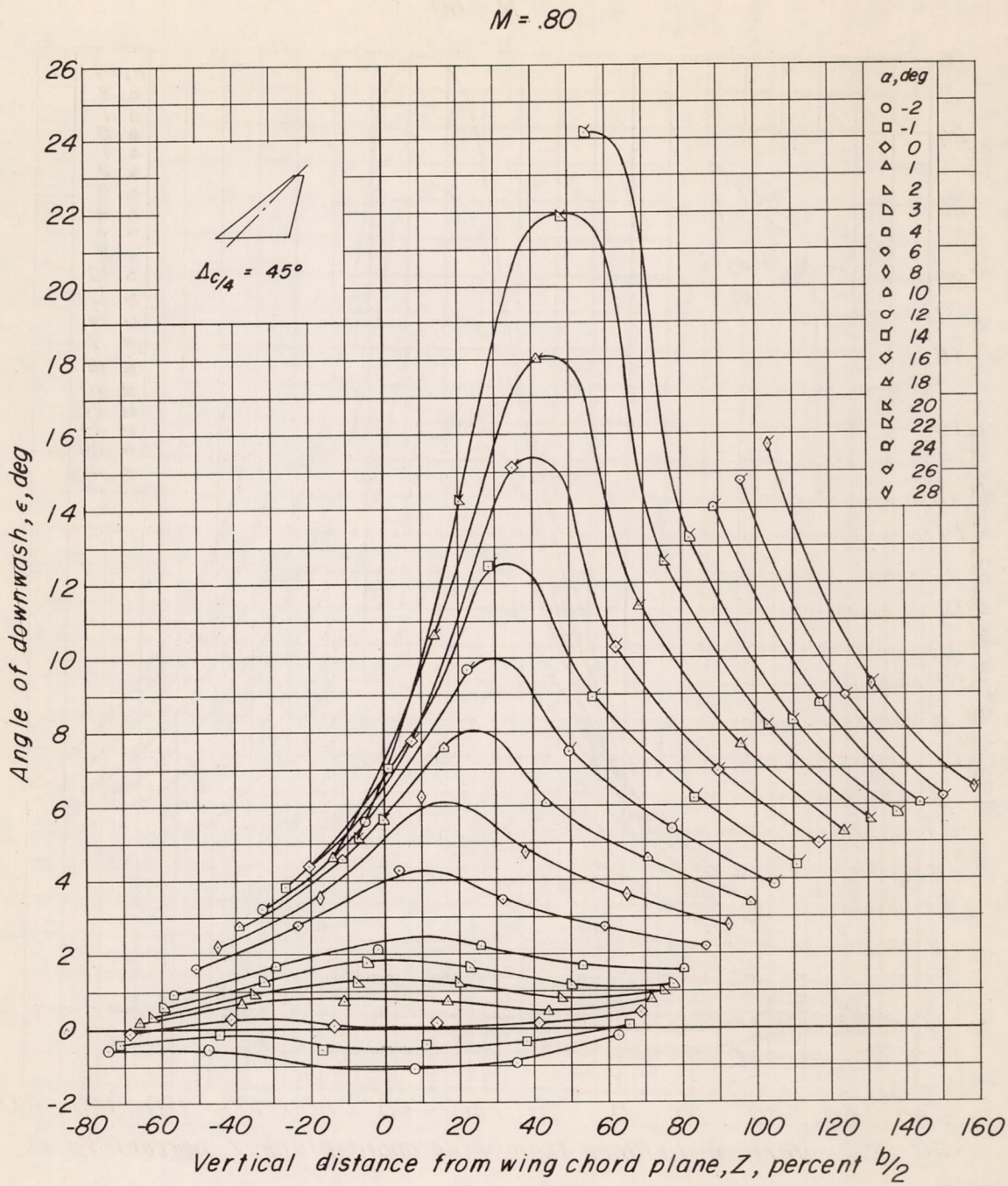
(f) M = 1.18.

Figure 7.- Concluded.



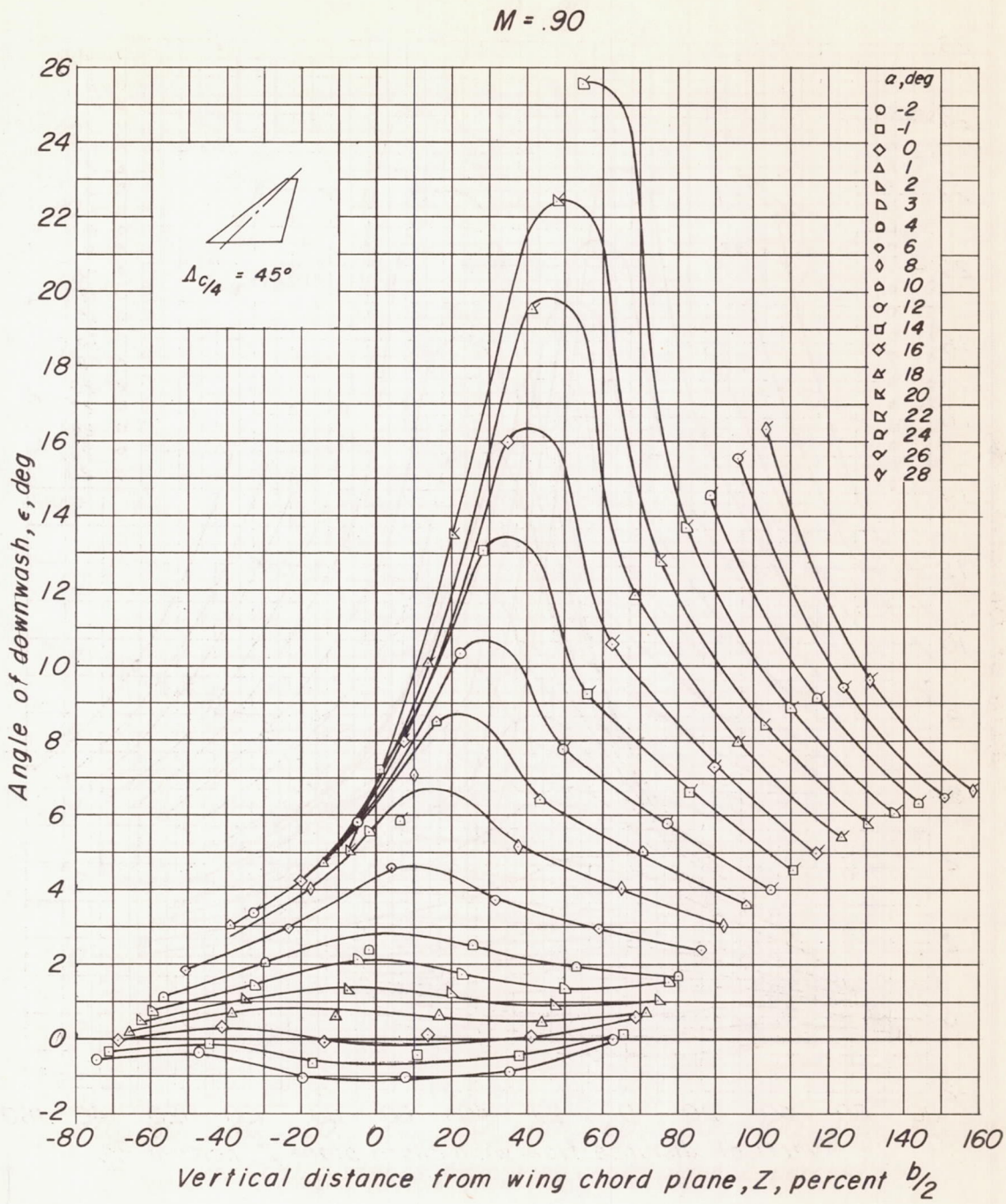
(a) M = 0.60.

Figure 8.- Effect of angle of attack on the variation of angle of downwash with vertical distance from the wing chord plane; Y = 0.20b/2; X = 1.69b/2; t/c = 0.03; $\Lambda_{c/4} = 45^{\circ}$.



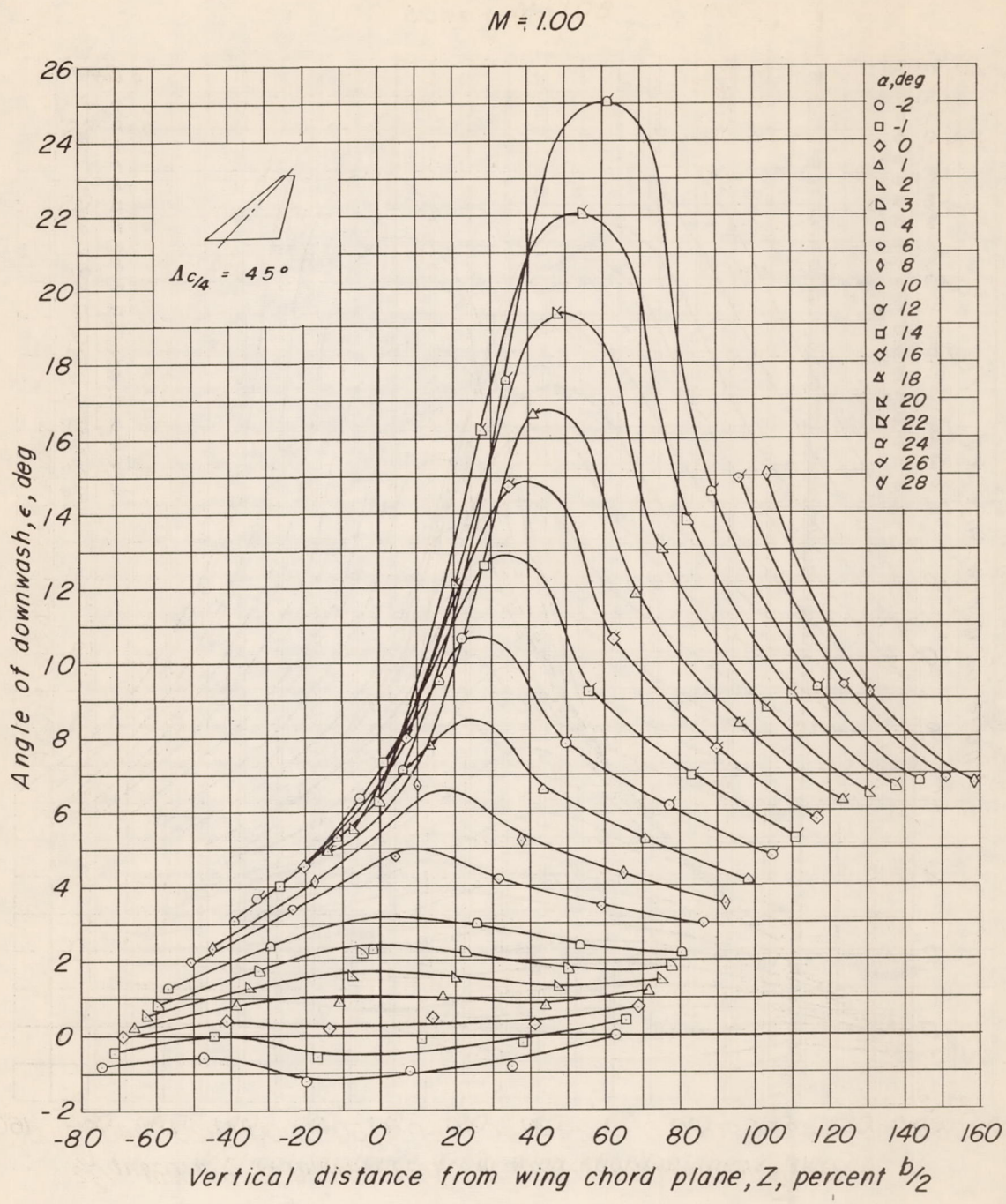
(b) M = 0.80.

Figure 8.- Continued.



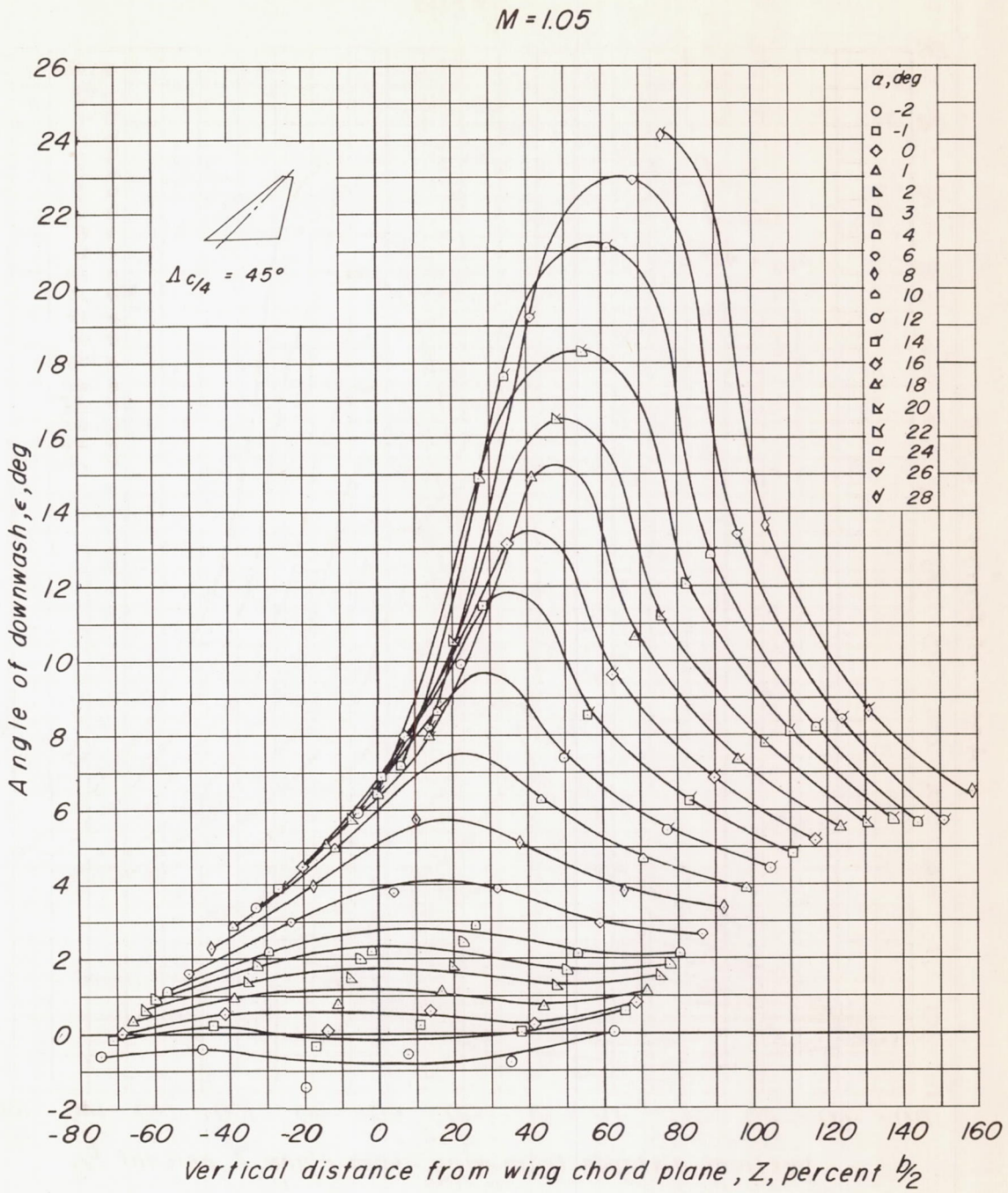
(c) M = 0.90.

Figure 8.- Continued.



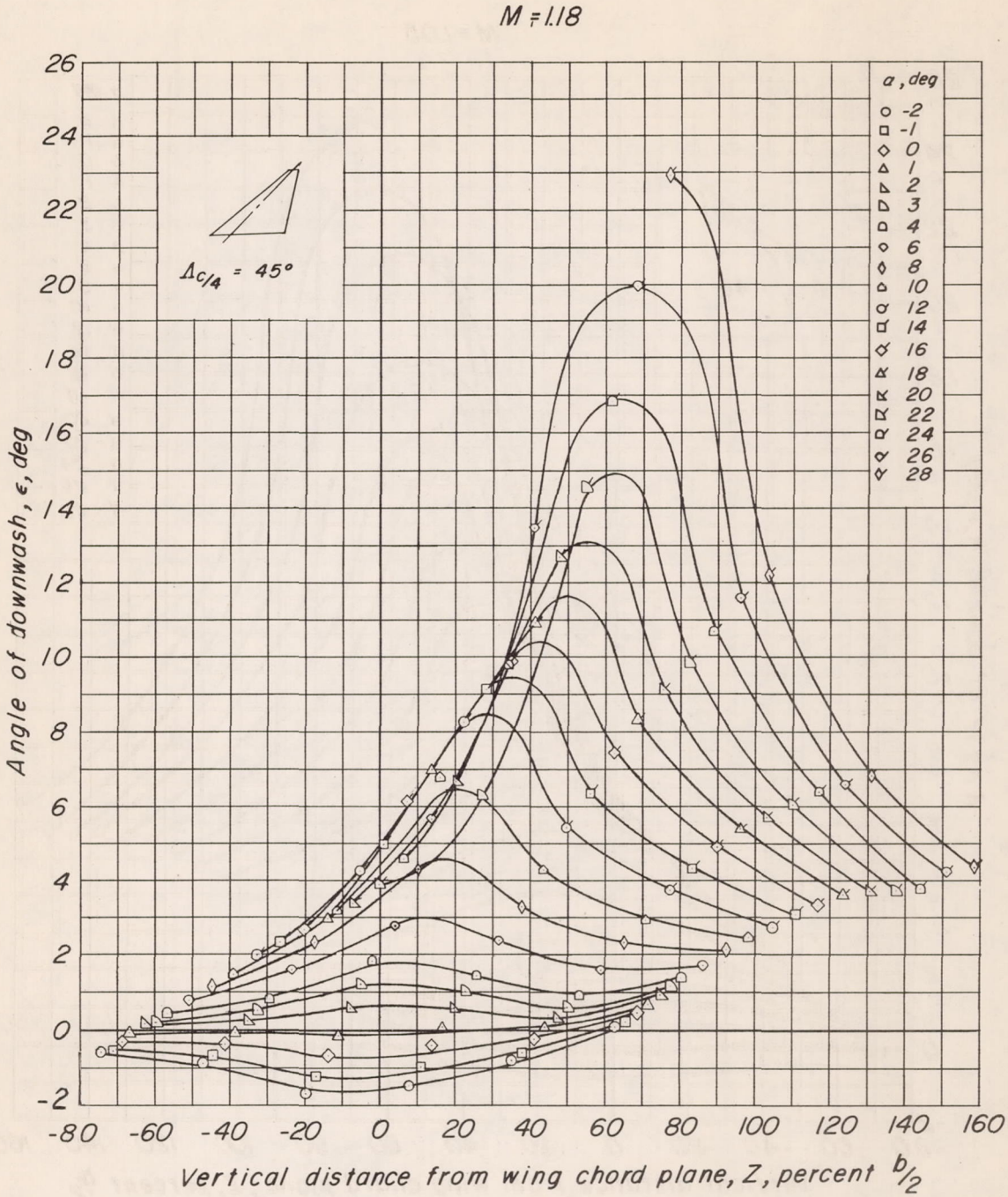
(d) M = 1.00.

Figure 8.- Continued.



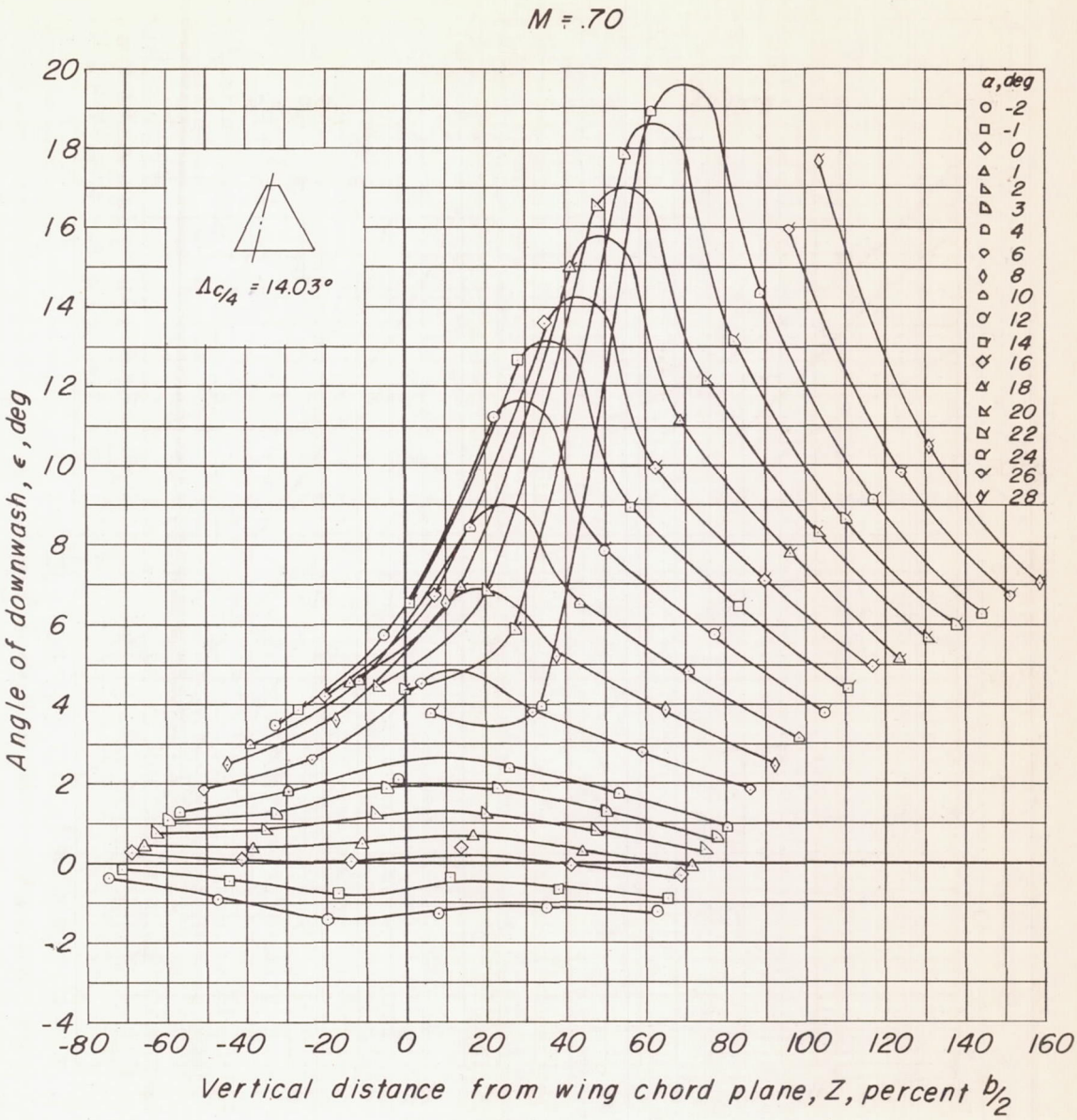
(e) M = 1.05.

Figure 8.- Continued.



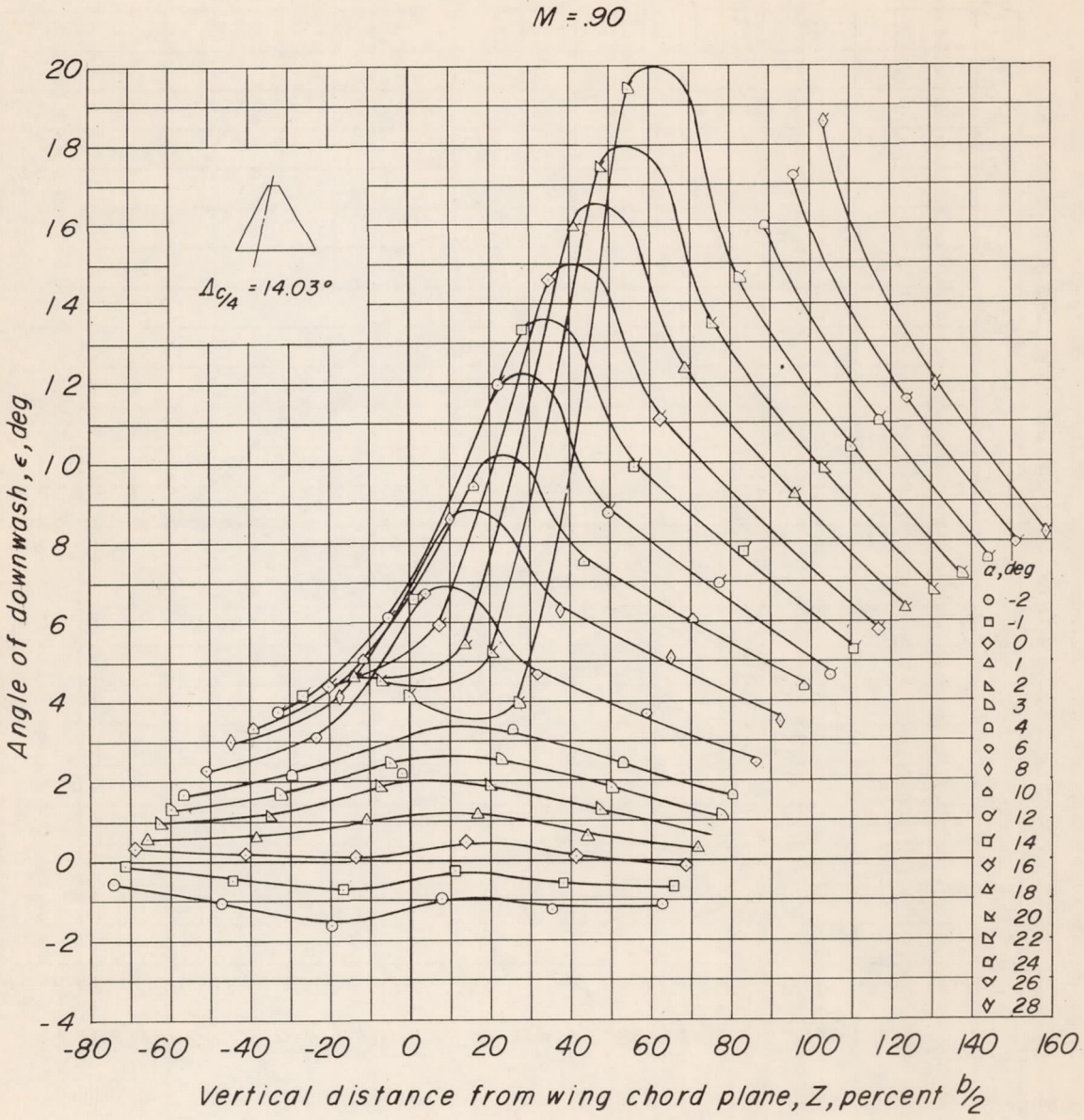
(f) M = 1.18.

Figure 8.- Concluded.



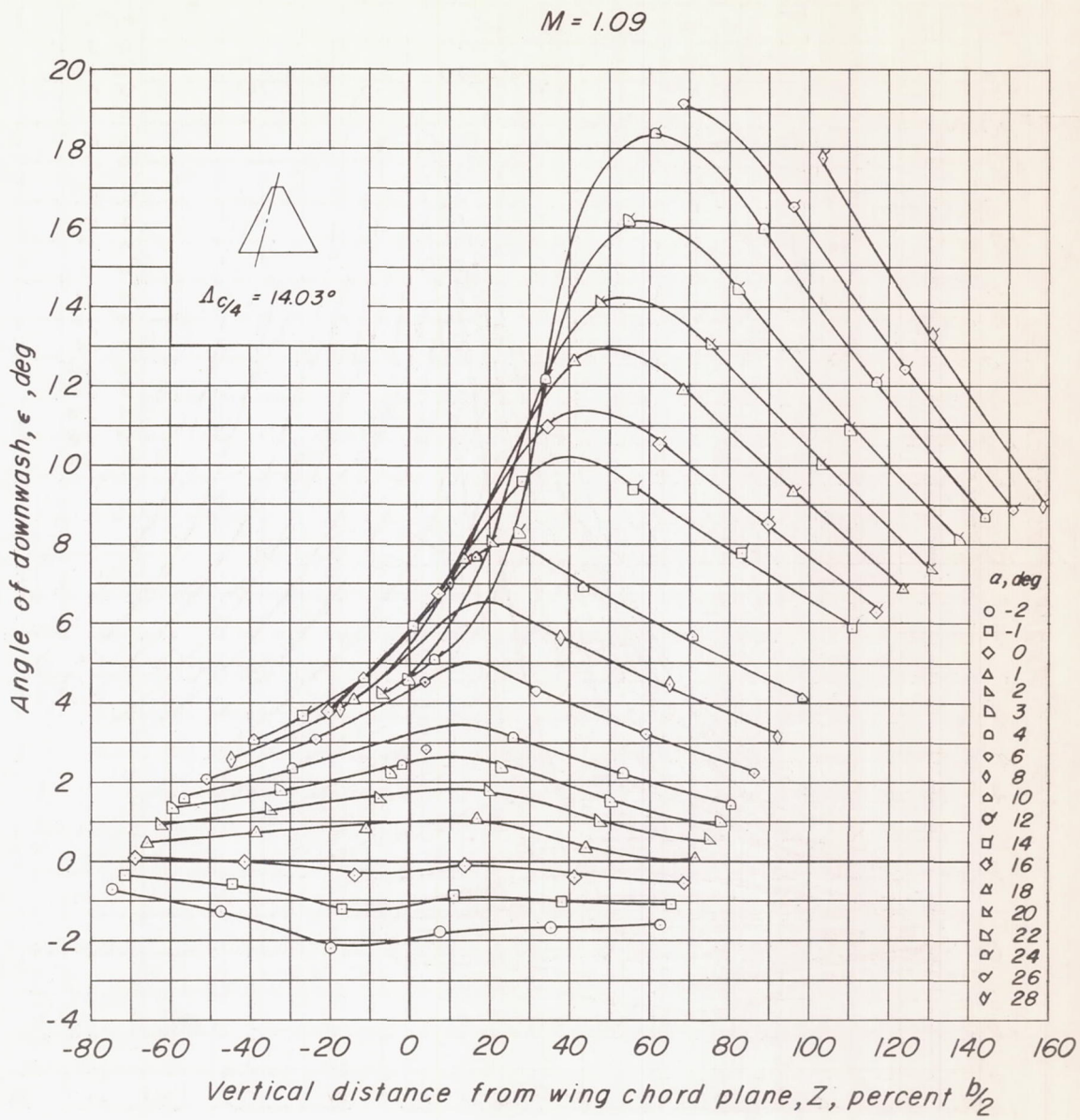
(a) M = 0.70.

Figure 9.- Effect of angle of attack on the variation of angle of downwash with vertical distance from the wing chord plane; Y = 0.20b/2; X = 1.92b/2; t/c = 0.02; $\Lambda_{c/4}$ = 14.03°.



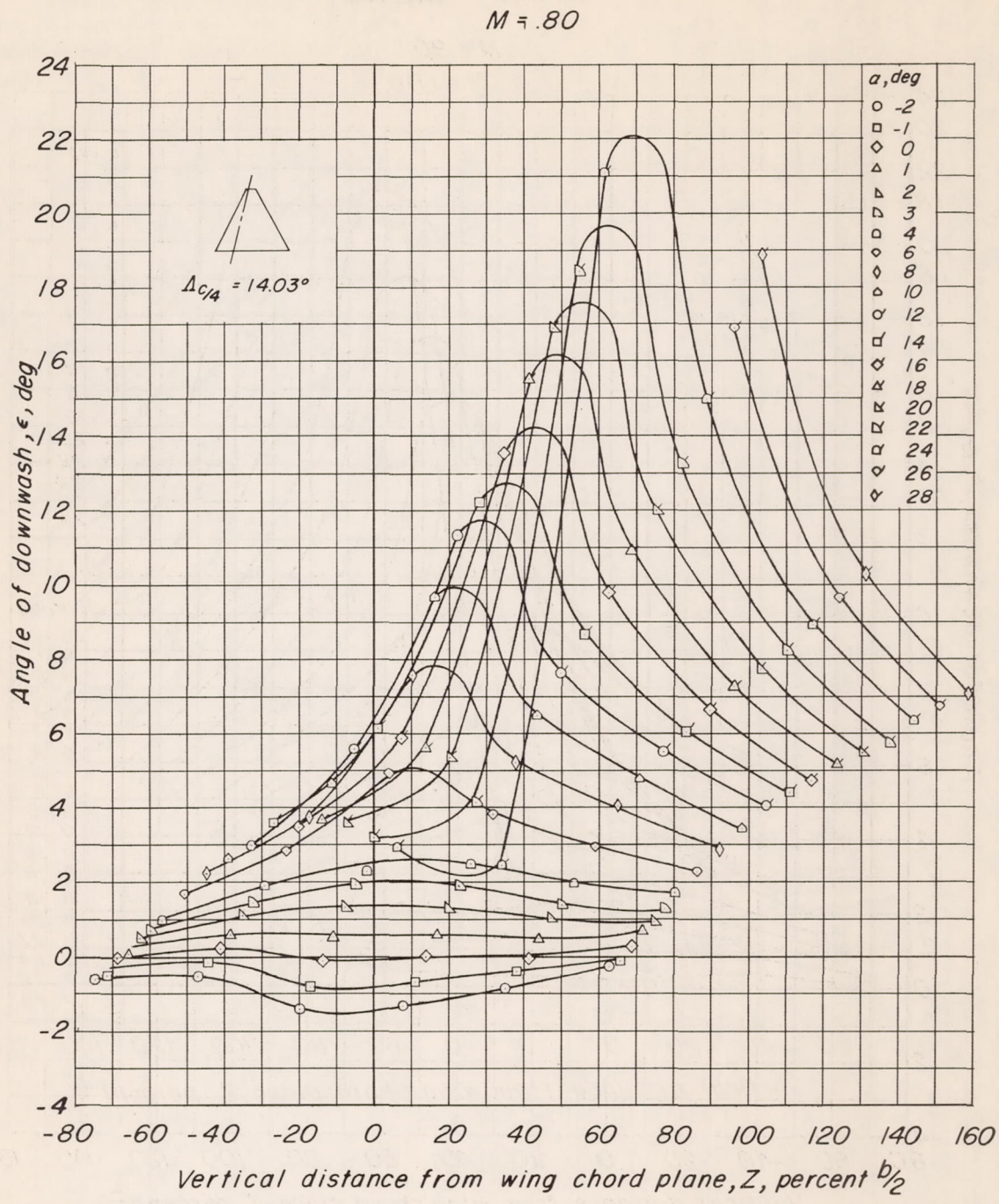
(b) M = 0.90.

Figure 9.- Continued.



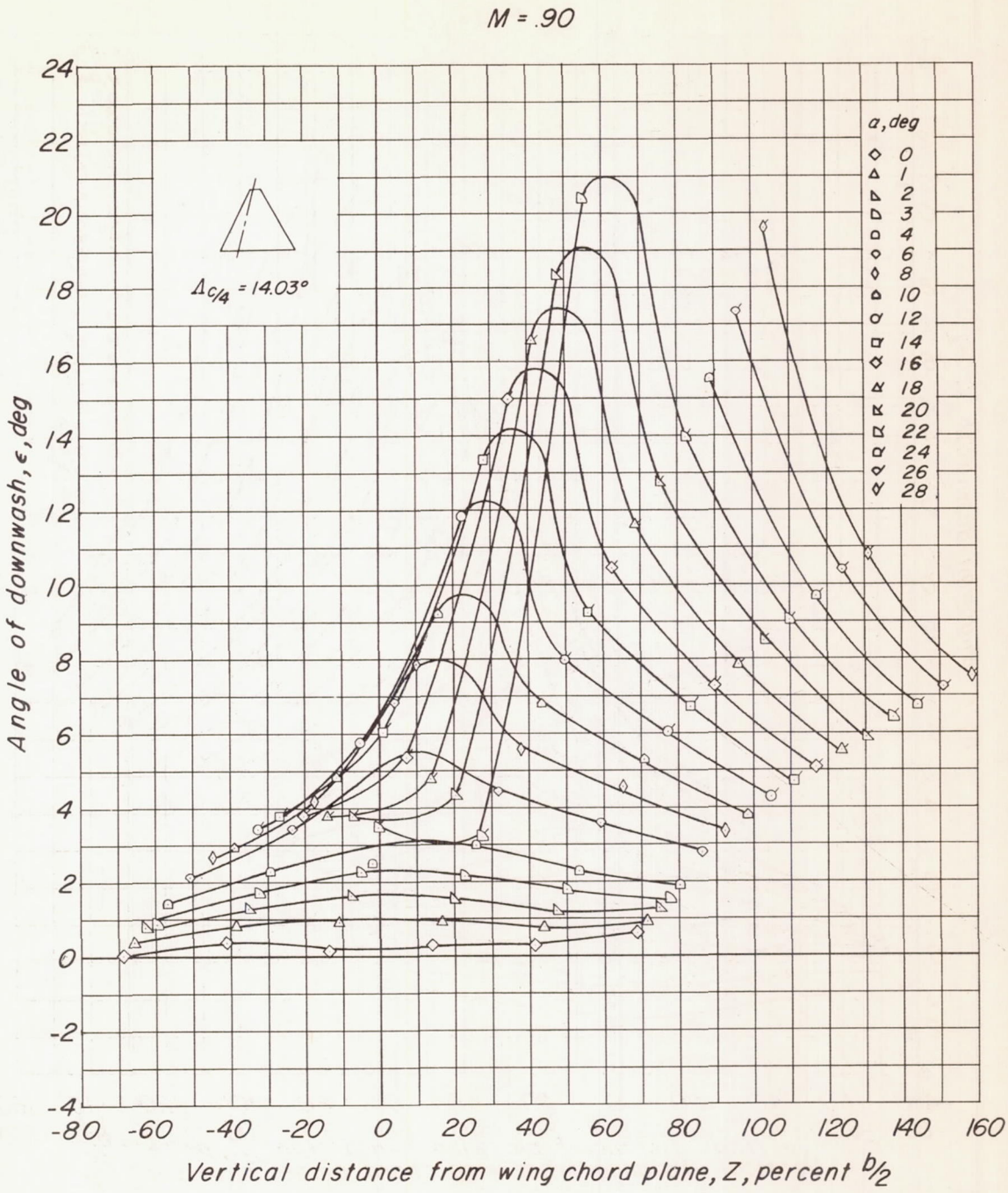
(c) M = 1.09.

Figure 9.- Concluded.



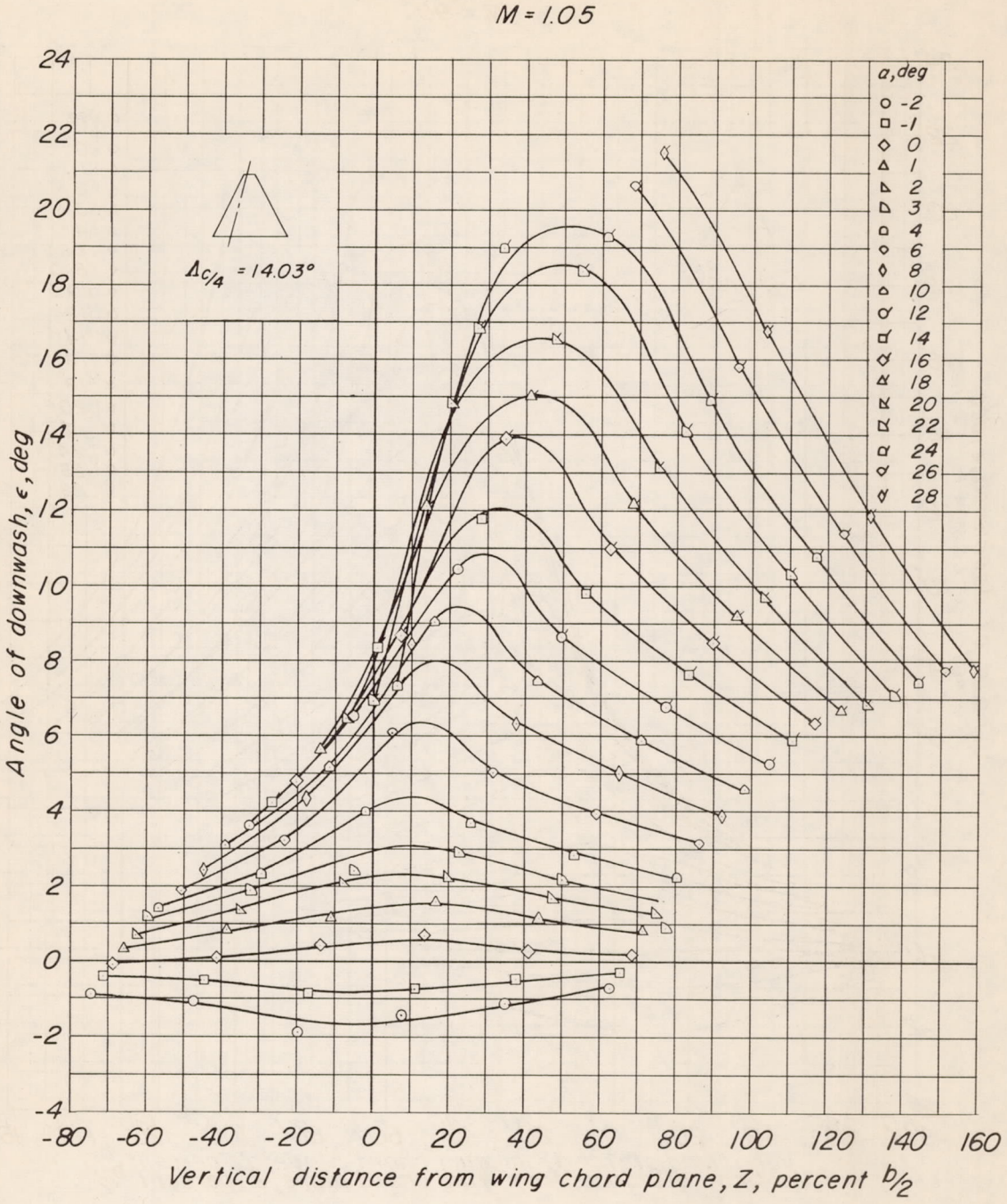
(a) M = 0.80.

Figure 10.- Effect of angle of attack on the variation of angle of downwash with vertical distance from the wing chord plane; Y = 0.20b/2; X = 1.92b/2; t/c = 0.045; $\Lambda_{c/4}$ = 14.03°.



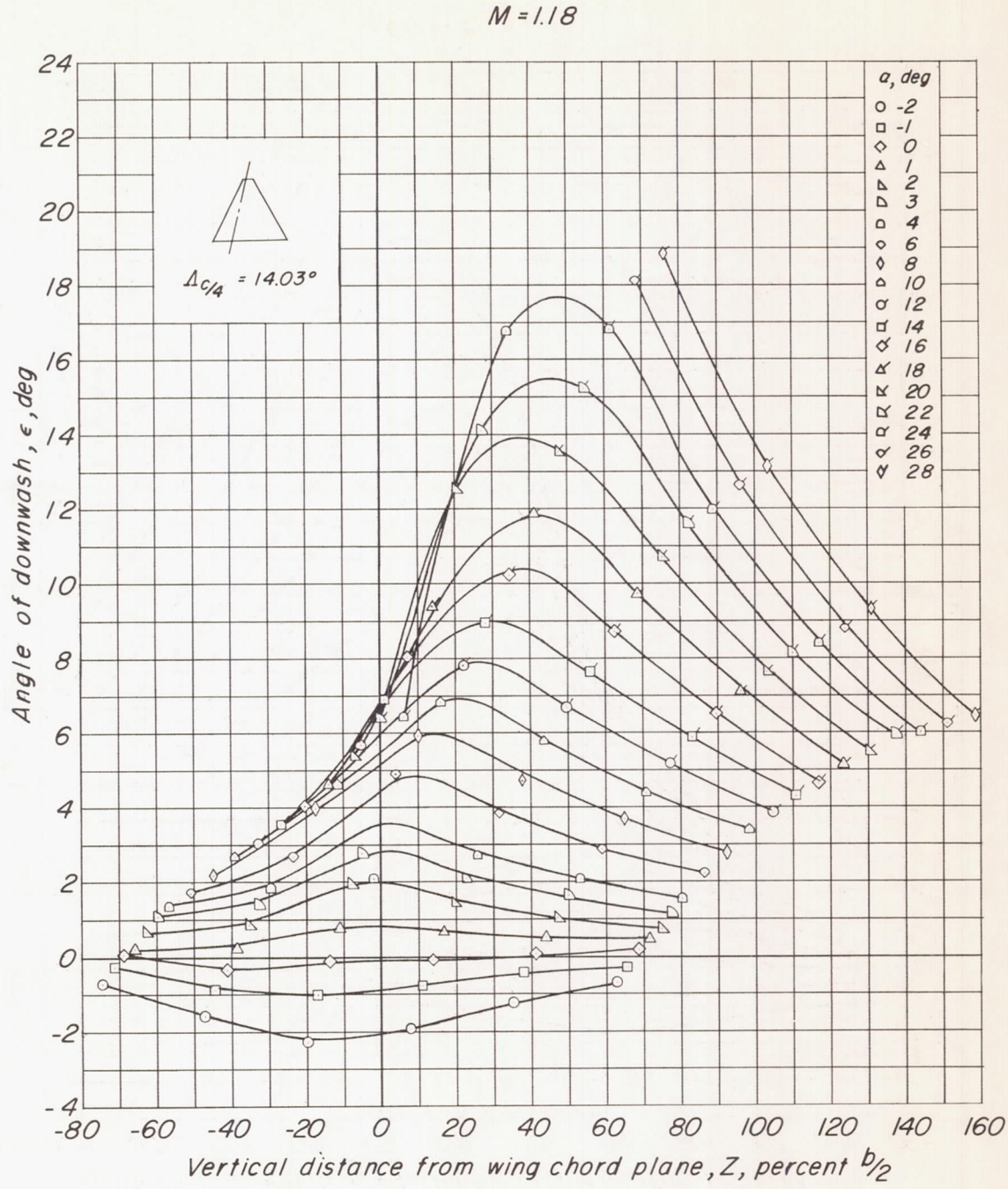
(b) M = 0.90.

Figure 10.- Continued.



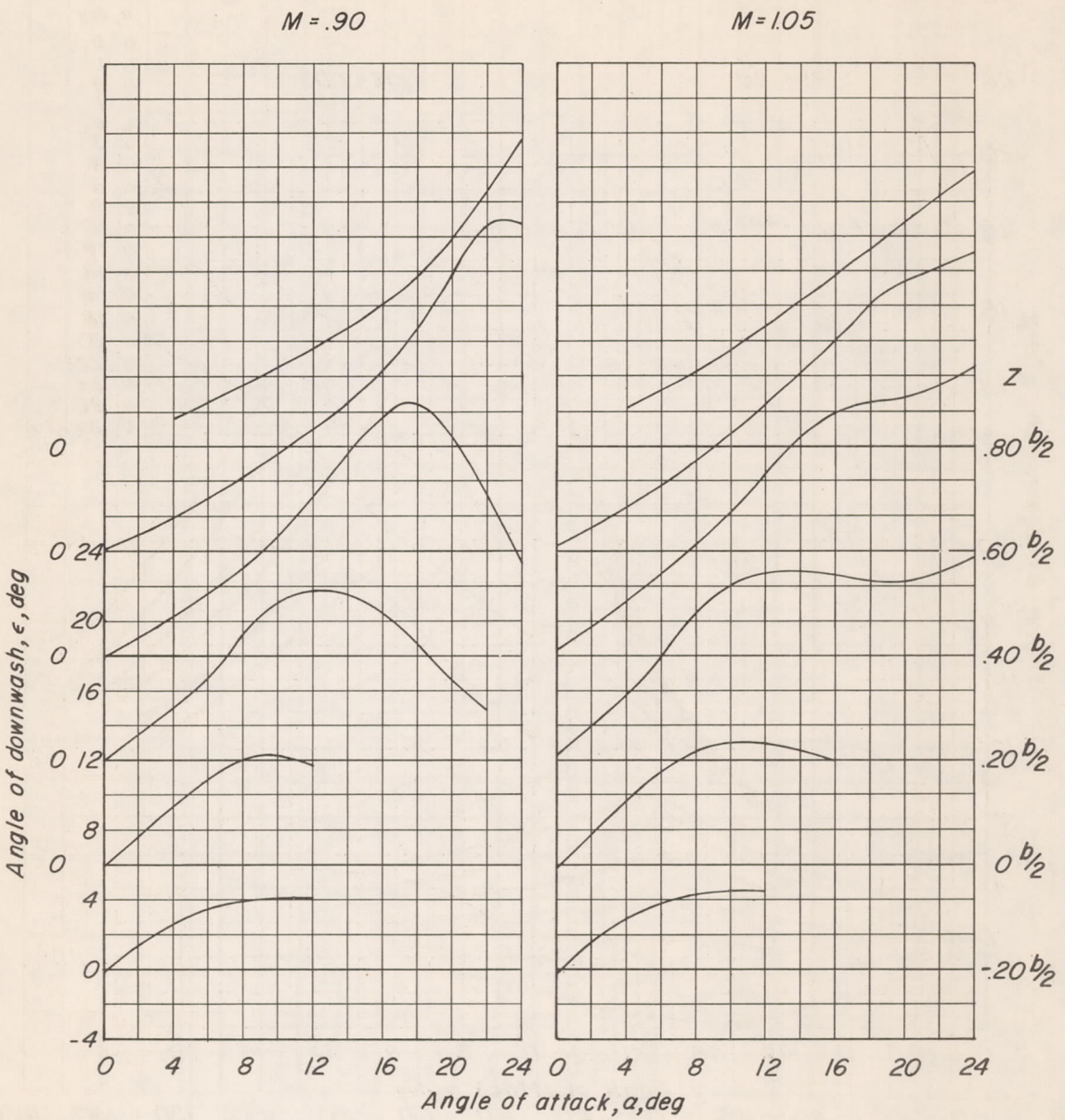
(c) M = 1.05.

Figure 10.- Continued.



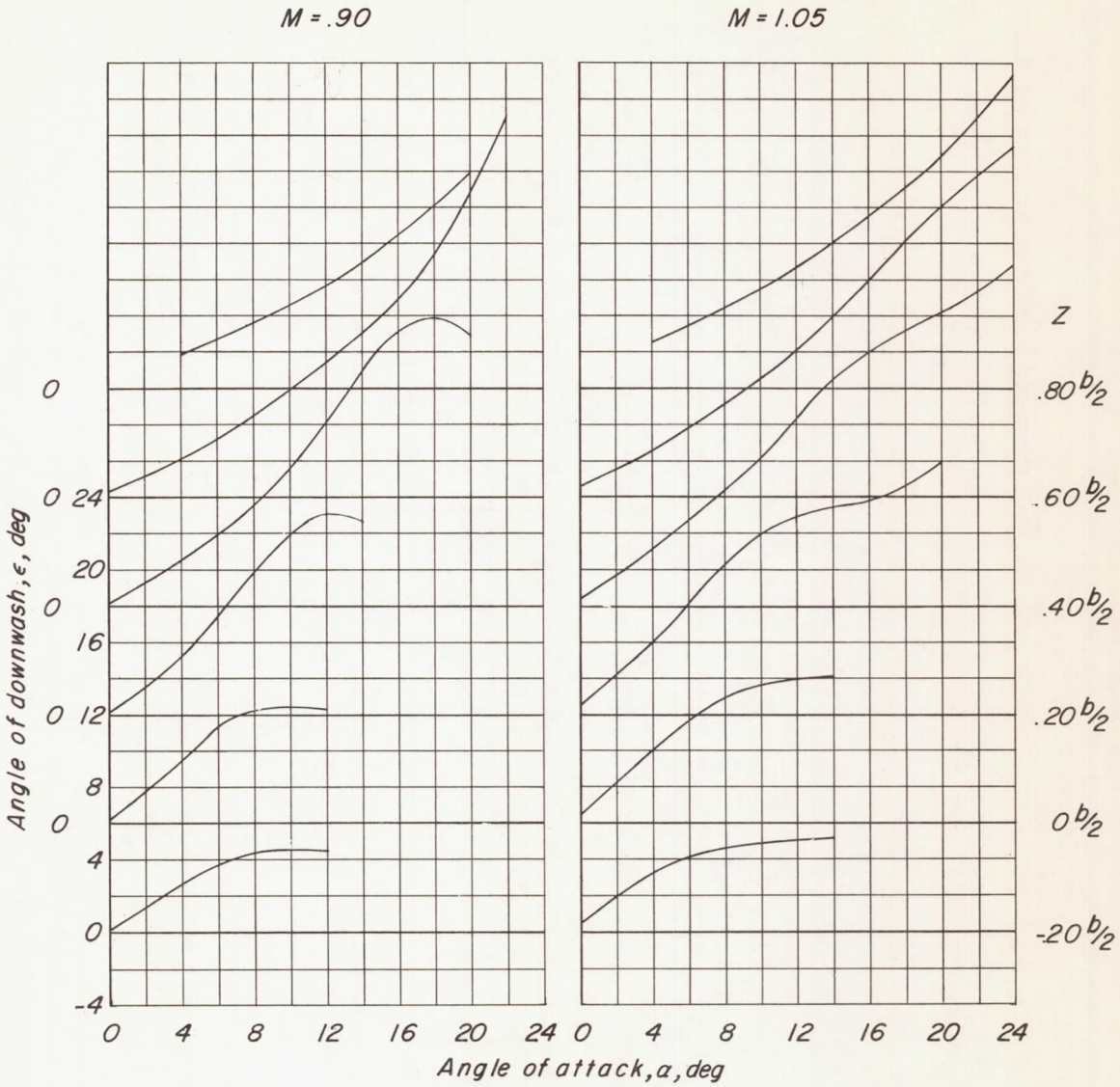
(d) M = 1.18.

Figure 10.- Concluded.



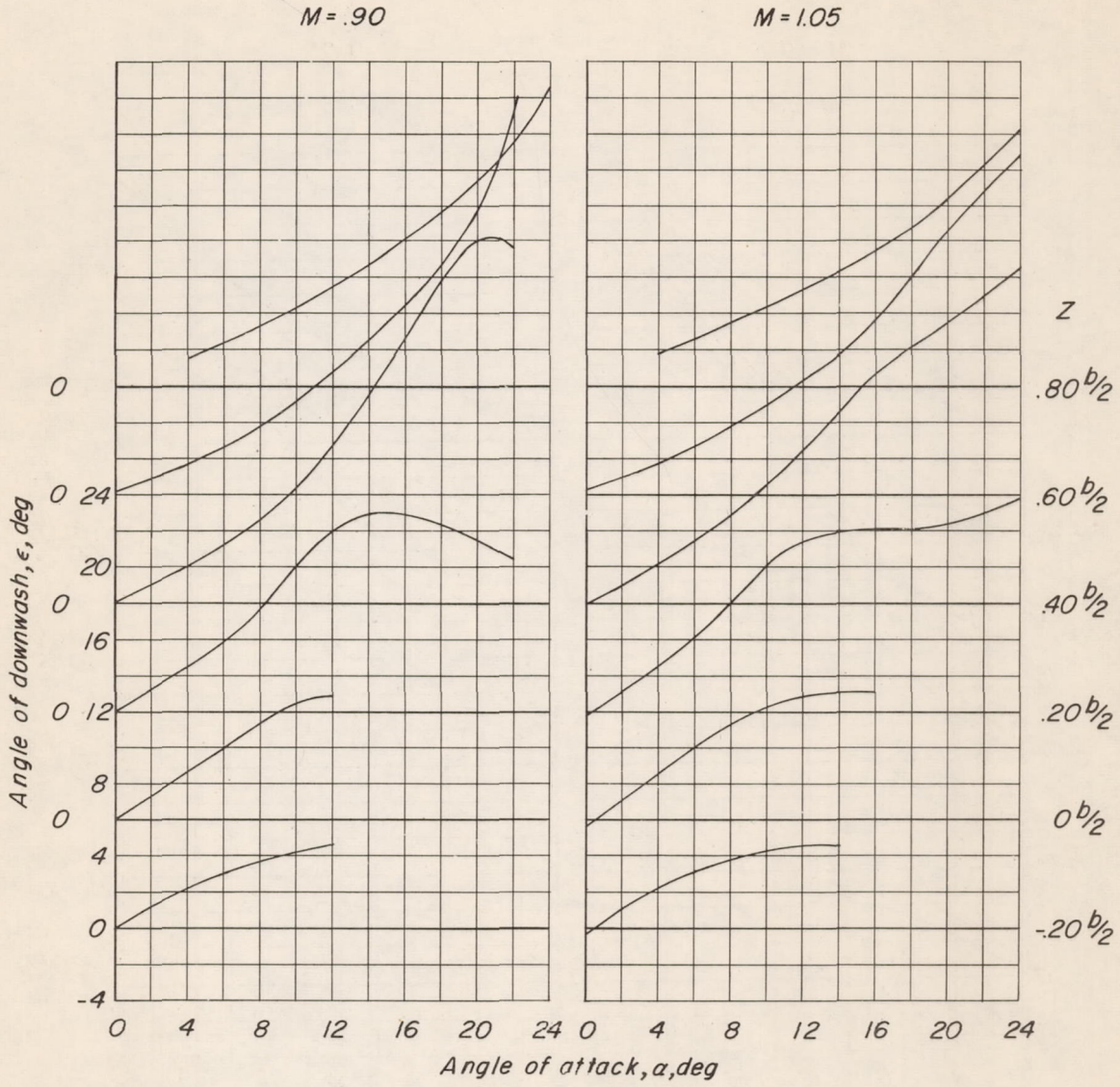
(a) $\Lambda_{c/4} = 0^{\circ}$; X = 2.05b/2; t/c = 0.03.

Figure 11.- Effect of vertical distance from wing chord plane on the variation of angle of downwash with angle of attack. Y = 0.20b/2.



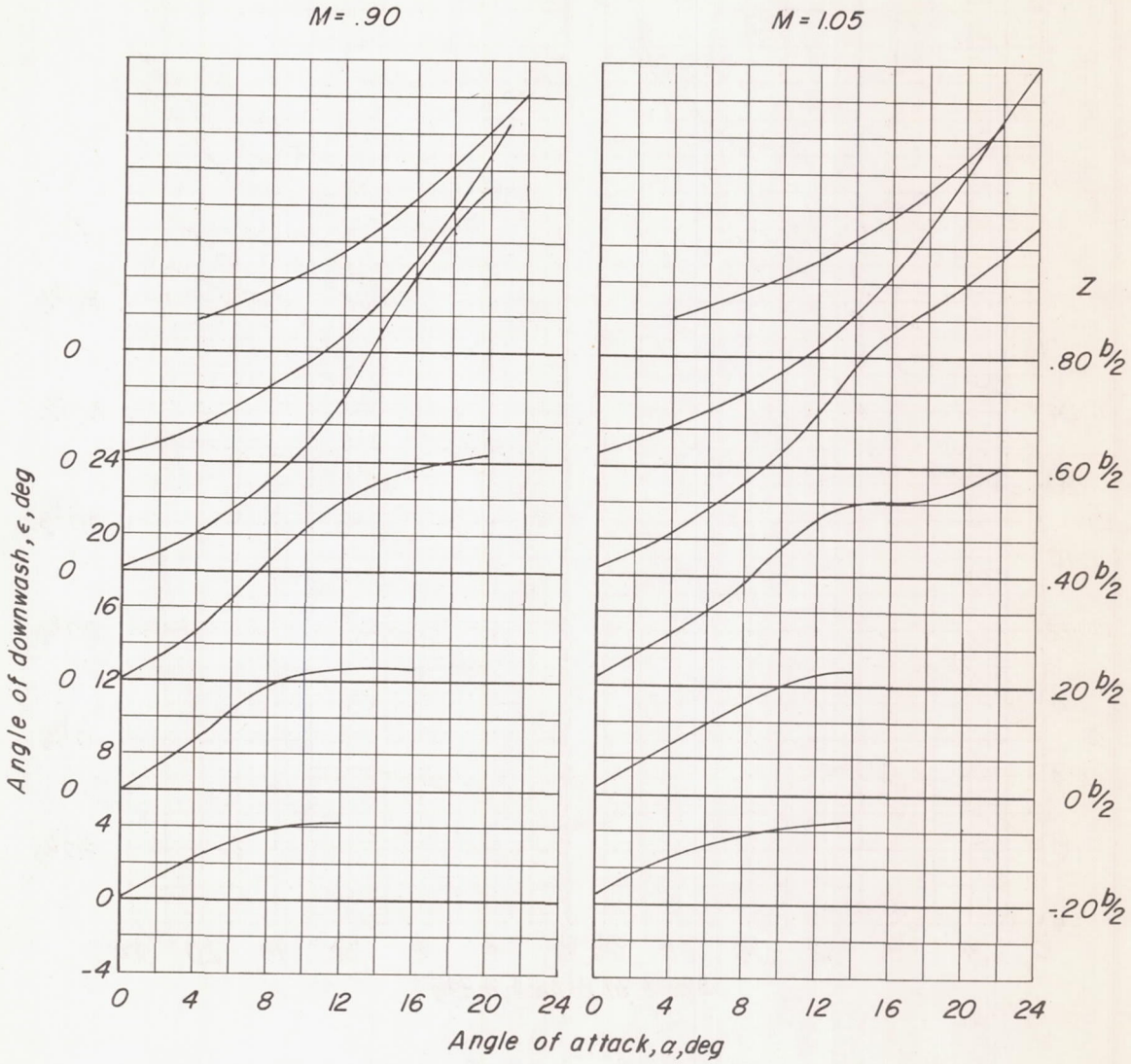
(b) $\Lambda_{c/4} = 14.03^{\circ}$; X = 1.92b/2; t/c = 0.03.

Figure 11.- Continued.



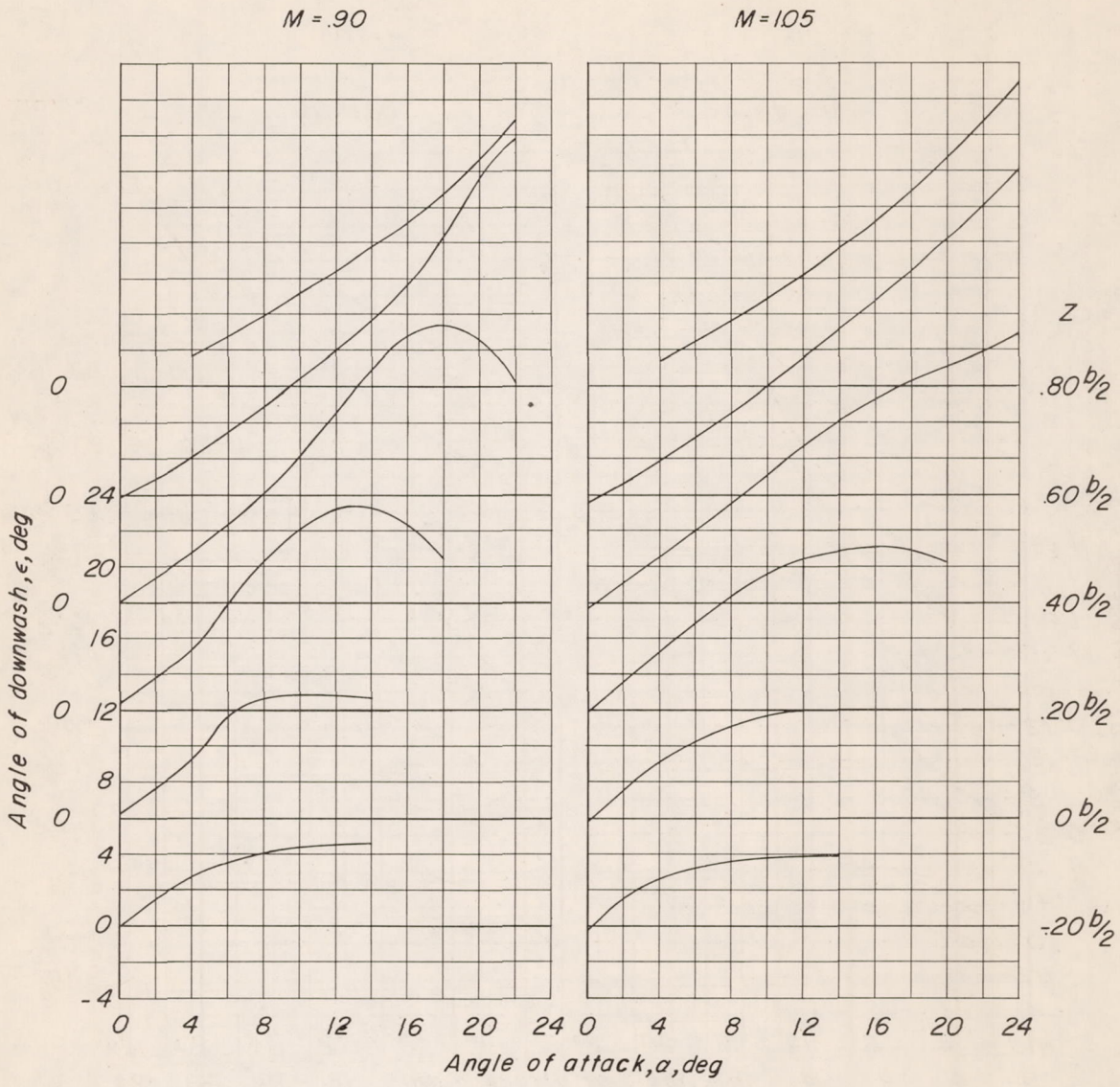
(c) $\Lambda_{c/4} = 36.87^{\circ}$; X = 1.69b/2; t/c = 0.03.

Figure 11.- Continued.



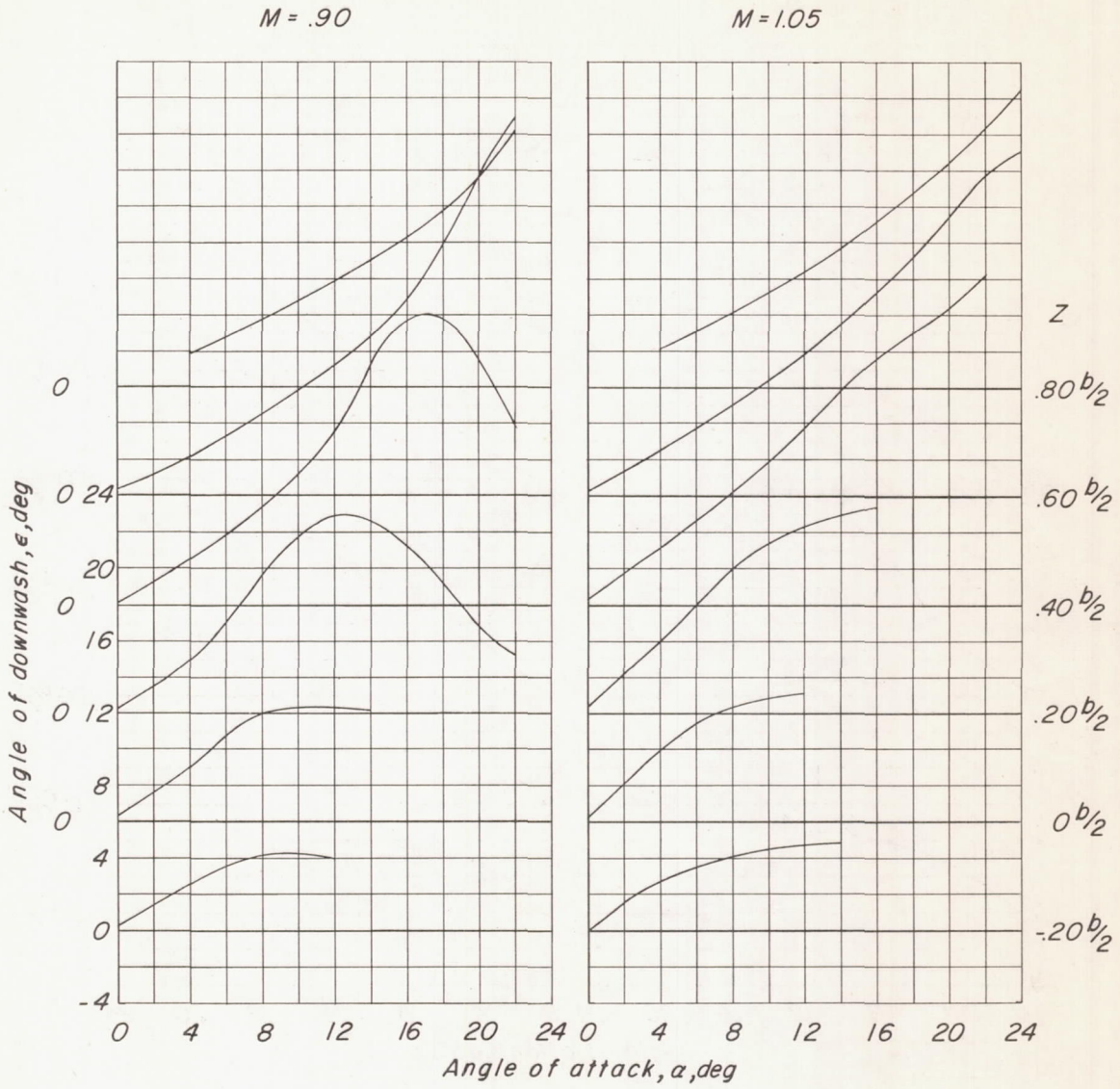
(d) $\Lambda_{c/4} = 45^{\circ}$; X = 1.69b/2; t/c = 0.03.

Figure 11.- Continued.



(e) $\Lambda_{c/4} = 14.03^{\circ}$; X = 1.92b/2; t/c = 0.02.

Figure 11.- Continued.



(f) $\Lambda_{c/4} = 14.03^{\circ}$; X = 1.92b/2; t/c = 0.045.

Figure 11.- Concluded.

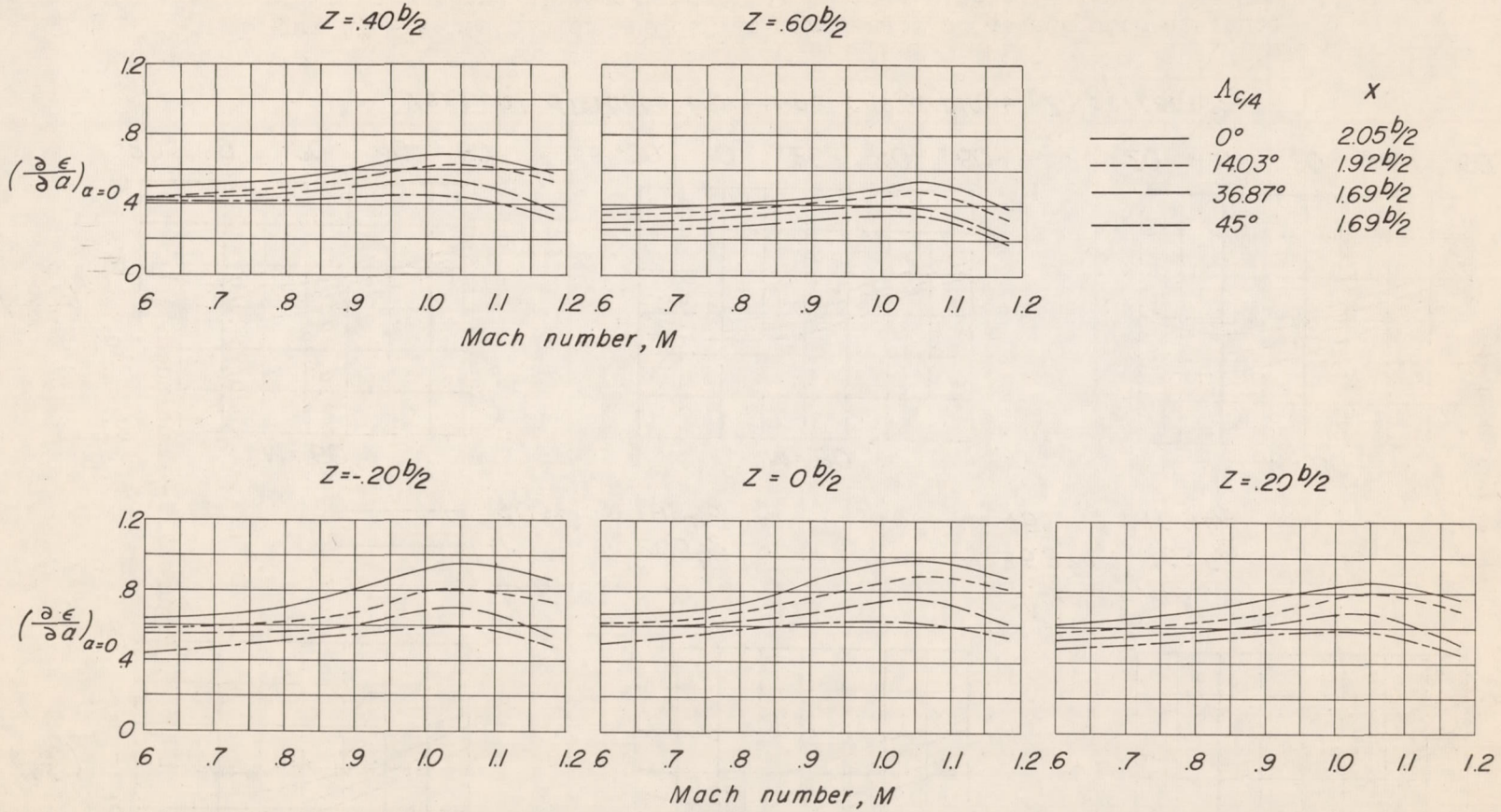


Figure 12.- Variation of $\partial\epsilon/\partial\alpha$ at zero angle of attack with Mach number for several wing plan forms; Y = 0.20b/2; t/c = 0.03.

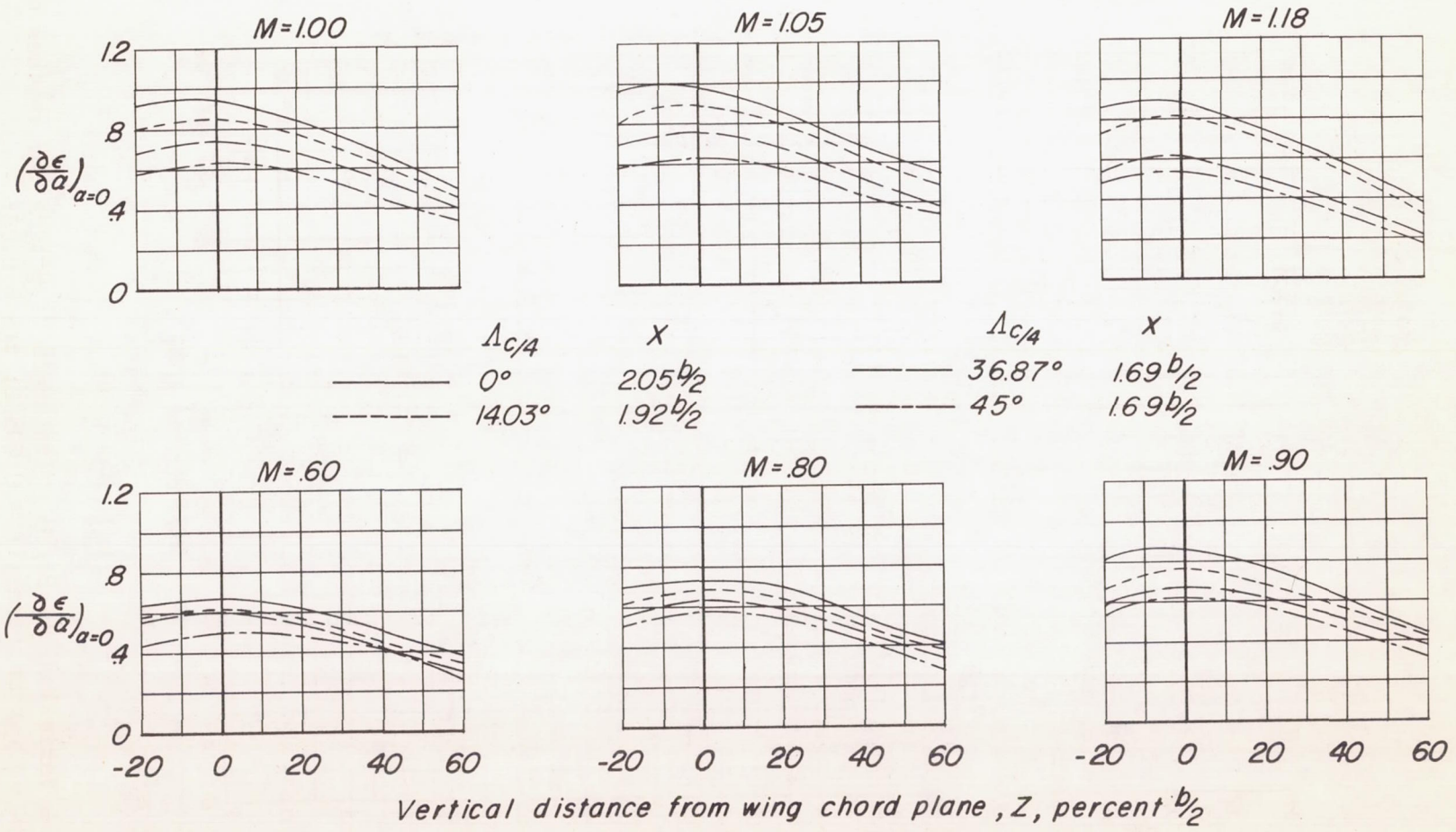
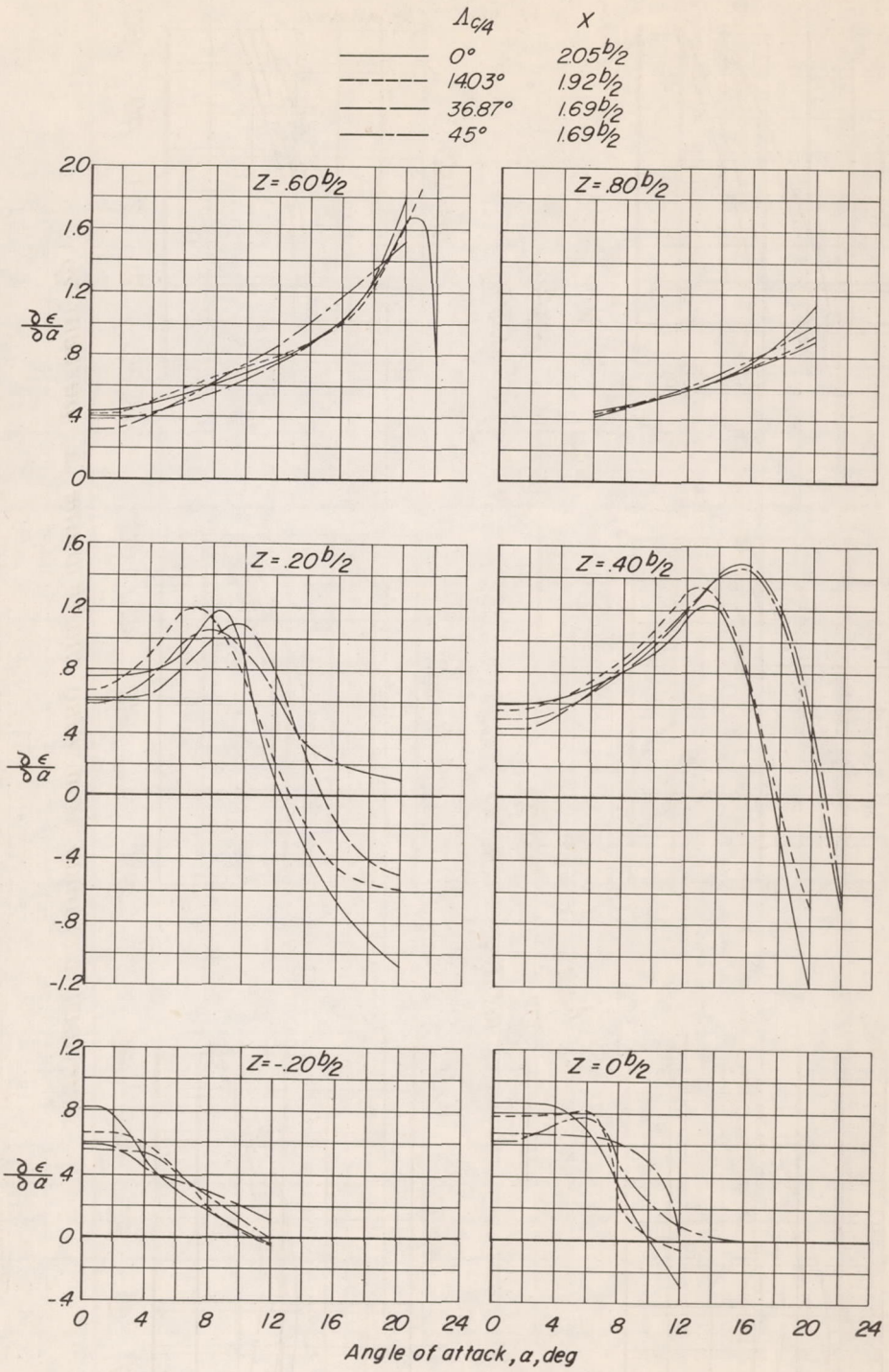
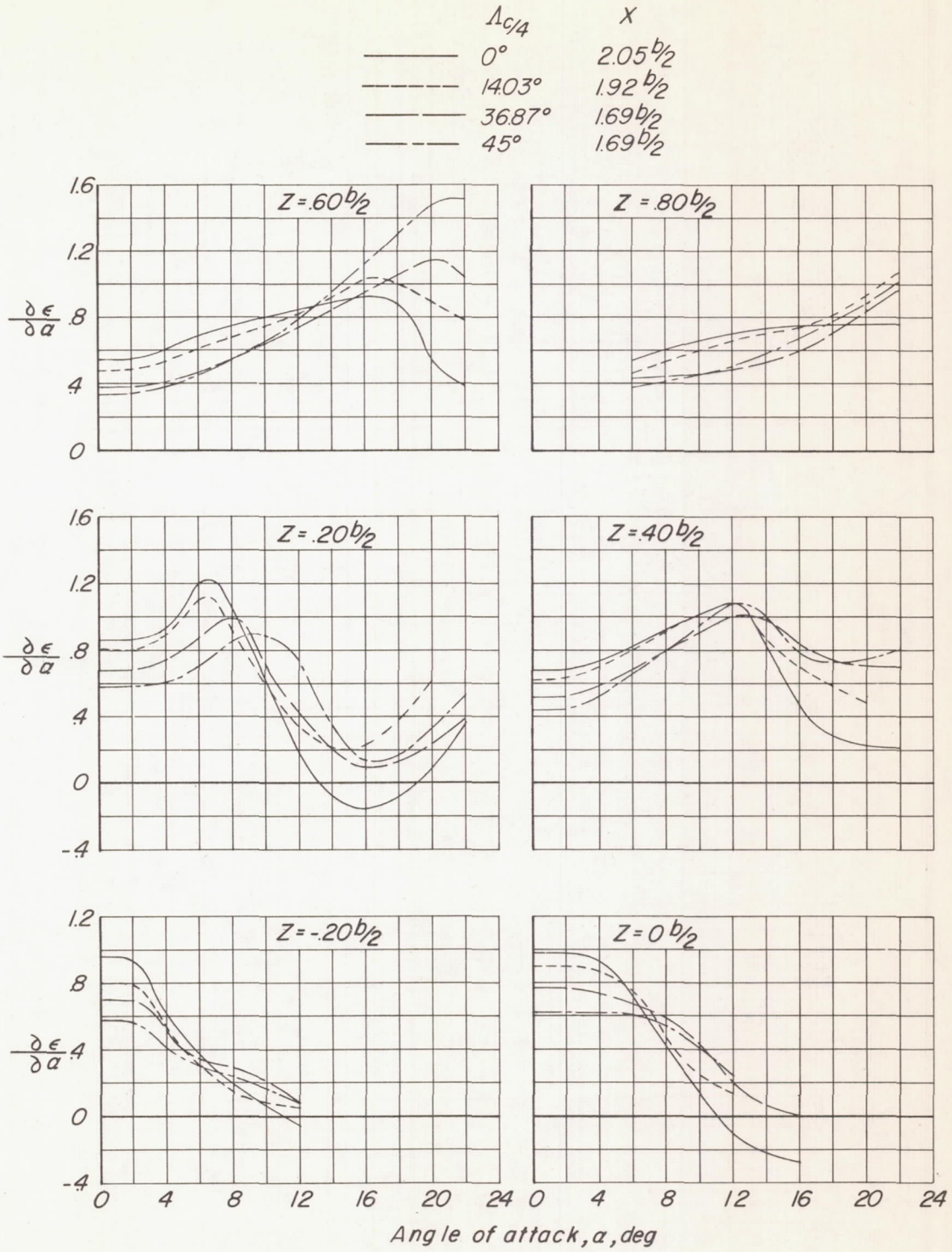


Figure 13.- Variation of $\partial\epsilon/\partial\alpha$ at zero angle of attack with distance from wing chord plane extended for various wing plan forms; Y = 0.20b/2; t/c = 0.03.



(a) M = 0.90.

Figure 14.- Variation of $\partial\epsilon/\partial\alpha$ with angle of attack for various wing plan forms; Y = 0.20b/2; t/c = 0.03.



(b) M = 1.05.

Figure 14.- Concluded.

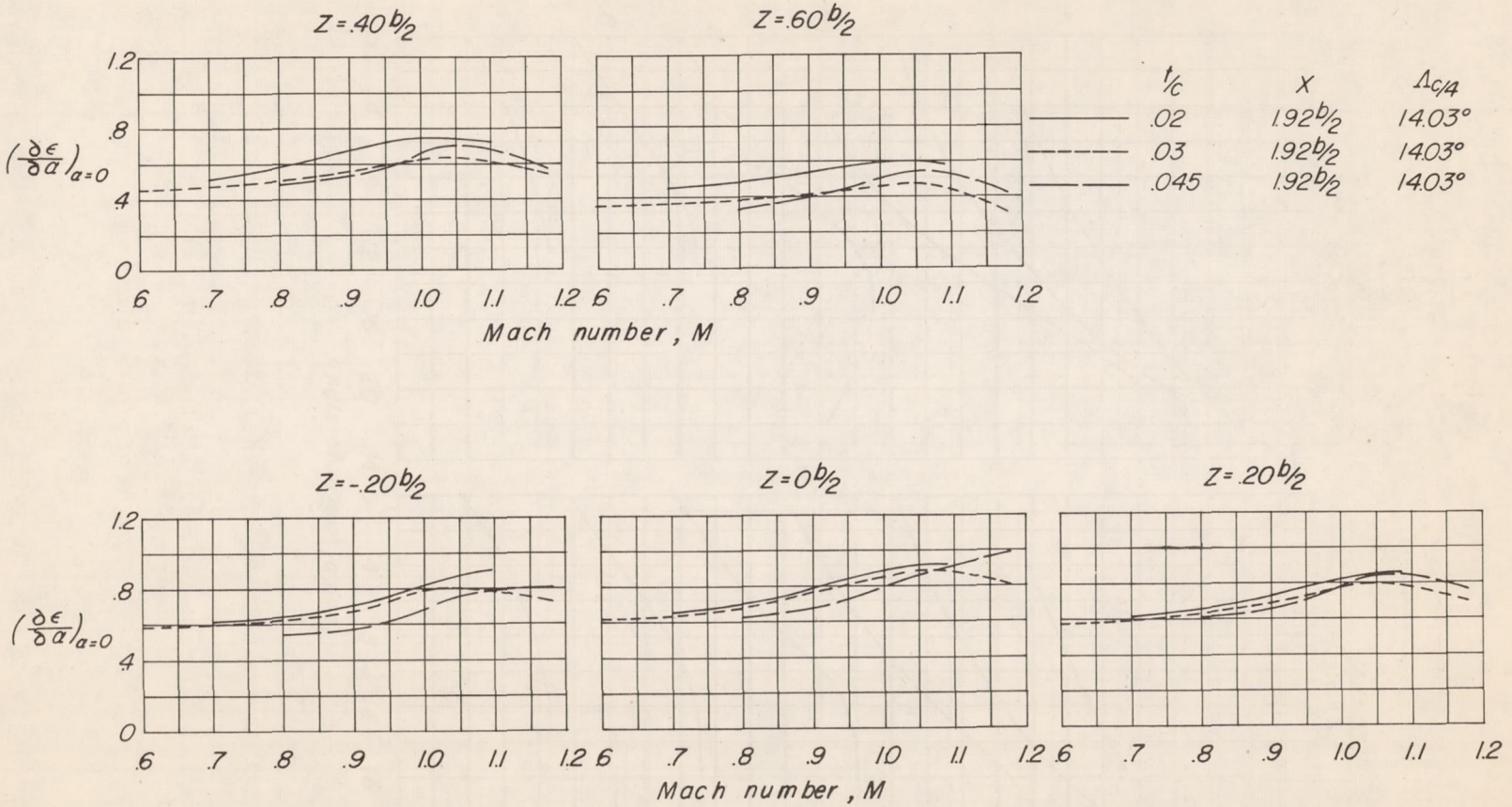
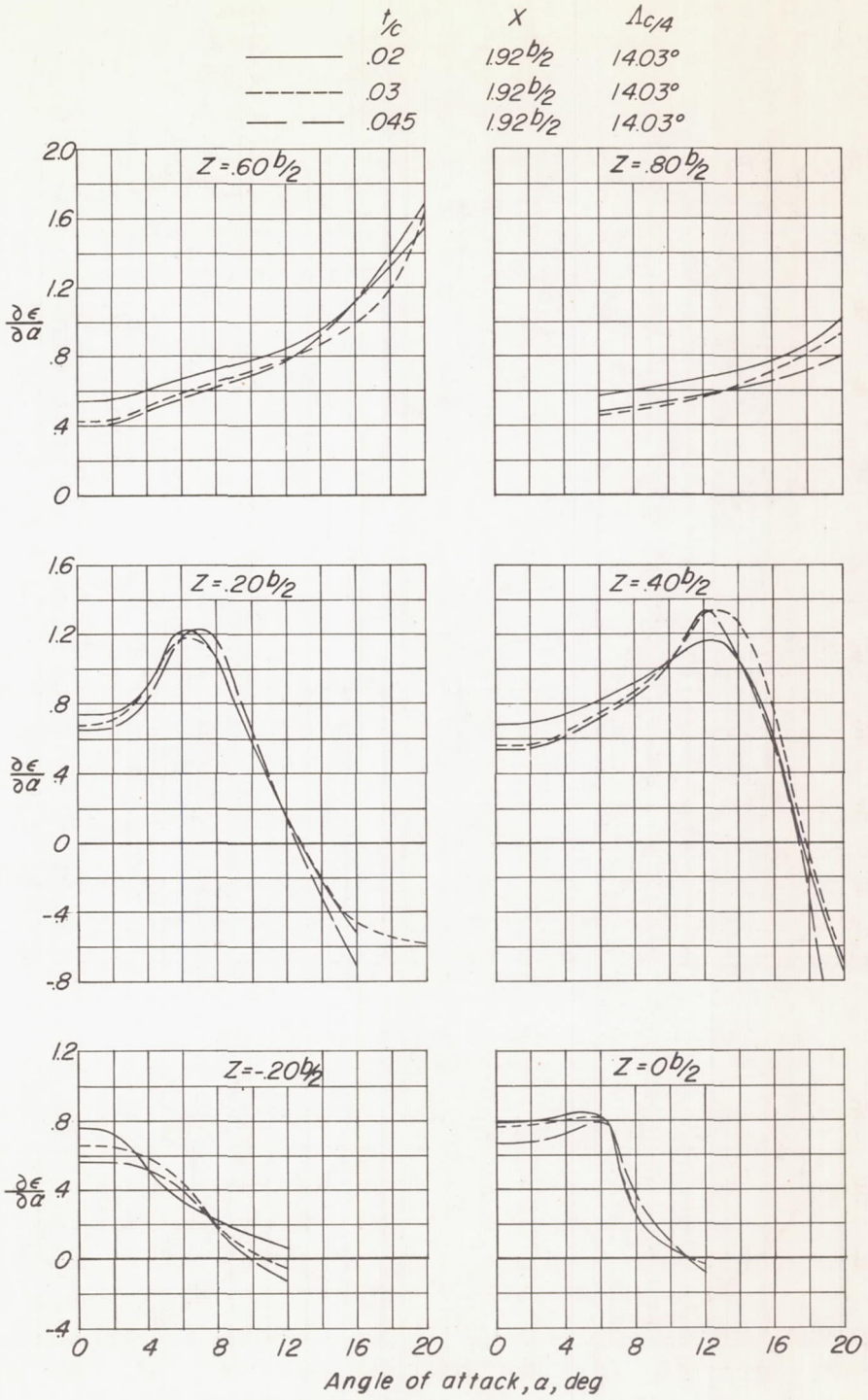
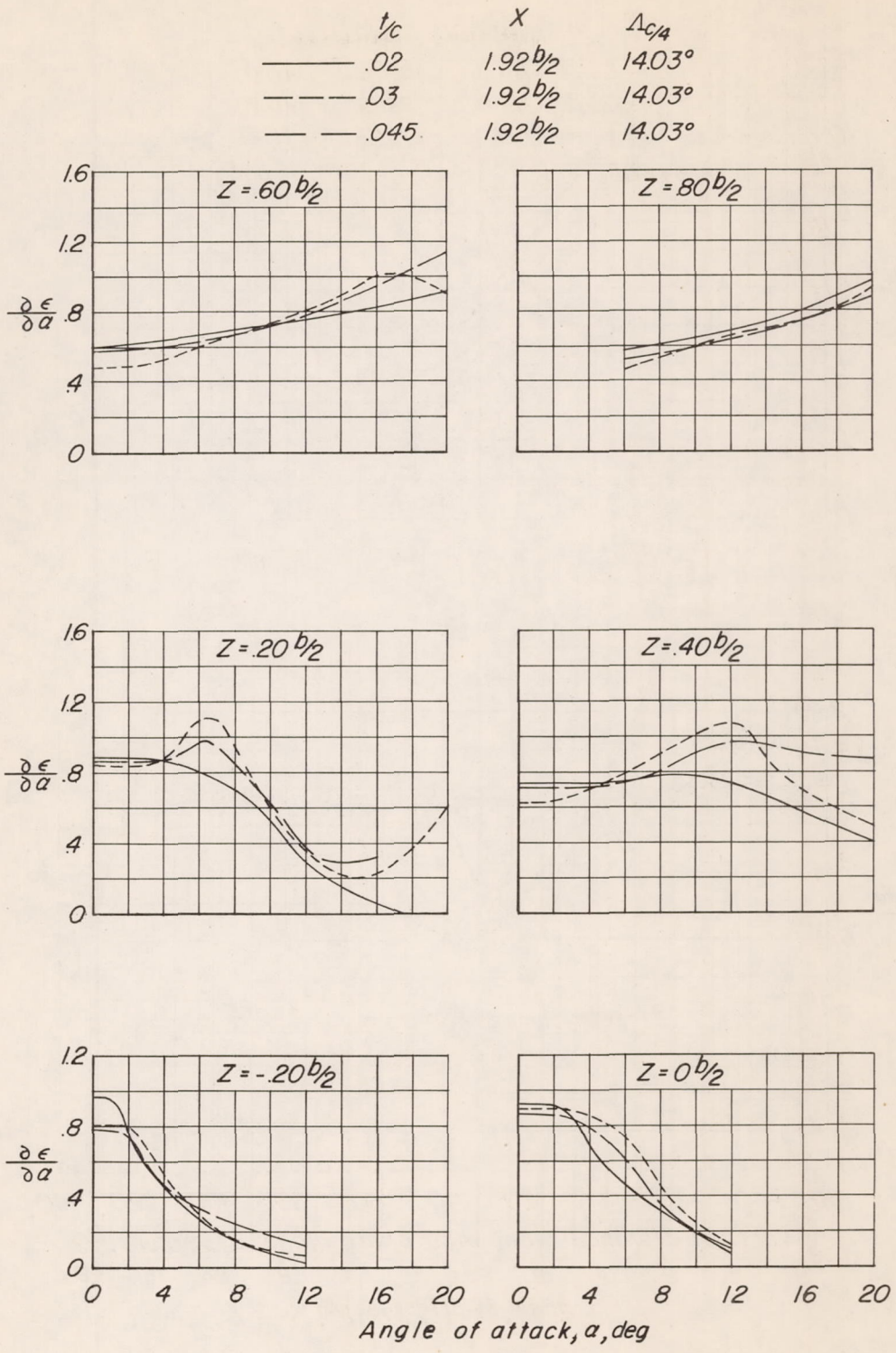


Figure 15.- Variation of $\partial\epsilon/\partial\alpha$ at zero angle of attack with Mach numbers for several wing thickness ratios; Y = 0.20b/2; $\Lambda_{c/4} = 14.03^{\circ}$.



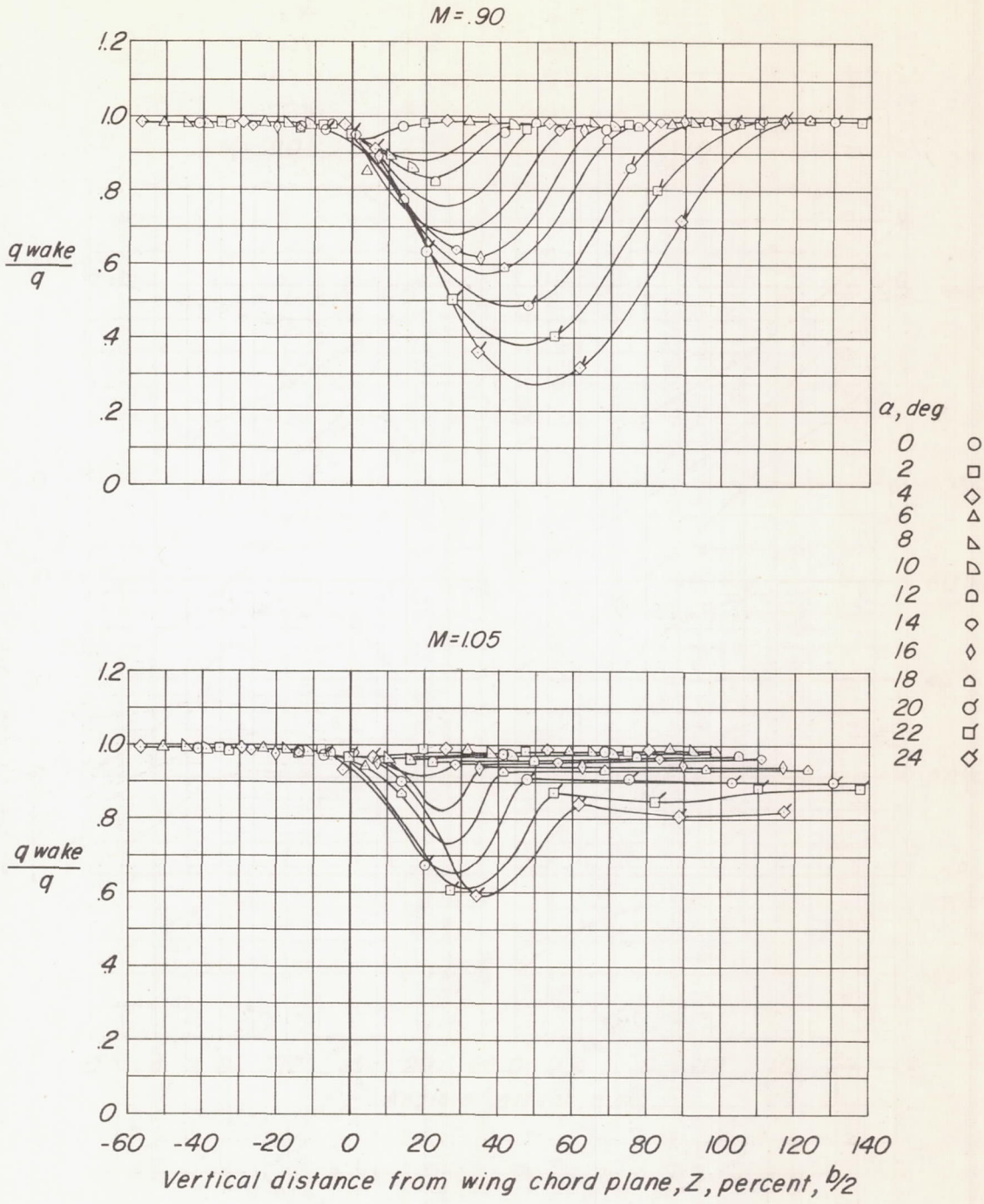
(a) M = 0.90.

Figure 16.- Variation of $\partial\epsilon/\partial\alpha$ with angle of attack for several wing thickness ratios; Y = 0.20b/2; $\Lambda_{c/4} = 14.03^{\circ}$.



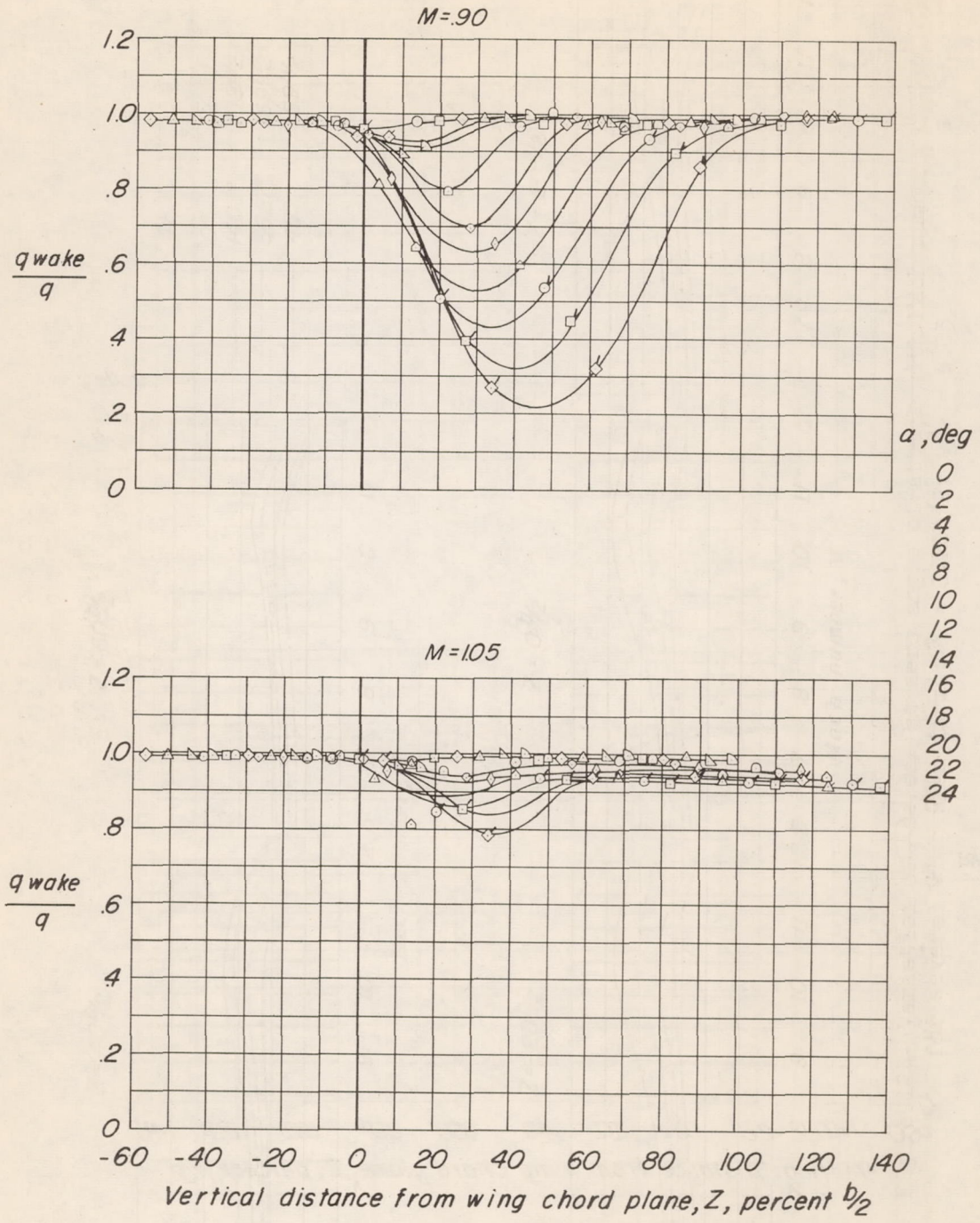
(b) M = 1.05.

Figure 16.- Concluded.



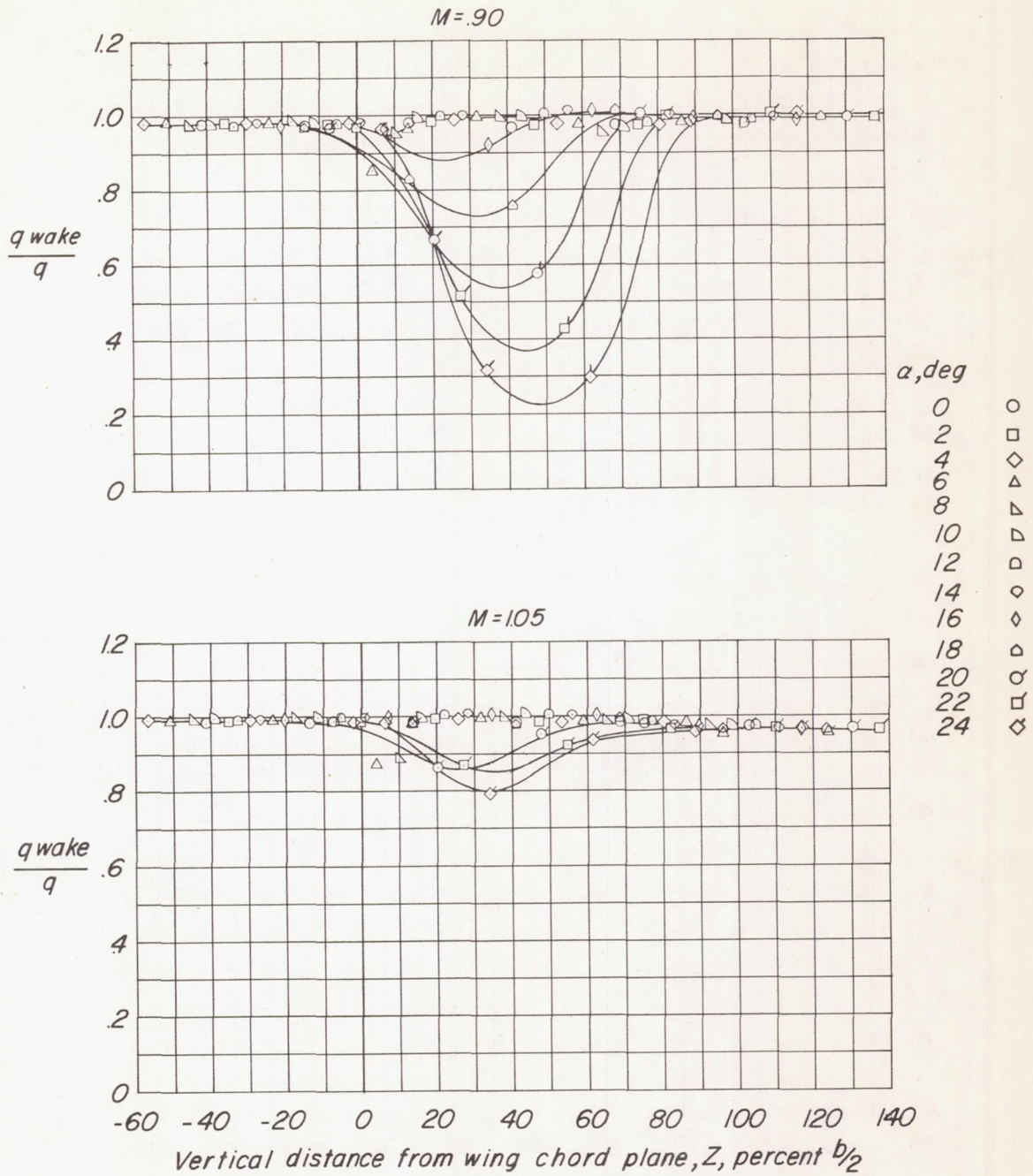
(a) $\Lambda_{c/4} = 0^{\circ}$; X = 2.05b/2; Y = 0.20b/2.

Figure 17.- Variation of dynamic pressure ratio with distance from wing chord plane extended for several angles of attack; t/c = 0.03.



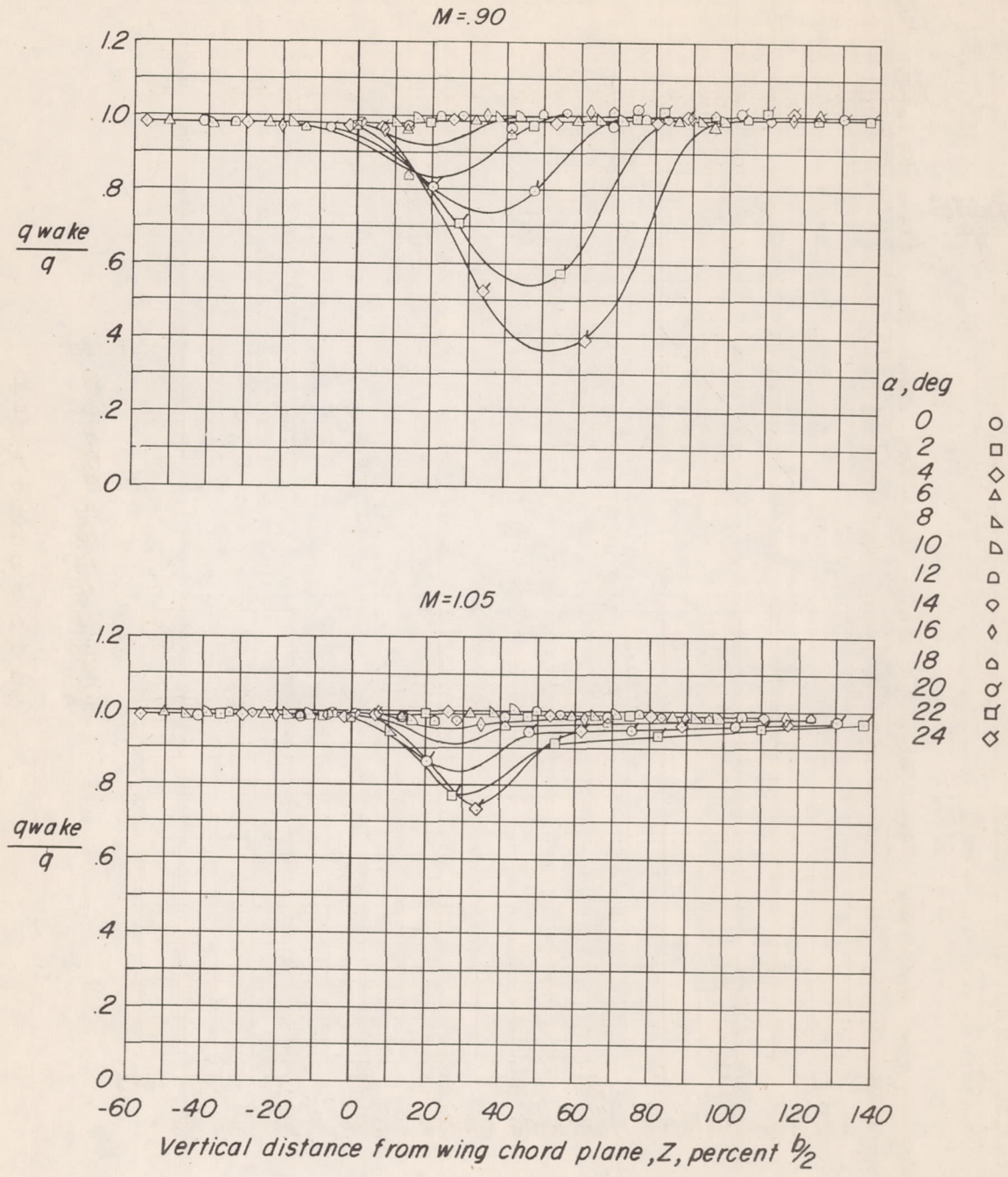
(b) $\Lambda_{c/4} = 14.03^{\circ}$; X = 1.92b/2; Y = 0.20b/2.

Figure 17.- Continued.



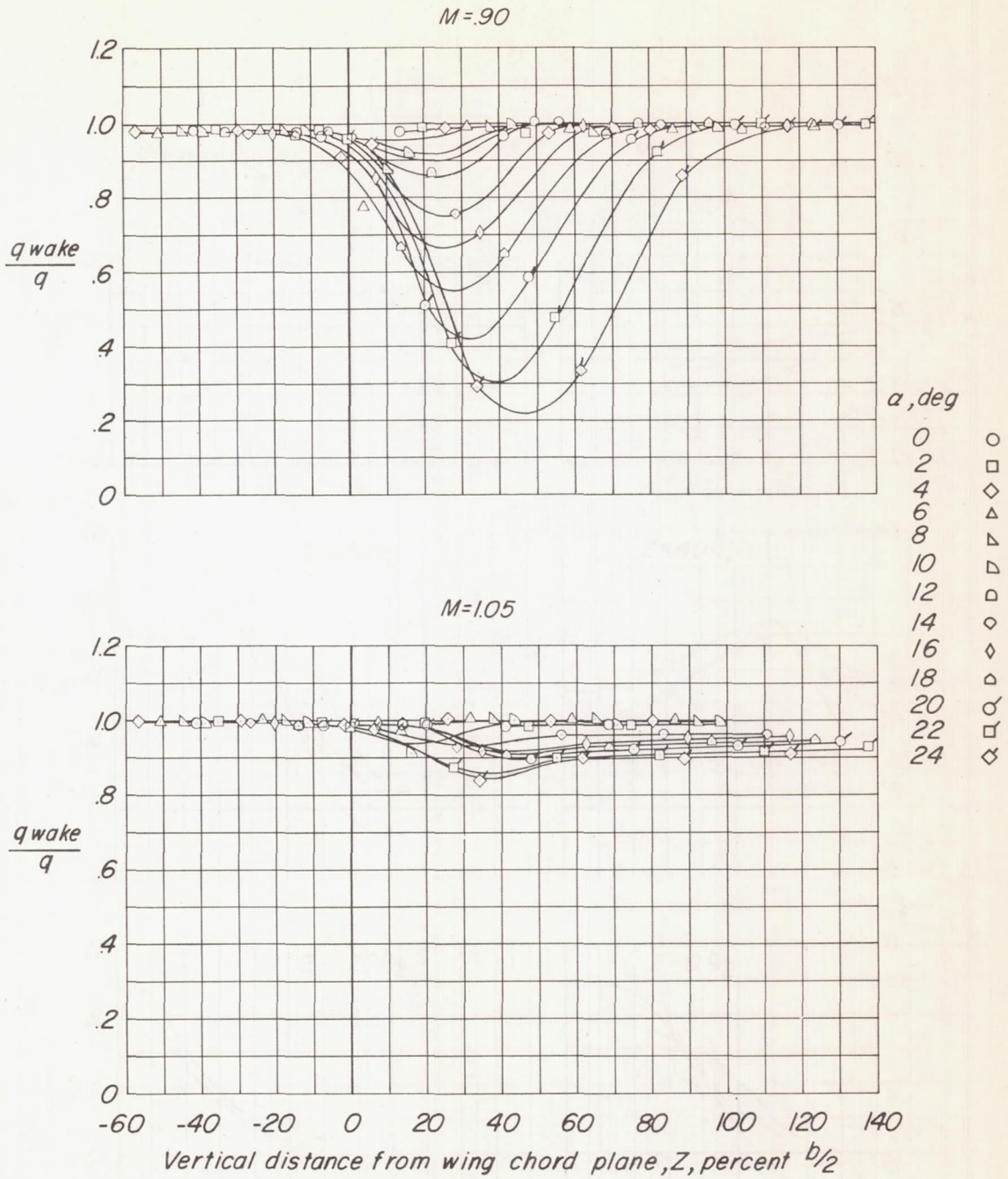
(c) $\Lambda_c/4 = 36.87^\circ$; X = 1.69b/2; Y = 0.20b/2.

Figure 17.- Continued.



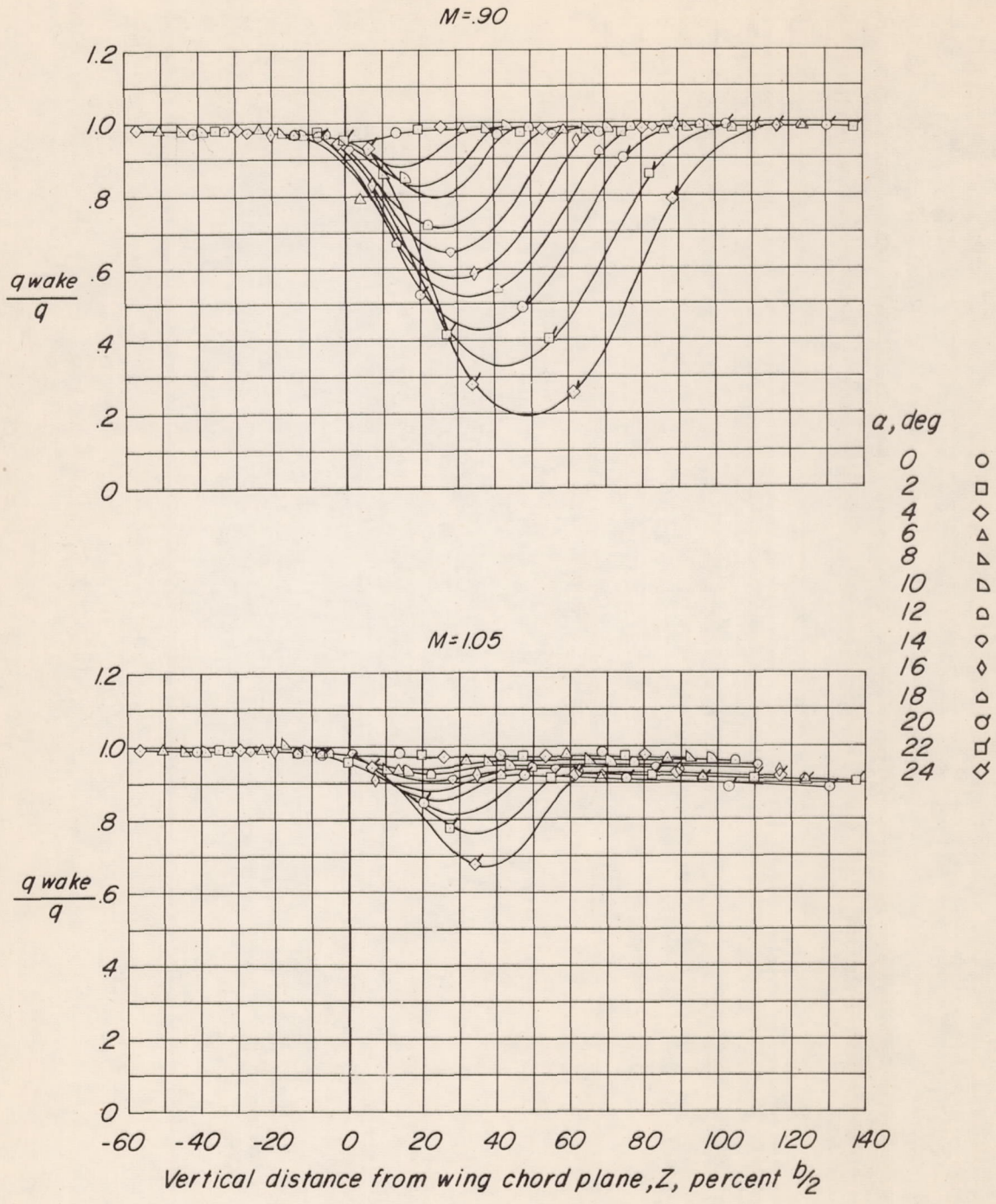
(d) $\Lambda_{c/4} = 45^{\circ}$; X = 1.69b/2; Y = 0.20b/2.

Figure 17.- Concluded.



(a) t/c = 0.02.

Figure 18.- Variation of dynamic pressure ratio with distance from wing chord plane extended for several angles of attack. $\Lambda_{c/4} = 14.03^{\circ}$; X = 1.92b/2; Y = 0.20b/2.



(b) t/c = 0.045.

Figure 18.- Concluded.

NACA - Langley Field, Va.